Combustion Characteristics of Ammonia as a Promising Alternative Fuel

by

Hadi Nozari

A Dissertaion Submitted to the

Graduate School of Sciences and Engineering

in Partial Fulfillment of the Requirements for

the Degree of

Doctor of Philosophy

in

Mechanical Engineering

June 16, 2017

Combustion Characteristics of Ammonia as a Promising Alternative Fuel

Koç University

Graduate School of Sciences and Engineering

This is to certify that I have examined this copy of a doctoral dissertation by

Hadi Nozari

and have found that it is complete and satisfactory in all respects,

and that any and all revisions required by the final

examining committee have been made.

Committee Members:

_____

Asst. Prof. Arif Karabeyoğlu

_____

Prof. Metin Muradoğlu

_____

Assoc. Prof. Alper Uzun

_____

Assoc. Prof. Onur Tunçer

_____

Asst. Prof. Çağlar Üçler

Date: 16. 06. 2017

to the memory of Hacımaman…

ABSTRACT

With its high hydrogen density and already existing infrastructure, ammonia (NH_3) is believed to be an excellent alternative fuel that can be used in energy generation and transportation systems. Combustion of ammonia has two main challenges that need to be addressed before its widespread use in practical systems: low flame speed (or weak flame stability) and its potential of generating fuel bond NO_x. The primary goal of the present research is to find a method to combust ammonia in an efficient and environmentally benign way. For this aim, the research is conducted in two parallel frameworks; chemical kinetics study and experimental investigation.

First we have investigated the combustion characteristics of NH_3/H_2/air mixtures at elevated pressure and lean conditions which are encountered in practical systems such as gas turbine combustors. Laminar premixed freely propagating flame model is used to calculate the combustion properties. The results of sensitivity study of total NO_x formation with respect to the equivalence ratio indicates the possibility of localized rich combustion as an effective way to reduce the NO_x concentration down to levels that are the same order as the modern gas turbine engines. One of the main objectives of the chemical kinetics study is to develop a reduced reaction mechanism for the combustion of ammonia which can be used to expedite the design of effective ammonia combustors through numerical simulations of realistic combustor geometries with accurate kinetics models. Accordingly by considering a wide range of conditions in terms of pressure, fuel mixture, and equivalence ratio we have developed two reduced mechanisms based on the well known Konnov mechanism. The reduced mechanisms are capable of predicting the total NO_x emission level and the laminar flame speed at an acceptable accuracy over a wide range of conditions. Evaluating the performance of the reduced mechanisms with respect to the full mechanism and experimental data shows that the mechanisms are able to predict the combustion properties almost at the same accuracy level as the Konnov mechanism, but at a nearly five times less CPU time expense.

The experimental study focuses on premixed ammonia-hydrogen-air flames under standard temperature and pressure conditions using an inert silicon-carbide (SiC) porous

block as a practical and effective medium for flame stabilization. Combustion experiments conducted using a lab scale burner resulted in stable flames with high combustion efficiencies at very high ammonia concentration levels over a wide range of equivalence ratios. Effects of some major influential parameters including equivalence ratio, ammonia mixture fraction, and diameter of the burner on flame stability have been investigated. Noticeable power output densities have also been achieved in the experiments. Results of NO_x emission measurements indicate NO_x concentrations as low as 35 ppm under rich conditions. The remarkable capability of this specific burner to operate efficiently and cleanly at high ammonia concentration levels, which can easily be achieved by partial cracking of NH_3, is believed to be a key accomplishment in the development of ammonia fired power generation systems.

ÖZET

Yüksek hidrojen yoğunluğu ve dünyada hâlihazırda mevcut bulunan üretim/dağıtım altyapısı amonyağı (NH_3) elektrik üretimi veya taşımacılık uygulamalarında kullanılabilecek, karbon içermeyen temiz yakıtlar arasında ön plana çıkarmaktadır. Amonyağın yakıt olarak geniş çaplı olarak kullanılmaya başlanabilmesi için iki teknik hususun çözülmesi gerekmektedir: yavaş yanma hızı dolayısıyla ortaya çıkabilecek yanma karasızlıklarının bertaraf edilmesi ve yanma sırasında oluşabilecek, molekül içeresindeki serbest nitrojenden kaynaklanan, NO_x salınımının minimize edilmesi. Bu çalışmanın esas hedefi amonyağın temiz ve verimli bir şekilde yakılabilmesi için gerekli teknolojilerin geliştirilmesidir. Bu amaca ulaşmak için hem kimyasal kinetik hesaplamalar, hem de deneysel çalışmalar beraberce yürütülmüştür.

Bu çalışmada öncelikle NH_3/H_2/hava sisteminin gaz türbinleri gibi pratik sistemlerde görülen yüksek basınçlarda ve yüksek hava/yakıt karışım oranlarındaki yanma dinamiğini incelenmiştir. Laminer ön karışımlı alev modeli yanma karakteristiklerinin belirlenmesi için kullanılmıştır. NO_x oluşum hassasiyet hesaplamaları NO_x seviyesini pratik sistemlerde istenen değerlere düşürmek için lokal olarak yakıt ağırlıklı yanma tekniğinin kullanılabileceğini göstermiştir. Kimyasal kinetik konusunda yapılan araştırmaların en önemli hedefi yanma odası tasarımını destekleyecek sayısal hesaplamaların yapılmasını kolaylaştırabilecek indirgenmiş yanma mekanizmalarının geliştirilmesidir. Bu bağlamda çok geniş basınç sıcaklık ve hava yakıt oranlarında, yüksek doğrulukla çalışan, Konnov mekanizmasından türetilmiş iki indirgenmiş yanma mekanizması geliştirilmiştir. İndirgenmiş mekanizmalar NO_x seviyelerini ve yanma hızını geniş bir operasyonel parametre aralığında oldukça doğru olarak hesaplayabilmektedir. Çıkan sonuçların değerlendirilmesi sonucunda indirgenmiş mekanizmaların deneysel ölçümler ve Konnov mekanizması ile yapılan hesaplamalar ile neredeyse ayni sonuçları verdiği görülüşmüş olup, indirgenmiş mekanizma ile yapılan hesapların Konnov mekanizmasına göre 1/5'lik bir CPU zamanında tamamlanabildiği tespit edilmiştir.

Deneysel araştırmalar NH_3/H_2/hava sistemi için atmosferik basınç ve sıcaklıkta yapılmış olup, yanma kararlılığını sağlamak için SiC bazlı geçirgen bloklar kullanılmıştır. Laboratuvar ortamında yapılan yanma deneylerinde geniş bir amonyak konsantrasyon ve hava yakıt oranı yelpazesi için kararlı alevler ve yüksek yanma verimleri elde edilmiştir. Yanma odası çapı, hava yakıt oranı, amonyak oranı gibi önemli parametrelerin yanma kararlılığına etkileri araştırılmıştır. Testler oldukça yüksek termal güç yoğunluğu değerlerinde yapılmıştır. NO_x değeri ölçümleri yakıt ağırlıklı hava yakıt oranlarında 35 ppm kadar düşük sevilerde salınım elde edilebileceğini göstermiştir. Test edilen konfigürasyonunun yüksek verimli, kararlı ve temiz bir yanma sağladığı tespit edilmiş olup ve bu tür sistemlerin amonyak bazlı endüstriyel yanma sistemlerine uygulanabilirliği için umut verici olduğu değerlendirilmektedir.

ACKNOWLEDGEMENTS

I would like to gratefully acknowledge the following people, who were instrumental in the writing and publication of this dissertation.

Foremost, I would like to express my sincere gratitude to my thesis advisor Assist. Prof. Arif Karabeyoğlu for his training, endless support, and the many opportunities he provided for me during the course of my PhD. I have learned a lot from him. He has always been a sourse of positive energy and motivation for me. I remember he used to say something like "That's a great news Hadi! You've nailed it!" when I presented him some promising results or "That's great Hadi! But I do not understand the X part! Why don't you also look into the …*here usually comes an absolutely helpful comment or a delicate tip about a critical point which I might have missed considering before! Based on my experience you never wanna miss a word of these statements!*..." when results did not make sense and he wanted to suggest a key point and at the same time encourage me to keep up the good work. He has always valued learning, profound understanding of concepts, and novelty as opposed to blindly publishing any obtained result. During the four years of advising me he always had a full trust on me which made me more confident and determined in my research. Last but not least, he never gave me deadline or any hierarchial orders! That's why I always considered him as a great advisor and most importantly a friend, as opposed to an academic boss! I am grateful to him being so generous for sharing his time, knowledge, and ideas. It was a great honor for me having conducted my PhD research under his supervision.

I am thankful to Assoc. Prof. Onur Tunçer at Istanbul Technical University, who gave me the opportunity to conduct experimental part of my research in his lab. I appreciate his support and assistance.

I am grateful to my thesis committee members, Prof. Metin Muradoğlu and Dr. Alper Uzun. They have always been supportive and their insightful comments in research progress meetings added to the quality of the thesis. It would be incomplete if I do not mention the contribustion of Dr. Çağlar Üçler for accepting to be a member of the PhD

dissertation jury and his valuable comments during the defense. I would like to thank all the dissertation jury members for their supportive comments and insightful suggestions.

I would like to give my special thanks to my friend Gizem Karaca for her valuable assistance in conducting the experiments. She set an example of a great experimental research assistant. I am also thankful to Gürkan Sarıkaya, Tanju Ergen, Muhittin Çelebi, and Tamer Şener, my friends and collueges in Istanbul Technical University for their endless support in the lab.

I would like to give my sincere thanks to my precious friends Ehsan Sarayloo, Selma Bulut, Sibel Çal, and Bengisu Seferoğlu for all the great moments we shared during the past years. We spent memorable quality time for hiking, biking, camping, traveling, running, brewing, celebrating, learning, and living! I will never forget their endless support and friendship.

A hearty thank you to my office mate, friend, and collogue Ozan Kara for his support and all the pleasant moments we shared during the past years. I am thankful to my former office mate and dear friend, Elena Toson for her support and hospitality and I wish her and dear Cristiano a great life ahead with their newcomer.

Vahid, my brother and my best friend; thank you for always being there for me. I don't know how to appreciate your precious presence and endless support during all the years we lived, learned, and grew up together. I just know that I have always counted on you in all the happy and sad moments of my life because you've always been there for me! My heartful thanks go to the delightful newest member of the family, Ayda, for all the pleasant freshness, joy, and positive nergy she brought with her to the family. She's always been a kind and supportive sister for me and I feel lucky for this.

Words are not enough to express my gratitude to the love of my life Darya. If I were to express one sentence about the impact of her green presense in my life I would say: She has always been the reason for my warm feelings about a place (not necessarily a physical space!) called home. Without her devotion and tolerance during the course of my studies, all the accomplishments and achievements would be impossible. She always did her best to motivate me to keep up the work. I cannot express in words how

devotedly involved she was not only as a fantastic wife in our day-to-day life, but also as a great friend and mentor in all the important events of my MSc and PhD years. I feel very lucky having her in my *home* she herself has made for me. İyi ki varsın Darya.

I finish with Tabriz, the name of a land where the most basic sources of my life energy reside: my parents. I would like to forward my heartful thanks to this fantastic couple for their continuous support, patience, and endless love during every step of my life and education. I have amazing parents, fantastic and unique in many ways. Their support has been unconditional during all these years; they have given up many things for teaching me and my brother how to learn, share, respect, tolerate, persist, and live the life to the fullest. They have supported me in all the important moments of my life whenever I needed it. Despite the physical distance between us, I always feel their vigorous presence and unconditional love in every stage of my life. Her zaman kölgeniz başımız üste olsun eziz Ata ve Ana.

TABLE OF CONTENTS

LIST OF TABLES

LIST OF FIGURES

NOMENCLATURE

Chapter 3

a_{stoi}	moles of air for stoichiometry
ICE	internal combustion engine
CR	compression ratio
b,c	coefficients of products in NH_3/H_2/Air chemical reaction
x,y	coefficient of reactants in NH_3/H_2/Air chemical reaction
k	rate constant of chemical reaction
E_a	activation energy (cal/mole)
LHV_{fuel}	lower heating value of fuel (kJ/kg)
NH_i	nitrogenous radicals, mainly NH and NH_2
OX	oxygenated species
X_i	mole fraction of i^{th} species in the fuel mixture
dn/dt	mole conversion rate (mole/s)
SI	spark ignition
STP	standard temperature and pressure
SSAS	solid state ammonia synthesis
T	flame temperature (K)
ϕ	fuel-air equivalence ratio
SMR	Steam methane reforming
SCR	Selective catalytic reduction
SNCR	Selective non-catalytic reduction

Chapter 4

ε_{H_2}	Hydrogen flow measurement error
S_l	Laminar flame speed (cm/s)
ε_{NH_3}	Ammonia flow measurement error
SLPM	Standard liters per minute
ε_{air}	Air flow measurement error
SiC	Silicon Carbide
$\varepsilon_{ø}$	Equivalence ratio measurement error
T	Temperature (K)
$\varepsilon_{\%NH_3}$	Ammonia percentage measurement error
T_{ad}	Adiabatic flame temperature (K)
FC	Flow controller
V	Mixture velocity (m/s)
NTP	Normal temperature and pressure
x_i	i^{th} measurement result
N	Number of experiments
$\bar{x}$	Mean value of measurements
PPI	Pores per inch
$\sigma_{\bar{x}}$	Standard error
q	Volume flow rate
ϕ , ER	Equivalence ratio
Re	Reynolds number
% NH_3	Percentage ammonia volume fraction

CHAPTER 1

INTRODUCTION

1.1 Background

Extensive use of fossil fuels has caused harmful problems to the environment and human welfare. As the problems have become noticeably upsetting, the search for alternative fuels has gained critical global concern. To reduce the environmental impact of industrial activities, some sustainable and renewable fuels have been proposed by scientists. Some of the major parameters noted in studies are economic viability, energy efficiency, and the environmental impact of alternatives. Liquefied petroleum gas, natural compressed gas, oxygenated fuels, biodiesel, and hydrogen are some of the fuels that have been studied extensively.

Carbon free ammonia (NH_3) is a promising green energy carrier/storage medium due to its high hydrogen density, which is higher than liquid hydrogen. As a matter of fact, 108 kg H_2 is stored in $1m^3$ of liquid ammonia at 20 °C and 8.6 bars. The hydrogen density of NH_3 is 4 times higher than the demonstrated density in the most advanced methods involving metal hydrides [1]. Furthermore ammonia's cost per volume of stored energy is about three times less expensive than that of hydrogen. It is a colorless gas, alkaline at standard conditions of pressure and temperature, with a characteristic pungent odor. Basic physical properties of this molecule are presented in Table 1-1 [2].

Compared to hydrogen, which is also considered a favorable alternative, ammonia is easier to produce, handle, store, and distribute with the existent infrastructure and is believed to have a promising commercial viability. Presently, ammonia is a strategically important chemical, which is widely used as a fertilizer or as a feedstock for most other synthetic fertilizers. Despite its toxicity, ammonia presents a significantly lower fire hazard compared to hydrogen and gasoline. High ignition temperature of ammonia makes it a relatively safe chemical in transportation and distribution, while hydrogen

systems are prone to explosions due to its wide explosion limits and very low minimum ignition energy [3].

Table 1 - 1 Physical properties of ammonia

Property	Value	Unit
Density	603	kg/m3
Molecular weight	17.03	g/mol
Vapor pressure @293 K	8.88	Bar
Auto-ignition T	651	°C
Boiling point at 1 atm	-34	°C
Peak Flame T	1850	°C
HHV	22.5	MJ/kg
LHV	18.65	MJ/kg
Price	0.25	$/kg
Price	151	$/m3
Energy price	11	$/GJ
Main synthesis process	Haber-Bosch	60-65% efficiency
Latent heat of vaporization @1atm & boiling point	1371.2	kJ/kg
Critical T & P	405.4 / 112.8	K / bar
Gas density @ 1 atm & boiling point	0.86	kg/m3
Compressibility factor @ 1atm, 288 K	0.9929	
Cp & Cv @ 1atm, 288 K	0.037 / 0.028	kJ/mol-K
Flammability limit in air	15%-28%	By volume
Octane rating	110-130	

Following items are some of the noticeable advantages of ammonia as a fuel [4]:

- A relatively high octane rate (110–130) makes it a practical fuel for internal combustion engines.
- It can be thermally cracked into hydrogen and nitrogen in a simple process by providing energy as low as 12% of its higher heating value.
- The distribution infrastructure already exists for ammonia to deliver it in amounts larger than 100 million tons yearly [5].

- Safer than many other fuels. Because of its lower density than air, in case of a leakage or spillage it dissipates rapidly.
- It is a self-alarming toxic chemical. Leakage even as low as 5ppm can be detected by nose.
- It has a narrow flammability limit and near zero explosion danger if transported properly.

1.2 Ammonia synthesis

Because of its many applications, NH_3 is in volume the second globally produced inorganic chemical. Dozens of chemical plants worldwide produce NH_3. Consuming more than 1% of all man-made energy, NH_3 production is a significant component of the world energy budget. Ammonia is synthesized by reaction of hydrogen and nitrogen molecules:

$$3\,H_2 + N_2 \rightarrow 2\,NH_3 \quad -45.2\,kJ/mol_{NH_3} \qquad (1)$$

Although it is an exothermic reaction, the activation energy of this reaction which is needed to break the triple bond of nitrogen molecule is challenging (~460 kJ/mol). The main process through which the reaction takes place is Haber-Bosch process which was invented at the beginning of the twentieth century. Hydrogen and nitrogen molecules combine thermo-catalytically under specific conditions. The principle of this process is based on increasing the temperature of the reactants to a level that nitrogen molecules get enough energy to be cracked. Modern NH_3-producing plants depend on hydrogen (H_2) from steam methane reforming (SMR) to react with atmospheric nitrogen (N_2) using a catalyst under high pressure and temperature (200 bar and 450 °C) to produce anhydrous liquid NH_3. This step is known as the Haber-Bosch synthesis. Production of ammonia by this process accounts for about 1% of the global CO_2 emissions. Many environmentally friendly methods have been developed for hydrogen production, which do not emit CO_2. For instance biomass, solar energy, or other renewable sources are used for hydrogen production [6].

1.3 Ammonia decomposition

Ammonia cracking to hydrogen and nitrogen molecules is simply the reverse of the synthesis reaction.

$$NH_3\,(g) \rightarrow 0.5\,N_2\,(g) + 1.5\,H_2\,(g) \qquad \Delta H = 46\,kJ/mol \qquad (2)$$

As presented the reaction is endothermic. Catalyst plays an important role in the decomposition process. There are a wide variety of materials that have been found to be effective. The required temperature for catalytic decomposition can vary between 650-1100 °C depending on the catalyst.

1.4 Ammonia-hydrogen-air reaction

If the initial composition of the reactants corresponds to the stoichiometric equation of the complete combustion reaction, the flame is a stoichiometric flame and the value of the equivalence ratio is unity. Ammonia, hydrogen, and air react under the following global reaction.

$$NH_3 + 0.5H_2 + (O_2 + 3.76\,N_2) \leftrightarrow 4.26N_2 + 2H_2O \qquad (3)$$

To describe the stoichiometric status of a reacting mixture, the concept of the equivalence ratio is defined by the following equation:

$$\emptyset = \frac{(\frac{Fuel}{Oxidizer})_{mixture}}{(\frac{Fuel}{Oxidizer})_{stoichiometric}} \qquad (4)$$

The ratios can be either volumetric or gravimetric. Regarding the ammonia-hydrogen-air global reaction, the stoichiometric fuel to air ratio is 0.315 volume-based (0.13 mass based). The mole fractions and corresponding volume flow rates of the fuel and air streams are presented in Appendix 1.

1.5 NO_x formation mechanisms

Nitrogen oxides formation is one of the major challenges of ammonia combustion. These chemicals are among the main environmental pollutants which are generated by

chemical reactions occurring in flames. Therefore, understanding the underlying kinetics of NO_x formation and decomposition in flames is essential for development of the associated reduction and removal technologies. NO_x formation is strongly dependent on the flame temperature as well as on the availability of some precursor radicals. The major NO and NO_2 formation mechanisms in H/N/O systems are presented in the following.

1.5.1 Thermal NO

The thermal (Zeldovich) NO mechanism is basically the oxidation of nitrogen molecules at temperatures greater than 1700 K. Nitric oxide is formed by involvement of oxygen and nitrogen molecules via the global reaction $N_2+O_2 \leftrightarrow 2\,NO$. However, the kinetic route of NO formation is not through the attack of an oxygen molecule on a nitrogen molecule. Dissociated oxygen atoms react with nitrogen molecules to start a chain. The next step is the fast reaction of the liberated nitrogen atoms with oxygen molecules.

$$O + N_2 \leftrightarrow NO + N \quad k_{f1} = 2 \times 10^{14}\exp(-315/RT) \qquad (5)$$

$$N + O_2 \leftrightarrow NO + O \quad k_{f2} = 6.4 \times 10^{9}\exp(-26/RT) \qquad (6)$$

Later the reaction of nitrogen atom and hydroxyl radical was also included as an influential step in the thermal mechanism.

$$N + OH \leftrightarrow NO + H \quad k_{f3} = 3.8 \times 10^{13} \qquad (7)$$

Activation energies are in kJ/mol. The combination of the three steps is referred as thermal (Zeldovich) mechanism. The mechanism is named after Zeldovich, who was the first to propose the chain [7]. It is important to note that the first of the three steps is rate limiting and due to a slower reaction rate compared to fuel oxidation, the radical concentrations of O and OH species are assumed to be at equilibrium yielding NO formation rate as:

$$\frac{d[NO]}{dt} = 2 \times k_{f1}[O_2]_{eq}[N_2]_{eq} \qquad (8)$$

The strong dependence of thermal NO formation on temperature is evident from the latter equation. Based on the very high activation energy of the first step, NO formation via the thermal mechanism is insignificant below 1500 K.

1.5.2 The fuel-NO

Fuel-bond nitrogen is an important source of NO in flames. In other words, combusting nitrogenous fuels leads to fuel-NO formation. A demonstration of fuel-bond NO formation reaction is as following.

$$NH_i + OX \leftrightarrow NO + H_iX \quad (9)$$

OX is an oxygenated species which reacts with a NH_i radical. Therefore, the NH_i radicals are known as fuel-bond NO precursors. For the case of ammonia flames the precursors are thus mainly NH_2 and NH and their formation occurs in the flame front.

In practical applications there are two widely used methods applied to reduce NO emissions during combustion. The first method is to modify the combustion conditions. Examples are reduction of the oxygen concentration and reduction of the combustions temperature. The second practical way is to apply reduction methods using ammonia itself. The latter method is based on NO_x reduction capability of ammonia. Ammonia injection on the way of exhaust gases starts a chain through which nitrogen monoxide is removed. First the NH_2 radicals are formed in a hydrogen abstraction reaction. The resulting radical reacts with NO to form water and nitrogen molecule.

$$NH_3 + (H; OH; O) \leftrightarrow NH_2 + (H_2; H_2O; OH) \quad (10)$$

$$NH_2 + NO \leftrightarrow N_2 + H_2O \quad (11)$$

This reaction chain is very influential in NO alleviation in industrial applications. It is important to note that the widely used SCR and SNCR techniques use ammonia as the NO_x removal agent.

1.5.3 NO_2 formation

Nitrogen dioxide is in equilibrium with nitrogen monoxide through the following reactions.

$$NO + O(HO_2) \leftrightarrow NO_2(+OH) \qquad (12)$$

$$NO_2 + H \leftrightarrow NO + OH \qquad (13)$$

In combustion processes, the above two reactions occur simultaneously. Based on the equilibrium concentrations, any NO formed at room temperature is converted to NO_2. At higher temperatures, the concentration of NO exceeds the concentration of NO_2. At conventional combustion temperatures (> 1800 K) appreciable amounts of NO formation are expected, while negligible amounts of NO_2 are formed. It is worth mentioning that the NO_2 formation levels throughout the present research were negligible compared to NO emission levels. Therefore, the focus is primarily put on NO emission.

1.5 Target markets

As elaborated in literature review section, ammonia has been studied as a transportation system fuel extensively. This is mainly due to its high hydrogen density. However, using ammonia as a fuel for electricity generation can be more advantageous and practical. Here are some important factors to consider:

- Safety: this is a critical issue in transportation vehicles but not as critical in electricity generation units. In the latter case normal people are not handling ammonia and ammonia fired combustion units in their everyday life. Ammonia handling health effects are presented in Appendix 2.
- Cracking: the current cracking reactors are mostly heavy and expensive. Therefore they are not ideal for transportation.
- Storage tank weight: weight is critical in transportation application bot not an issue in terrestrial power generation systems.

- Startup: engine startup with pure ammonia is not trivial. Even with a combustion promoter it may be tricky in engines. For electricity generation we do not need many startups.
- Operational safety: it is considered a drawback in transportation sector due to the possibility of handling the fuel pumps by nonprofessionals. In power generation systems, skilled and professional people handle the system.

For power generation application, lightweight and micro gas turbines can be considered as a primary potential target market for ammonia replacement [8]. Even with the current production technologies and excluding the CO_2 emission related issues ammonia is an economically viable option for oil fired light weight gas turbine systems and also oil fired micro gas turbines used for stranded power generation. Note that since CO_2 sequestration is not feasible for these relatively small power generation units, ammonia has huge environmental advantages over fossil fuels. This market opportunity exists currently and does not require the development of new production, distribution, and storage technologies for ammonia. It is important to note that since the heavy duty gas plants utilize natural gas, switching to ammonia may not be economically viable within the current paradigm.

Another potential market for ammonia combustion based gas turbine power generation can be distributed renewable energy generation units. Most of the renewable energy sources such as solar or wind have very low capacity factors. This requires a backup power system. Instead of connecting to the grid (in case of which the utilities and companies would charge for this), excess power can be used to make ammonia which can be stored and burned in a micro turbine to generate electricity and heat when needed. This requires the development of an efficient synthesis technology for ammonia from water and air. Since ammonia is a widely used fertilizer, its use for electricity generation in rural and agricultural areas makes perfect economic sense.

Also ammonia as energy carrier has the potential to solve the stranded renewable energy problem. Most of the renewable energy sources such as solar, geothermal, or wind are not accessible by the existing electric grid system. Extending the grid to remote areas is

not economical. On the other hand, in most cases extension of the grid system is politically difficult (if not impossible). Using a synthesis method such as SSAS ammonia can be produced at the stranded site from water and air. Consequently, the produced ammonia can be shipped via trucks, railroad, or pipelines to the power generation plants to generate electricity.

1.6 Thesis Organization

Chapter 3 presents a comprehensive chemical kinetics study of ammonia-hydrogen-air mixtures under mid and high pressure conditions. The combustion characteristics (laminar flame speed, NO_x formation, and ignition delay time) are thoroughly investigated. Two reduced reaction mechanisms are established as a major outcome of the chemical kinetics study. The reduced mechanisms are capable of predicting combustion characteristics with a high precision and efficiency levels. The content of Chapter 3 was published as:

H. Nozari, A. Karabeyoglu, "*Numerical study of combustion characteristics of ammonia as a renewable fuel and establishment of reduced reaction mechanisms*", Fuel, 2015, DOI 10.1016/j.fuel.2015.06.075

H. Nozari, A. Karabeyoglu, "*Combustion characteristics of ammonia as a renewable energy source and development of reduced chemical mechanisms*", AIAA JPC Proceedings, 2015, DOI: 10.2514/6.2015-3917.

The forth chapter includes the experimental study on flame stability and NO_x formation sensitivity of ammonia-hydrogen-air mixtures in standard temperature and pressure conditions. A silicon-carbide porous medium based burner is designed and introduced as an effective way to enhance the combustion quality of ammonia doped flames. Flame stability is investigated and stability criteria are established for the burners. A simple volumetric heat release CFD model is used to examine the combustion efficiency of the burners. Power output density and NO_x emission are other important characteristics investigated in this chapter. The content of Chapter 4 is elaborated in the following articles:

H. Nozari, G. Karaca, O. Tunçer, A. Karabeyoglu, "*Porous medium based burner for efficient and clean combustion of ammonia-hydrogen-air systems*", International Journal of Hydrogen Energy; 2017; DOI 10.1016/j.ijhydene.2017.03.234.

H. Nozari, O. Tunçer, A. Karabeyoglu, "*Evaluation of ammonia-hydrogen-air combustion in SiC porous medium based burner*", accepted for publication by Elsevier Energy Procedia.

H. Nozari, O. Tunçer, A. Karabeyoglu, "*NO_x formation sensitivity analysis of ammonia-hydrogen-air premixed flames in a 30 KW porous medium based burner*", under preparation for submission to International Journal of Hydrogen Energy.

In Chapter 5 concluding remarks of the conducted research are put forward and potential future research directions are suggested.

CHAPTER 2

LITERATURE REVIEW

2.1 Chemical kinetics research

Several chemical kinetics models have been developed and implemented to analyze the ammonia oxidation and NO_x formation reactions. The first reaction mechanism related to ammonia chemistry was proposed in 1973 by Kaskan and Hughes [9], introduced as the mechanism of ammonia decay in an NH_3/O_2 flame. The main goal was to predict the rates of change of NH_3, NO, and NH during the process. The mechanism contained only 12 species and 26 elementary reactions. They concluded that the ammonia decay mainly occurs through a set of reversible reactions that convert the various NH_i's (i = 0-3) into each other, and another set of irreversible reactions that permanently remove one or more NH_i. Even though the model could not predict the observed phenomena during the combustion with an acceptable precision, since it did not take into account important species like HNO or N_2O, it is considered as a first interpretation of ammonia combustion.

The first detailed mechanism for ammonia combustion was proposed in 1983 by Miller et al. [10] based on several burner-stabilized and freely propagating NH_3/O_2 and $NH_3/H_2/O_2$ flames. The species concentration profiles generally matched the experiments, except for very rich flames where kinetic model was missing important pyrolysis steps. However, the important NO and N_2 formation reactions were correctly identified and nitric oxide in lean flames was mainly produced through the nitroxyl (HNO) intermediate, which was formed either by the reactions of NH_2+O, $NH+OH$ or $NH+O_2$. The NO conversion to N_2 in lean flames is supposed to occur by reaction with NH_2 or NH, forming NNH or N_2O, respectively, as intermediates. Under rich conditions, NH_2 and NH are supposed to be rapidly converted to nitrogen atoms

followed by formation of NO and conversion of NO to N_2 by the extended Zeldovich mechanism [7].

To improve the Miller mechanism [10], combustion of ammonia has then been studies in various conditions with different pressures and temperatures. Dean et al. [11] analyzed ammonia flames at atmospheric pressure. They highlighted the importance of reactions between NH_1 and NH_2 species to form N-N bonds. The N_2H_j (j=1-3) species could then lose H atoms via dissociation to ultimately form N_2. Ammonia oxidation was also studied by Salimian et al. [12] in a shock tube operating at temperature range of 1600-2100 K using N_2O as a thermal source of O atoms. They reported that the reactions involving HNO radicals, mainly formed by reaction of O atoms with NH_2, were the major pathways of NO production. They concluded that the reactions of N and NH_2 with NO were significant NO removing steps while NH_i-NH_i interactions were very influential in the fast removal of ammonia and production of N_2 through non-NO pathways.

Together with Bowman, Miller proposed an improved version of his former mechanism in 1989 [13]. The main focus was on nitrogen oxides formation, considering both thermal and prompts NO as well as fuel nitrogen conversion, thermal De-NO_x and Rapid Reduction of NO_x (RAPRENOx) processes. Parallel to NO, NO_2 and N_2O formation and removal processes were also investigated. Subsequently the improved mechanism was used by Davidson et al. [14] as a starting platform to elaborate a pyrolysis mechanism for ammonia. Also they conducted measurements of some NH reaction rates [15,16] which provided further insight into the consumption reactions of NH_2 and NH. Although the model presents ammonia degradation in conditions very different from combustion, some reaction steps and related rate constants remarkably attracted interest reflected as benchmark in later studies. The Bian et al. [17] developed a model specific to ammonia oxidation which has been tested on H_2/O_2/Ar flames seeded with ammonia and nitrogen monoxide (NO) and for ammonia flames burning in oxygen or in nitrogen monoxide. Consequently, Vandooren et al. [18] presented a detailed mechanism for ammonia combustion based on the Bian et al. model [17]

providing valuable data on the reactions. For this aim they had conducted experiments mainly focusing on the formation of NO and N_2O. Furthermore, they concluded that the reaction $NH_2+NO \rightarrow N_2+H+OH$ plays a critical role in burning of NH_3/NO mixtures by providing the essential hydrogen atoms and hydroxyl radicals for the primary decomposition of NH_3. Based on the Miller and Vandooren mechanisms [13,18], Lindstedt et al. [19,20], developed a reaction mechanism with acceptable prediction accuracy for laminar premixed $NH_3/H_2/O_2$, $NH_3/NO/H_2/O_2$, and NH_3/O_2 flames. They reported that the relative significance of the various NO formation pathways is highly dependent on the flame condition: (a) $NH_2 + O$ plays a critical role in all flames, (b) $NH + OH$ becomes significant in pure ammonia flames, (c) the Zeldovich mechanism [7] becomes more important with increasing fuel concentrations in hydrogen flames with ammonia and ammonia flames with nitrogen monoxide. They also concluded that the conversion of NO to nitrogen is mainly accomplished by reactions involving NH_2 and N radicals, with NH radicals having a less significant role in this conversion. Finally, they specified the major NO conversion paths: $NO + NH_2$ in pure ammonia and ammonia doped lean hydrogen flames and $NO + N$ in ammonia doped stoichiometric and rich hydrogen flames.

Some other detailed reaction mechanisms exist which were mainly developed for methane or natural gas but also used for ammonia combustion. The well-known Gas Research Institute mechanism (GRI-mech) [21] is an example which is used to simulate natural gas flames burning in oxygen or air but also takes into account nitrogenous species like ammonia, radical amidogen, and nitrogen monoxide. San Diego mechanism [22] is another example which was initially a basic model designed for methane systems but gradually developed to a more complete model capable of being applied to more complex systems such as hydrocarbons up to n-heptane.

Followed by an experimental study of methane oxidation in the presence of NO and NO_2 in an isothermal plug flow reactor, Glarborg et al. [23] suggested a detailed mechanism for low temperature oxidation of methane based on a previous mechanism [24]. They also investigated a part of the mechanism for ammonia oxidation under fuel

rich conditions and moderate temperatures [25]. Since the study was performed at lower temperatures (750-1250 K) than flame temperatures, it highlighted the role of pathway $NH_3 \rightarrow NH_2 \rightarrow N_2$ (directly or via NNH) rather than the sequence $NH_3 \rightarrow NH_2 \rightarrow NH \rightarrow N$ which is important in flames. They also concluded that the major conversion of fuel bond nitrogenous species to N_2 occurs by reaction of amine radicals with NO, particularly via $NH_2 + NO$. A more precise mechanism was proposed by Konnov et al. developed for the combustion of small hydrocarbons. Based on this mechanism they developed a complete detailed mechanism for N/H reactions [26] and validated with experimental data for ammonia pyrolysis in shock waves [14]. They reported the significance of implementing reaction steps including N_2H_3 and N_2H_4 into the mechanism which noticeably influenced the calculated rise-time and peak concentrations of the NH and NH_2 radicals. It is important to note that the pressure and temperature conditions of ammonia pyrolysis in shock waves are not similar to those of ammonia combustion in flames. In a later study [27] Konnov improved the previous mechanism by implementing modifications on the rate constants of some prompt NO formation pathways. The modifications led to a better accuracy in prediction of NO concentration in lean and rich flames of methane, ethylene, ethane, and propane. The revised mechanism is considered one of the most reliable detailed reaction mechanisms for ammonia chemistry. Based on experimental and modeling studies of several premixed $NH_3/CH_4/O_2/Ar$ flames at low pressure (4.0 kPa) and stoichiometric conditions, Tian et al. [13] proposed a detailed kinetics mechanism. The mechanism was capable of successfully predicting the structure of CH_4–NH_3 and nitro-methane flames. It is important to note that the latter two mechanisms by Konnov and Tian are much more detailed and comprehensive, including extensive reaction steps for ammonia chemistry, when compared to the former mechanism by Miller and Bowman [13]. The full versions have about 4 times more species and 10 times more reaction steps.

In all the reaction mechanisms the prediction precision mainly depends on the method applied to obtain the reaction pathways and rate constants. Many experimental methods are used to examine or improve accuracy of the rate constants of certain reaction steps in literature. For instance, Harrison et al. [28] used laser induced florescence to study

$NH+NO/NO_2$ pathway and Lozovsky et al. [29] studied NH_2+O by a laser spectroscopy technique. Cheskis et al. [30] applied intracavity laser spectroscopy to investigate $HNO+HNO$ and $HNO+NO$ pathways and Zabielski et al. [31] used a molecular beam sampling mass spectrometer to measure NH_3 level regarding the reaction $NH_3+OH \rightarrow NH_2+H_2O$. Duynslaegher [32] has presented some other methods and reaction steps with more details on the applied methods. In certain studies, comparison of results obtained by the reaction mechanisms and experimental data was performed to investigate the accuracy of mechanisms in predicting the combustion process [33–36]. Based on the fuel mixture and the combustion conditions, each mechanism has shown agreement/disagreement with experimental results. This fact implies that for each numerical study, the choice of reaction mechanism is an important factor in obtaining reliable results.

To apply the detailed chemical kinetics to complete combustion modeling, reaction mechanisms are usually reduced. In other words, reduced mechanisms are significant, since they make it possible to apply accurate chemical kinetics to commercial or research CFD codes for combustion modeling within a reasonable simulation time for solving real life engineering problems. The main concern is to maintain the accuracy of reaction mechanism in an acceptable range to avoid inaccurate and possibly misleading results. In the open literature there exists few reduced mechanism focusing on ammonia flames. A reduced mechanism was established by Duynslaegher et al. [33] for ammonia combustion and another reduced mechanism developed by Xiao et al. [35] for ammonia/methane flames. Both the reduced mechanisms are developed based on the full Konnov mechanism [27].

2.2 Experimental research

In 1941 A. Macq [37] suggested ammonia as a potential alternative fuel for the first time. His suggestion was made mainly based on the fact that ammonia was produced in large quantities in Belgium making it a readily available chemical for substitution in car engines. The problem of combustion initiation was thus encountered since, for

conventional compression ratios used in spark ignition engines, ammonia does not ignite without a little boost. Therefore, a small part of ammonia was transformed into hydrogen which allowed the ignition when it was present in amounts greater than 5%. This hydrogen formation was performed using a catalyst composed of iron, aluminum oxide, and potassium carbonate. Since ammonia decomposition is endothermic, the heat required for this reaction was supplied by the exhaust heat.

A second study was performed in 1966 by Starkman et al. [38]. The objective was to extend the area of basic and applied information relative to successful substitution of hydrocarbons by anhydrous ammonia as a spark ignition engine fuel. The experiments were performed using nominal compression ratios between 6:1 and 10:1, normal ignition systems, atmospheric or throttled manifold pressures, and dissociation or regeneration methods compatible with domestic or military installations. They concluded that the successful application of ammonia as a spark ignition engine fuel at conventional compression ratios in such engines needed its introduction as a vapor and its partial decomposition into H_2 and N_2 before introduction into the cylinder. Also, specific fuel consumption was increased by a factor of 2 over that of hydrocarbons when compared at peak power and 2.5 when compared at maximum economic viability due to the smaller lower heating value of ammonia.

Since 2006, Grannell et al. [39,40] performed research on the possibility to use ammonia in a dual fueled spark ignition engine with gasoline. They investigated the operating features of a stoichiometric, ammonia and gasoline dual fueled SI engine using a single cylinder, variable compression ratio, supercharged Cooperative Fuel Research (CFR) engine at varying ratios of gasoline to ammonia. They concluded that a significant part of the gasoline used in SI engines can be replaced by ammonia. Near idling, the use of mainly gasoline is required while mainly ammonia can be used at higher loads. Higher compression ratios and higher loads can be obtained without knock using ammonia or ammonia with gasoline than with gasoline alone. A compression ratio of 12:1 was allowed with 65% ammonia and 35% gasoline whereas the limit for gasoline alone was 9:1. Operation at 10:1 compression ratio is the best mode from the

standpoint of both efficiency and also the fuel replacement rate when ammonia and gasoline are used.

In 2007, to demonstrate the practical use of ammonia as an alternative automobile fuel, Grannell et al. converted a Chevrolet S10 pick-up into an ammonia-powered vehicle and ran from Detroit to San Francisco (2500 miles) [41]. The truck was dual-fueled, meaning it could be switched seamlessly from 100% gasoline fuel to a mixture of 80% NH_3 and 20% gasoline. The truck ran the same, no matter which fuel it was burning. The technology that makes this NH_3 car possible is the control system that managed the perfect mixture of fuel for the amount of engine load. They concluded that most of the gasoline burned by SI engines can be replaced by ammonia when the indicated mean effective pressure is higher or equal to 400 kPa. However, they suggested that a SI engine cannot generally give acceptable performance while fueled by ammonia alone.

Finally in 2009 [42] Grannell et al. measured the engine-out and post-catalyst emissions of ammonia, hydrocarbons, nitric oxide, carbon monoxide, and nitrous oxide of the engine. They found that an ordinary three-way catalytic converter can be used to clean up these emissions but lean operation must be absolutely avoided. The clean-up region has been found to occur between stoichiometric and 0.2% rich. The engine-out exhaust emissions reflected appropriately the proportion of ammonia in the intake fuel mixture when the engine was operating satisfactorily from the standpoint of combustion stability and overall thermal efficiency. The effect of rich and lean operation on post-catalyst NH_3, NO, and N_2O emissions becomes much stronger whenever any ammonia doped fuel is used. For that reason, they suggested that the inclusion of a post-catalyst oxygen sensor is necessary when ammonia is used.

Morch et al. [43] investigated the use of ammonia-hydrogen mixtures in a SI engine using metal amine complexes for ammonia storage. Ammonia and hydrogen were introduced into the intake manifold of a CFR engine. They performed several experiments with varying excess air ratios and ammonia to hydrogen ratios. They found that, with respect to efficiency and mean effective power, a fuel mixture with 10 vol.% hydrogen was the optimum. This has been explained by the higher heat loss during

combustion of the mixtures with high levels of hydrogen. In order to investigate the possibility of using $MgCl_2$ as an ammonia carrier in SI engine, a fuel system was modeled. The model was used to analyze the possibility of using exhaust heat for desorption and decomposition of ammonia. The investigation showed that it is possible to cover a major part of the needed heat for a metal amine complex based fuel system with the exhaust heat. They observed a noticeable NO_x emission with the largest one occurring with a high hydrogen content and an excess air ratio between 1.1 and 1.4. In order to reduce the NO_x they proposed to use selective catalytic reduction (SCR) since ammonia was already onboard. They performed also a comparison with gasoline concluding that higher power and efficiency with NH_3/H_2 was achievable due to the possibility of higher compression ratios. The overall emission levels of NO_x on ammonia/hydrogen and gasoline were the same.

As previously mentioned in some of the studies, a practical way to make ammonia operable in internal combustion engines as well as gas turbine combustors is to premix it with a vigorous fuel which acts as combustion promoter. Gross and Kong [44] combusted ammonia-dimethyl ether mixtures in a compression-ignition engine and Reiter and Kong [45] studied the combustion and emission characteristics of ammonia-diesel mixtures in the same type of engine. A novel dual fuel combustion system featuring the direct injection of diesel and NH_3 has been proposed by Boretti [46]. Results revealed the feasibility to achieve diesel-like power densities and efficiencies, and load control by adjusting the quantity of the injected fuel. Additionally, ammonia has proven to be a satisfactory substitute for hydrocarbon fuels in gas turbine engines. Past experience with ammonia fueled gas turbines by Solar Company [47] and UC Berkeley [48] in the 60's showed that acceptable levels of efficiencies were achievable in well-designed ammonia combustors. In a study by SPG Group, the feasibility of ammonia based fuels for environmentally friendly power generation in gas turbine engines was investigated [49]. Similarly, in a study on ammonia-methane combustion in tangential swirl burners, potential of ammonia was evaluated as a gas turbine fuel [50]. With resulting weak flame stability and high emissions, stratified injection with low swirl was recommended as a possible way to burn the mixture effectively.

In order to enhance the desirable characteristics of ammonia combustion while keeping its carbon-free chemistry merit, hydrogen can be mixed as a combustion promoter. As a more desirable method for practical applications, ammonia can be partially cracked to generate hydrogen prior to combustion. Presence of hydrogen increases the flame speed, decreases the ignition delay time, and also extends the narrow flammability range of ammonia making the fuel mixture possible to burn in a wide range of practical engines. It can be argued that combustion of NH_3-H_2 mixtures are more attractive compared to pure hydrogen due to the improved safety associated with narrower the explosion limits and visually detectable flames. There have been a few studies exploring the effect of hydrogen addition on combustion characteristics of ammonia. Potential of hydrogen-ammonia mixture is evaluated for combustion in a premixed burner by Li et al. [51]. Burning velocity, Markstein number, and NO_x emissions are measured as functions of equivalence ratio and H_2 mixture fraction supporting the potential of NH_3-H_2 as a promising fuel mixture with moderate burning velocities and reasonable NO_x emissions (1100-1700 ppm). Um et al. have evaluated the effects of ammonia substitution on non-premixed H_2-air flames regarding extinction and NO_x emission [52]. The results support the potential of NH_3 as an effective green additive for improving the safety of H_2. By implementing a designed electronic fuel injection system, the performance of a twin-cylinder spark ignition engine was examined by Frigo and Gentili using ammonia and hydrogen as fuels [53]. Main focus was on the evaluation of the engine stability and exhaust pollutants. With the necessity of controlling hydrogen-ammonia ratio based on engine load, a general decrement in engine performance was reported with respect to the original gasoline version. The effect of hydrogen addition on the burning velocity and Markstein length of stoichiometric premixed NH_3-H_2-air flames at atmospheric and elevated pressures was reported by Ichikawa et al. [54]. NO_x emission and flame stability were investigated for ammonia substituted H_2-air flames with low ammonia mixture fractions in a study by Joo et al [55]. They reported a reduction in stability limits and an increase in absolute value of NO_x emission with NH_3 substitution. Furthermore, the extinction limits, flame temperature, and morphology of the counter flow non-premixed NH_3-H_2-air flames were determined at elevated temperatures and

under atmospheric pressure in a study by Choi et al. [56]. The results verify the potential of H_2 as an effective additive for improving the flame reactivity, and also the shrinkage of extinction limits with increasing flame strain rates.

Recent research have shown that using porous blocks is an advantageous and practical way to stabilize premixed flames [57–60]. Basically, the interest in porous medium based combustion has been directed by the needs of industry to develop high performance radiant heaters while complying with environmental concerns. Porous media have been widely used for flame stabilization of hydrocarbons. In a review by Howell et al. characteristics of the media as well as the mechanisms of interior combustion and heat transfer in the porous blocks are discussed in detail [59]. In a basic sense porous media enhance the heat, momentum, and mass transfer leading to an increase in the burning speed. This is specifically critical for better stabilization of the flames with high ammonia mixture fraction. With a chemically inert characteristic and a low thermal expansion coefficient compared to metal, SiC is a ceramic compound of silicon and carbon. It is one of the hardest known materials and generally considered to yield a higher flow rate as a function of pressure compared to other ceramic materials. In addition, the high thermal conductivity of SiC porous blocks elevates the heat conduction from the flame zone to pre and post flame zones which can accordingly decrease the thermal NO_x due to the lower peak temperature [61]. Alavandi et al. have experimentally demonstrated fuel flexibility of a two-section SiC porous burner by studying lean premixed combustion of hydrogen–syngas/methane fuel mixtures [62]. Heat recovery rates of hydrogen flame modes in porous medium combustion are studied by Su et al. using oxide-bonded silicon carbide and two other porous media to hold the flame [63]. Regarding the literature, the SiC porous media can be used in a wide range of applications including internal combustion engines, low calorific gas burners, volatile organic compound oxidizers, and radiation heaters [57].

CHAPTER 3

Combustion characteristics of ammonia-hydrogen-air mixtures: chemical kinetics study

3.1 Introduction

For effective combustion of ammonia as a fuel in practical applications, it is essential to have a profound understanding of the reaction mechanisms using detailed chemical kinetic models. In the first part of this study, we aim to theoretically investigate the combustion characteristics of NH_3/H_2/air mixtures at elevated pressures and under lean premixed conditions, which are commonly encountered in gas turbine combustors. The conditions are similar to the study by Strohle et al. [64], which focused on hydrogen combustion under gas turbine combustor conditions. For simulating the combustion characteristics, we use the detailed Konnov mechanism [27] which is proven to be one of the most reliable mechanisms for ammonia chemistry. No previous numerical study has investigated the autoignition process or the laminar flame speed sensitivity for NH_3/H_2/air mixtures under gas turbine conditions. The present study includes predictions for the ignition delay time, laminar flame speed, and related sensitivity coefficients. Also the main reaction pathways of ammonia oxidation and NO_x formation are identified. A main objective in this study is to develop reduced mechanisms applicable to the steady state conditions of practical combustion systems. Combustor design for high efficiency and minimal ammonia slip along with the minimum NO_x level of pollutants are the major objectives in the design of most engines (such as gas turbine system). For that reason, flame speed, ignition delay time, and NO_x emission selected to be the most dominant combustion properties to be addressed in this study. As major contribution of this study, two reduced reaction mechanisms are established based on Konnov mechanism to predict the flame speed and total NO_x emission under a wide range of combustion conditions. Comparing the results obtained by the reduced

mechanisms with those of Duynslaegher et al. [33] shows better consistency of our reduced mechanisms with the full mechanism and corresponding experimental data.

3.2 Materials and methods

In chemical kinetics simulations we assume laminar, one-dimensional, premixed, and freely propagating flames. The laminar premixed model in the Cosilab software [65] is used to calculate the flame speeds, species profiles, reaction rates, and sensitivity analyses. Although flames with these conditions rarely exist in reality, this assumption leads to a basic research tool meaningful to be investigated by removing the complexities which are not the target of this study. Also in simulating the autoignition process for predicting the ignition delay times, a homogeneous closed reactor model is implemented.

The Konnov mechanism [66] was previously used by Duynslaegher et al. [67] to study the combustion characteristics of near-stoichiometric ammonia–air mixtures at elevated pressure and temperature conditions. Proven to generate the most accurate results among some of the widely-used mechanisms for high ammonia content flames [34], in the present study we also use an updated version of the Konnov mechanism [27] to simulate the combustion properties of pure ammonia and NH_3/H_2 mixtures. The complete Konnov mechanism has over 85 species and 1200 reactions for C, H, N, and O elements. It has been used for a wide range of fuel mixtures, including NH_3, H_2, N_2O, NO, NO_2, and carbon containing species. However, in this study, all carbon containing species and associated reactions are eliminated due to the absence of carbon in the fuel mixture. The full Konnov carbon free mechanism includes 30 species and 240 reactions.

3.2.1 Combustion characteristics at high pressure lean conditions

Based on the typical operational conditions of combustors, the initial composition of the fuel mixture is calculated and listed in Table 3-1. As illustrated in the table we study

five major cases based on fuel composition. The NH_3 percentage, which is based on energy fraction of ammonia in the fuel mixture, is defined in Eq. (14).

$$\%E\ NH_3 = \frac{X_{NH_3} \times LHV_{NH_3}}{X_{NH_3} \times LHV_{NH_3} + X_{H_2} \times LHV_{H_2}} \times 100 \quad (14)$$

The overall chemical reaction used to calculate equivalence ratios is presented in Eq. (15).

$$xNH_3 + yH_2 + a_{stoi}(O_2 + 3.76\ N_2) \rightarrow b\ H_2O + c\ N_2 \quad (15)$$

Table 3 - 1 Mole fraction of initial fuel/air mixture with ϕ = 0.5.

% E NH_3	NH_3	H_2	O_2	N_2
100	0.1228	0	0.1843	0.6929
80	0.0958	0.0382	0.1819	0.6840
60	0.0701	0.0745	0.1797	0.6757
40	0.0456	0.1091	0.1776	0.6677
20	0.0223	0.1421	0.1755	0.6600

In the simulations we assume an adiabatic condition, since the heat loss is not noticeable especially for high ammonia content mixtures [34]. This is mainly due to the relatively low flame temperatures of high ammonia content flames. For laminar flame studies a freely propagating premixed flame in a lean NH_3/H_2/air mixture at 17 bars and an initial temperature of 400 °C is simulated for different mixture blends. The simulations have been performed in a computational domain of *x= 0-0.3* cm with a grid resolution about 1000 points, which is sufficient to produce grid-independent solutions. For sensitivity analysis of laminar flame speed, the impact of variations in the magnitude of the pre-exponential rate constant of reactions on the predicted flame speed is presented by the normalized sensitivity coefficient (S_i) for the ith reaction which is defined as Eq. (16).

$$S_i = (A_i/S_u) \times (\partial S_u/\partial A_i) \quad (16)$$

For determination of the ignition delay time two indicators are implemented; the maximum NH_2 mole fraction and the maximum temperature inflection criteria (dT/dt).

The effects of thermal diffusion and multicomponent diffusion are included, since they are important in hydrogen seeded mixtures.

3.2.2 Reduced mechanism establishment

In this study, the reduced mechanisms are obtained based on successive steps briefly illustrated in Figure 3-1.

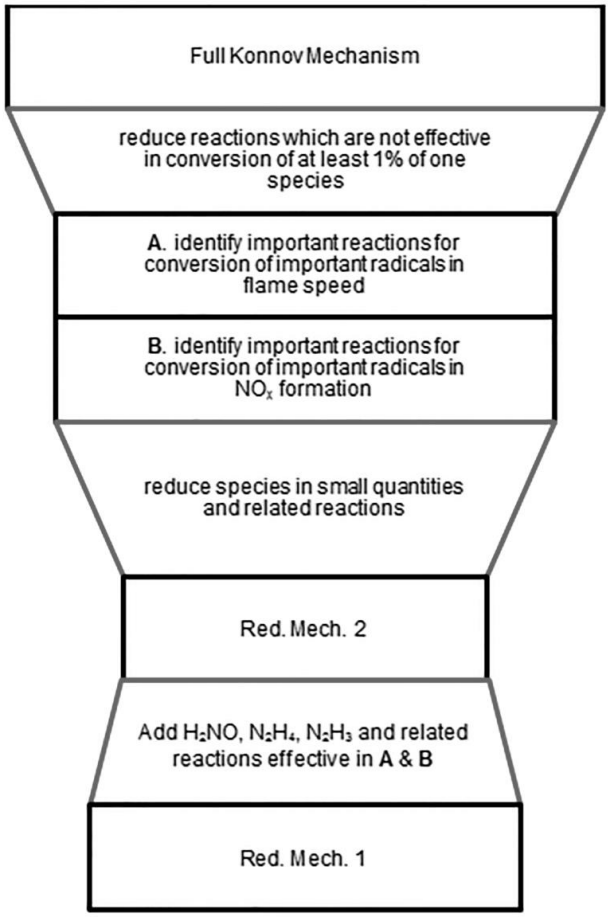

Figure 3-1 Obtaining reduced mechanisms from the full Konnov Mechanism.

As the first step, contribution rates calculation is performed under atmospheric and high pressure conditions. Based on the contribution rates calculation, only the reactions that contribute for at least 1 % in formation/decomposition of at least one species are kept and other reactions are eliminated.

Followed by that, formation/decomposition analyses for some of the key radicals in flame speed and emissions formation (i.e. NH_2, OH, O, H, NH, NO) are performed. As a result, the key reactions responsible for formation/decomposition of the radicals are revealed. As the next step, to further reduce the mechanism, the species in very small quantities (X<1E-8) and the corresponding reactions are removed. The species with small quantities are NO_3, N_2O_3, N_2O_4, H_2O_2, N_2H_3, N_2H_4, HNO_3, HNNO, HONO, HNOH, H_2NO, and NH_2OH. Based on the previous algorithm, the reaction mechanism # 2 with 18 species and 80 reactions is obtained. The major difference of the reduced mechanism with that obtained by Duynslaegher et al. [33] is the presence of reactions 105 ($N_2O+H\leftrightarrow NH+NO$), 61 ($NH+H_2\leftrightarrow NH_2+H$), and 142 ($HNO+NH\leftrightarrow NH_2+NO$) in our reduced mechanism. Due to the formation/decomposition analysis, the reaction 105 is one of the most influential reactions in the decomposition of NH and NO in the NH_3/H_2/air flames. The reaction 61 is one of the main contributors to NH_2 decomposition and NH formation. Also the reaction 142 has an important role in NH_2 formation.

We also obtained a more comprehensive reduced mechanism based on the formation/decomposition analysis. Due to the noticeable contribution of some reactions which include the species H_2NO, N_2H_4, and N_2H_3 in conversion of key radicals, we added the three species and the related reactions to the mechanism #2 to obtain mechanism #1. As a result the more comprehensive reaction mechanism #1 has 21 species and 91 reactions. The reduced mechanisms are provided in Appendix 3.

3.3 Results and Discussion

The results presented in subsections 3.3.1-3.3.5 correspond to the detailed kinetics investigation of ammonia flames under the high pressure lean conditions, while section 3.3.6 is comprised of the reduced mechanism predictions and performance analyses.

3.3.1 Laminar flame speed sensitivity analysis

Sensitivity analysis provides the first order sensitivity coefficient of the predicted flame speed with respect to variations in the magnitude of the pre-exponential rate constant. The sensitivity coefficients at 17 bar and 673 K for pure NH_3/air as well as 80%NH_3/20%H_2/air mixtures are shown in Figure 3-2. To make it clearly visible, only top 15 reactions with the highest sensitivities are illustrated.

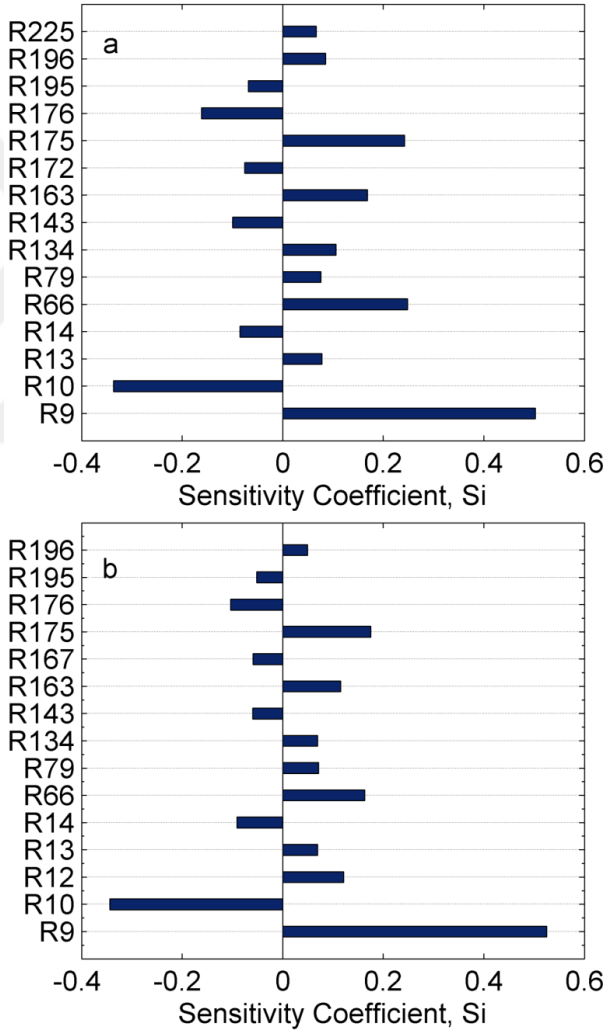

Figure 3-2 Sensitivity coefficient, S_i, of the most influential reactions to the laminar flame speed for (a) NH_3/air mixture and (b) 80%NH_3/20%H_2/air mixture at ϕ = 0.5, 17 bar, and 673 K.

It is observed that the reactions $H+O_2 \leftrightarrow OH+O$ and $H+O_2 \leftrightarrow HO_2$, which are presented as R9 and R10 respectively, have the highest sensitivity coefficients in terms of absolute

values. The reaction R9 has the largest impact on the laminar flame speed in both mixtures. In other words, more than any other reaction, an increase of the reaction rate of R9 will enhance flame speed. The sensitivity coefficient of R9 is higher in the 80%NH_3 case compared to the pure ammonia case. The sensitivity is further enhanced as the H_2 content in the mixture is increases, which is not shown here. On the other hand, reaction R10 is in the negative side of the sensitivity diagram for both mixtures which means that, by increasing the reaction rate of R10 the flame speed will decrease and this negative impact is larger than other reactions. The absolute value of the sensitivity coefficient gets larger by increasing the H_2 content of the mixture. Followed by these two most dominant reactions with positive and negative sensitivities, R66 and R175 also greatly enhance the flame speed. Some other reactions such as R163, R134, and R143 also have noticeable sensitivity coefficients. Considering them altogether, it is concluded that flame propagation is mainly controlled by competition of these few dominant reactions with positive/negative sensitivity coefficients. All the 240 reaction steps of Konnov mechanism with corresponding rate constants are demonstrated in Appendix 3.

3.3.2 Ammonia decomposition analysis

To further understand the contribution of specific radical species on the laminar flame speed, ammonia decomposition analysis is performed under the high pressure lean condition (ϕ=0.5, T=673K, P=17bar). The peak heat release point along the flame is chosen as the location for the analysis. The major reactions responsible for ammonia decomposition for three different fuel mixtures are presented in Table 3-2. Also the top 15 important reactions are demonstrated in Figure 3-3.

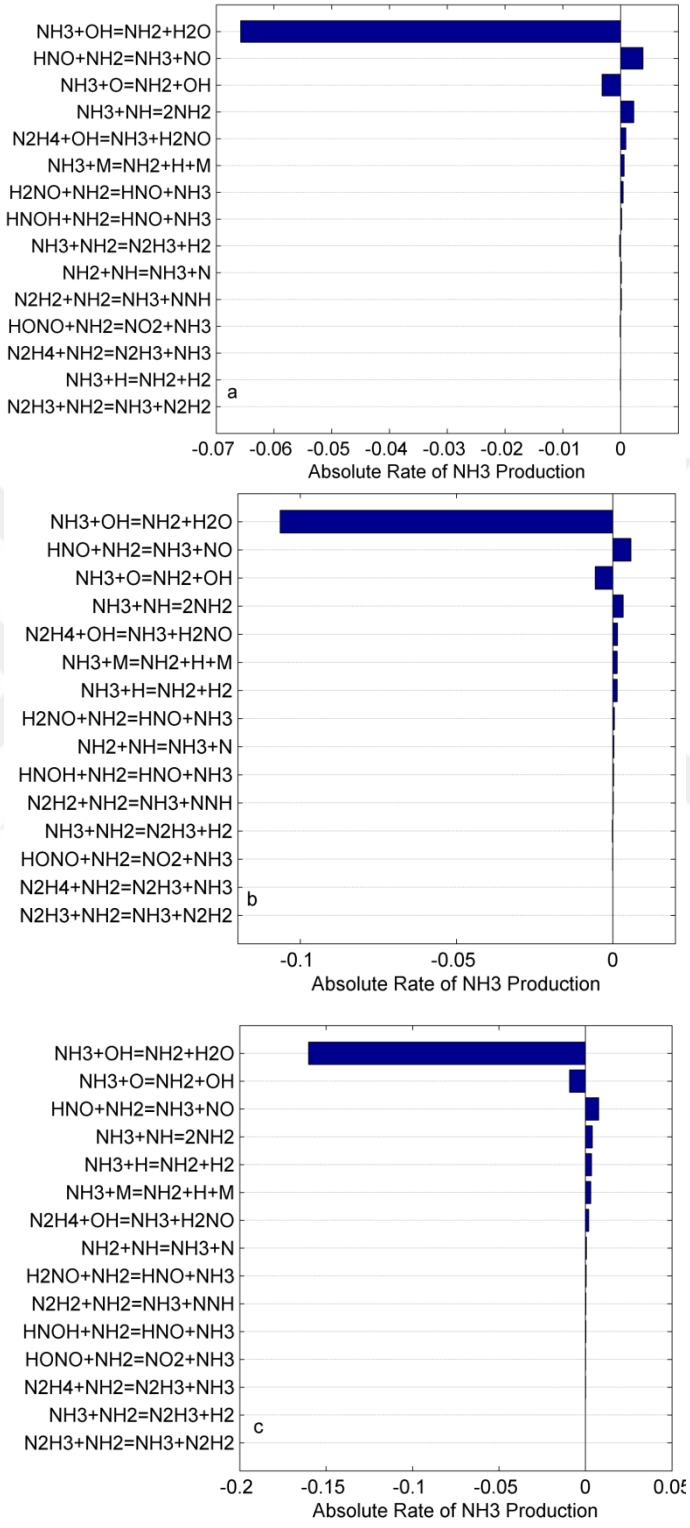

Figure 3-3 Contribution of reaction steps in molar conversion of NH_3 in (a) pure ammonia, (b) 80%NH_3 and (c) 60%NH_3 cases at ϕ=0.5, T=673 K, P=17 bar.

Table 3 - 2 Contribution percentage of major reaction pathways of NH_3 decomposition at ϕ=0.5, T=673 K, P=17 bar.

Fuel mixture	$NH_3+OH \leftrightarrow NH_2+H_2O$	$NH_3+O \leftrightarrow NH_2+OH$	$NH_3+NH_2 \leftrightarrow N_2H_3+H_2$
Pure NH_3	95%	4.64%	0.23%
80%NH_3	94.8%	5.04%	0.11%
60%NH_3	94.5%	5.45%	ignorable

Positive and negative values of the conversion rate in the Figure 3-3 mean that the species is formed and consumed by the reaction, respectively. The analysis shows that the most critical radical which impacts the ammonia decomposition and laminar flame speed, is OH. Reaction of this species with ammonia is responsible for more than 94% of ammonia decomposition in all the studied mixture blends. This is indeed a well-known fact and shows consistency with the study of Kumar et al. [34] who showed that the consumption of NH_3 in lean and stoichiometric premixed flames primarily occurs through reactions with OH, O, and H with higher contribution of OH in NH_3 decomposition and laminar flame speed. After OH, the radical O also has noticeable effect on ammonia decomposition showing roughly the same level of influence for all three mixtures. The significance of OH radical in ammonia decomposition is consistent with the fact that the higher flame speed in higher H_2 content mixtures corresponds to the larger accumulation of OH radicals near the flame front. This fact is shown in Figure 3-4 and Figure 3-5. It is observed that the H_2 addition has a tremendous influence on the flame speed.

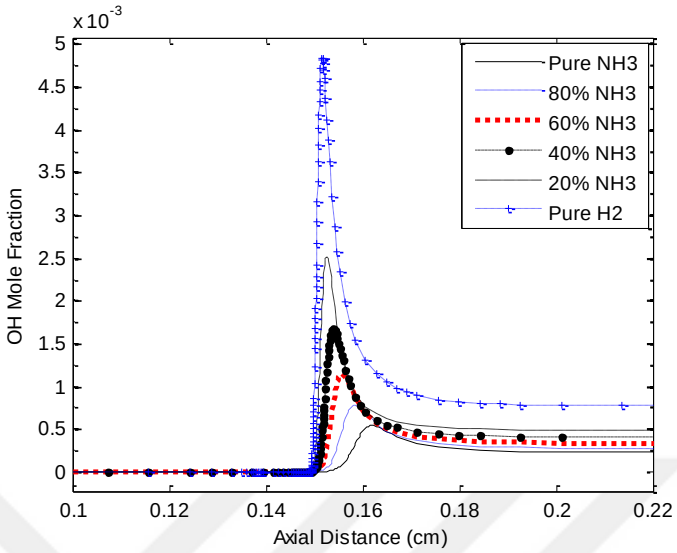

Figure 3-4 OH mole fraction near the flame front in different fuel mixtures, ϕ=0.5, T=673 K, P=17 bar.

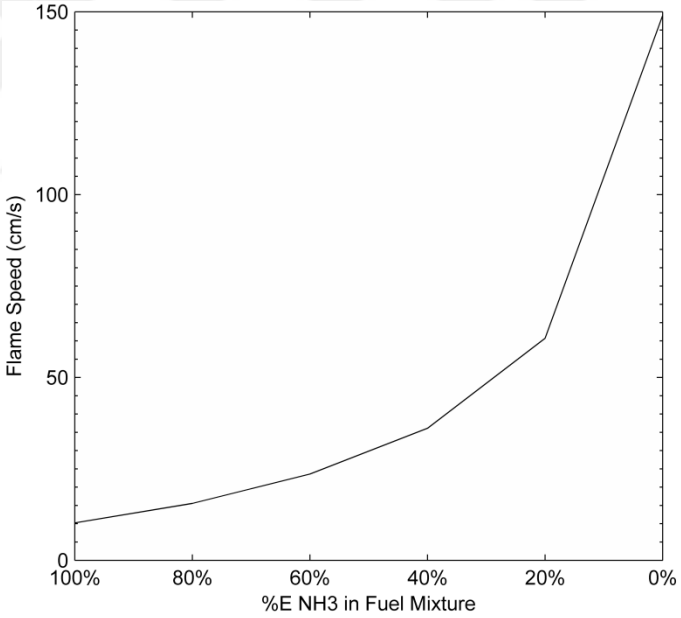

Figure 3-5 Laminar flame speed as a function of NH_3 fraction in the fuel mixture, ϕ=0.5, T=673 K, P=17 bar.

3.3.3 Autoignition

Autoignition time which is a critical kinetic parameter for gas turbines and ICEs is strongly affected by fuel composition. For investigating the combustion properties related to autoignition we consider fuel air mixtures at 17 bar and an equivalence ratio

of 0.5. For simulations a homogenous reactor model is used. At an initial temperature of 400 °C, the calculated ignition delay time is greater than 100 s, which is obviously too long to be applicable for gas turbine combustors. However, in real life applications, the reactants are heated by the recirculated hot combustion product gases. Hence ignition would actually take place at temperatures higher than that of the unburned fuel/air mixture. The computed mole fraction profiles of the most influential radicals for the pure ammonia case at 17 bar and 1300 K are presented in Figure 3-6.

Considering the mole fraction values in Figure 3-6a, ignition process seems to be dominated by the OH, NH_2, O, and H radicals. The concentration of other radicals is negligible compared to these species. The same figure in a larger scale focusing on the radicals with relatively low concentrations close to the ignition time (3.8E-04 s) is illustrated in Figure 3-6b.

As demonstrated in the figure, there is a noticeable accumulation of some radicals such as N_2H_2 which peak prior to the ignition time and rapidly decrease during the ignition. N_2H_2 is mainly produced by the contribution of NH_2 radicals through R66 and R63 and quickly destroyed by R79 close to the ignition time. The N_2H_4 and H_2NO radicals show the same behavior however in relatively lower concentrations. In the case of 80%NH_3 as shown in the Figure 3-7, ignition is dominated by OH, NH_2, O, and H radicals, similar to the pure ammonia case.

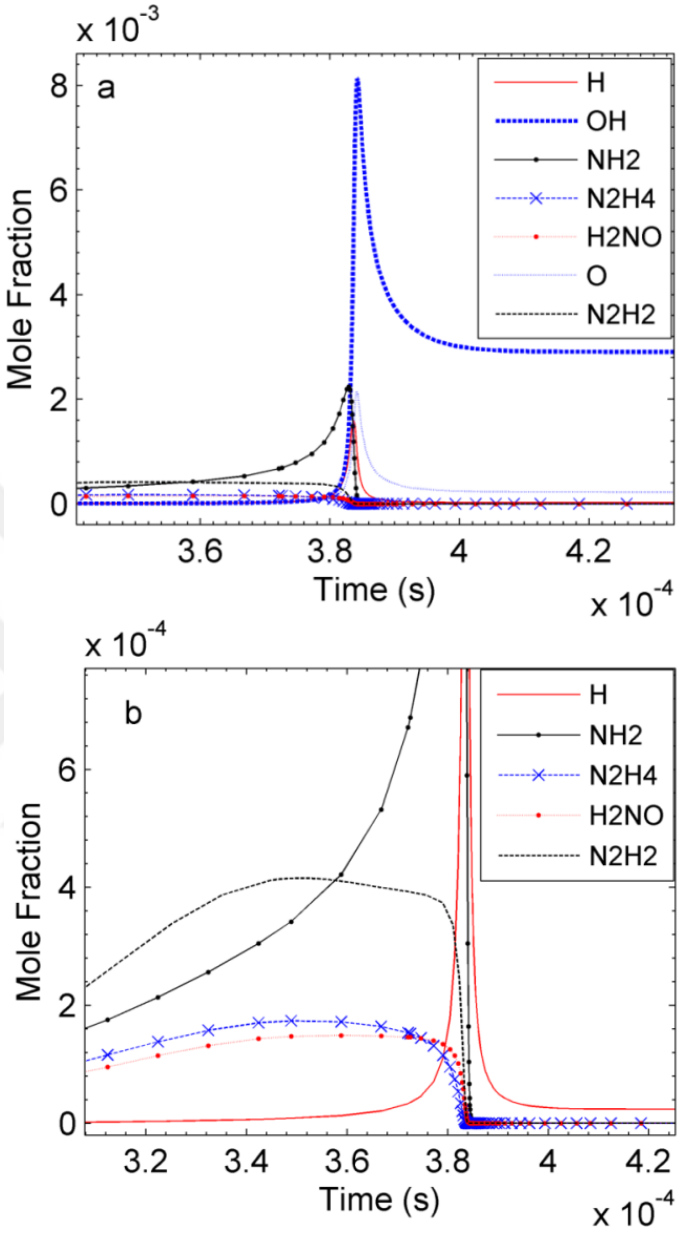

Figure 3-6 Mole fraction of radicals as a function of time in pure NH3 case, ϕ=0.5, T=1300 K, P=17 bar, depicted in (a) normal view, (b) larger scale view focusing on the radicals' profiles close to the ignition time.

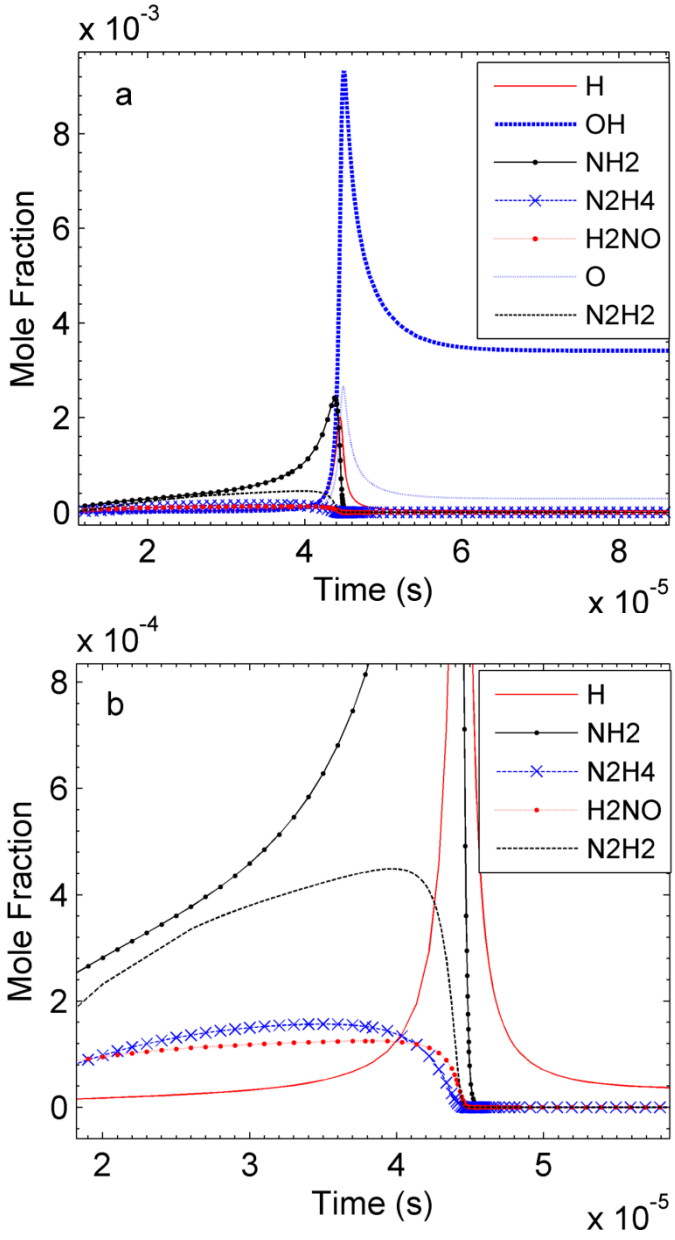

Figure 3-7 Mole fraction of radicals as a function of time in 80%NH3 case, ϕ=0.5, T=1300 K, P=17 bar, depicted in (a) normal view, (b) Larger scale view focusing on the radicals' profiles close to the ignition time.

Similar to the pure ammonia case we can see accumulation and local maximum concentration for N_2H_2, N_2H_4, and H_2NO. Similar trend is obtained for other mixture compositions with some differences in mole fraction levels.

The investigation shows that under the studied conditions (17 bar, ϕ=0.5 and 1300K), the species OH and NH_2 are generally the radicals with the highest concentrations in

pure ammonia and 80% NH_3 cases followed by the H radical. In the case of 60% NH_3 the H radical concentration exceeds that of NH_2. This is in complete agreement with the ammonia decomposition sensitivity and flame speed analysis as discussed in previous section. Also, the accumulation of the radical pools prior to ignition seems to have an important role in the ignition initiation.

Other than the fuel composition, autoignition is highly dependent on the initial temperature. Figure 3-8 demonstrates the ignition delay time as a function of 1000/T.

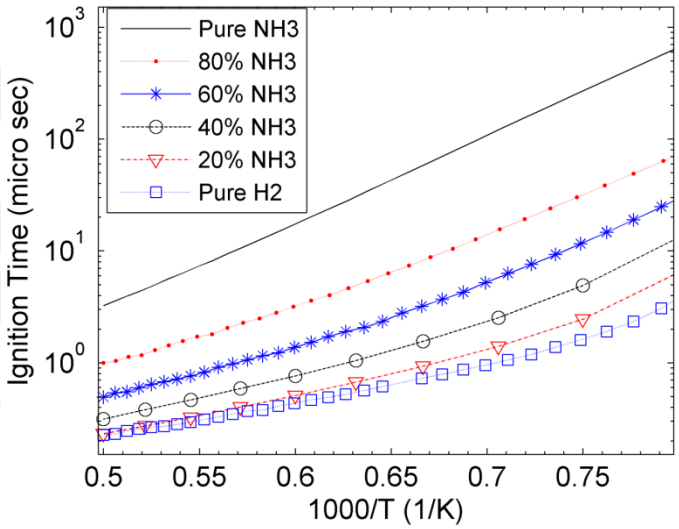

Figure 3-8 Ignition delay time as a function of the inverse temperature 1000/T for different mixture compositions, ϕ=0.5, P=17 bar.

As expected, ignition time decreases as the mixture temperature increases. Also there is a noticeable decline in ignition time by increasing the fraction of H_2 in the fuel mixture. The increase of hydrogen molecules in the fuel composition reduces the overall resistance of the fuel mixture to the autoignition because of the lower autoignition temperature of hydrogen compared to that of ammonia (500 °C for H_2 versus 651 °C for NH_3).

3.3.4 NOx formation

Nox Production Analysis

As one of the most important challenges in ammonia combustion, NO_x production analysis is performed to further understand the impact of certain reactions on NO_x formation. Since the concentration of NO_2 in the studied conditions is negligible compared to that of NO (*<1/100 [NO]*), the formation sensitivity analysis is performed only for NO which has the dominant contribution in NO_x level. The NO formation/decomposition rate, i.e. *dn/dt*, for each involved reaction is integrated over the entire domain. The contribution of the most important reactions in the formation/decomposition of NO for pure ammonia and 80% NH_3 cases are shown in Figure 3-9.

As shown in the figure, the main reactions contributing to the NO formation are R134 (*H+NO↔HNO*), R122 (*NO_2+H↔NO+OH*), R136 (*HNO+OH↔NO+H_2O*) and R143 (*HNO+NH_2↔NH_3+NO*) while the main reaction pathways leading in NO decomposition are R176 (*NH_2+NO↔N_2+H_2O*), R175 (*NH_2+NO↔NNH+OH*), and R123 (*NO_2+OH↔HO_2+NO*). These reactions are the major contributors in NO conversion in all three mixtures with different level of significance. A quantitative summary of main reactions along with their contribution fractions in NO formation is presented in Table 3-3 for three studied mixtures. Also the total NO_x mole fraction as a function of NH_3 content in the fuel mixture is plotted in Figure 3-10.

Table 3 - 3 Contribution percentage of the main reactions in NO formation dn/dt (mol/s), ϕ=0.5.

Formation	H+NO↔HNO	NO_2+H↔NO+OH	HNO+OH↔NO+H_2O	HNO+NH_2↔NH_3+NO
Pure NH_3	18.96	16.97	14.58	14.10
80% NH_3	14.27	22.14	15.61	11.49
60% NH_3	9.46	28.04	16.32	8.67

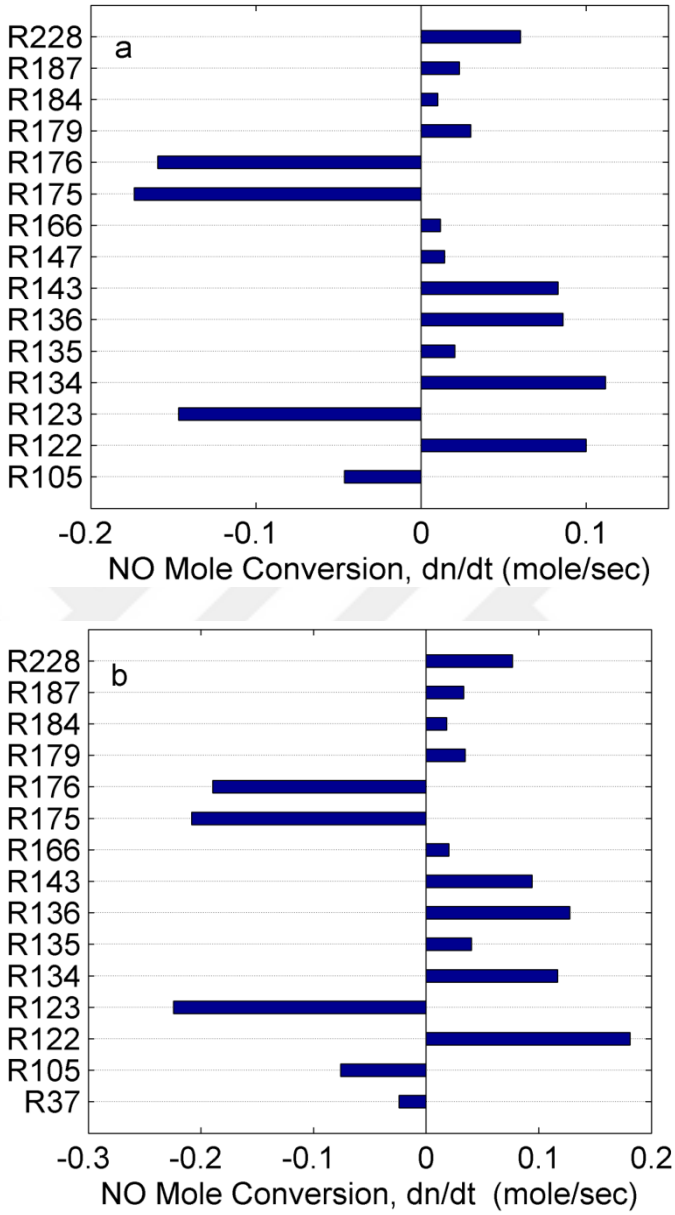

Figure 3-9 Contribution of each reaction to the NO molar conversion *dn/dt* for (a) pure NH_3 and (b) 80%NH_3 cases at ϕ=0.5, T=673 K

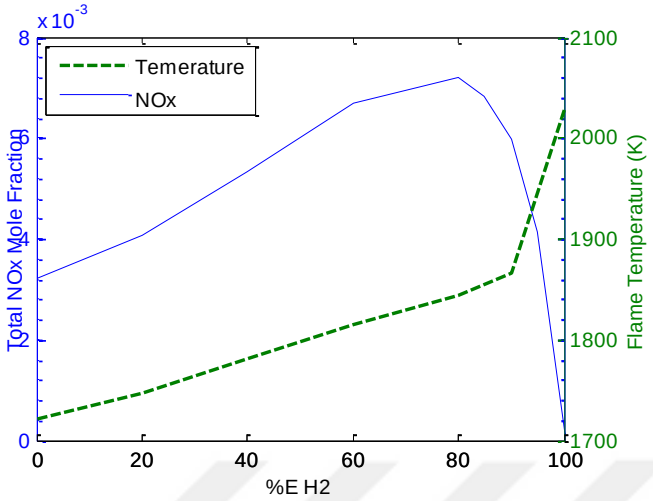

Figure 3-10 Total NO_x mole fraction as a function of NH_3 content in the fuel mixture, ϕ=0.5.

It is observed that as hydrogen content in the fuel mixture is increased up to 80%, the NO_x formation level increases as well. In this case in which the inlet temperature of the mixture is constant (400 °C), flame temperature increases with increasing hydrogen content of the mixture. Also in order to examine the contribution of thermal NO_x in the total NO_x emission we consider another case in which the flame temperature is held fixed (Figure 3-11(a)). A comparison of NO_x production level in two different cases, 1) constant inlet temperature and 2) constant flame temperature of 1725 K (pure ammonia flame temperature), is presented in Figure 3-11(a).

When keeping the flame temperature constant, an interesting phenomenon takes place. Based on the general understanding of fuel bond versus thermal NO_x production, one would expect a decrease in the total NO_x production with decreasing NH_3 concentration in the fuel under the assumption of constant flame temperature. However, as shown in Figure 3-11(a), the total NO_x emission keeps increasing with increasing mixture hydrogen fraction up to a very high hydrogen concentration level over which the NO_x concentration rapidly drops to its pure hydrogen level.

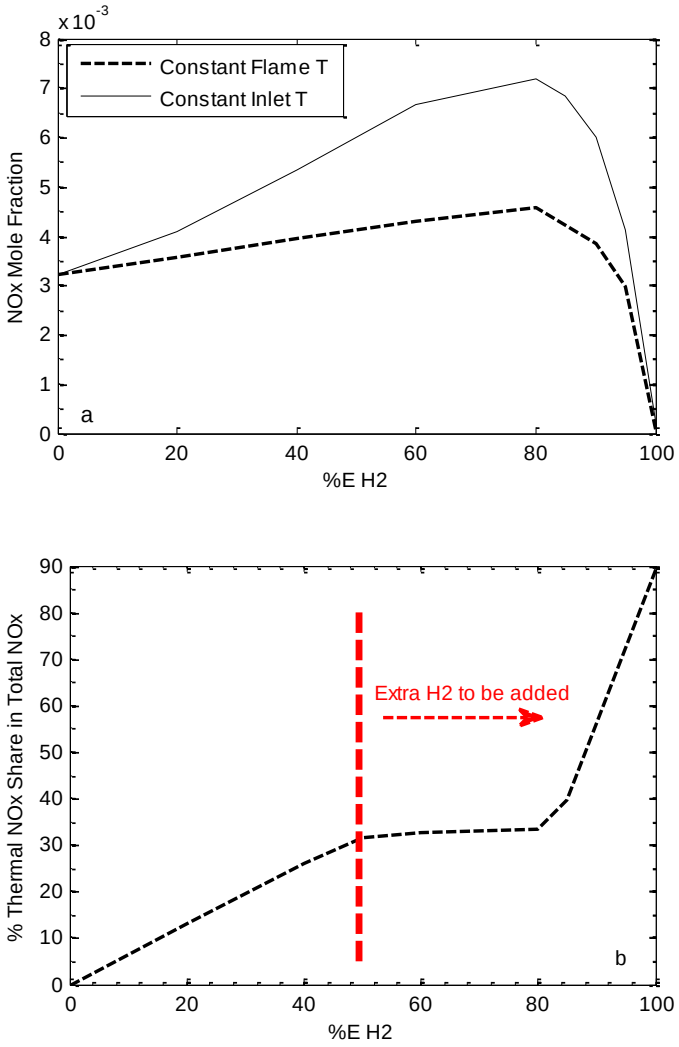

Figure 3-11 (a) NO_x emission levels with constant inlet temperature and constant flame temperature; (b) Percentage of thermal NO_x share in the total NO_x production as function of mixture hydrogen fraction, ϕ=0.5.

A careful investigation of the rate of production of NO_x for various mixture compositions revealed that H, OH, and HNO radicals play an important role in this increasing behavior. The rate of production analysis shows that the reactions $NO_2+H \leftrightarrow NO+OH$, $HNO+H \leftrightarrow NO+H_2$ and $HNO+OH \leftrightarrow NO+H_2O$ are the most influential steps in NO production. It has been determined that with increasing hydrogen content in the fuel, the rate of production of NO by these reactions increases noticeably. Namely an increase in the accumulation of the hydrogen and hydroxyl radicals close to the flame front is the primary culprit for the observed trend. Note that nitroxyl is also

available (mainly by the precursor conversion $NH_2 \rightarrow HNO$) to participate in the reactions leading to NO production. The contribution of the fore mentioned reactions in the production of NO keeps increasing until a point (for instance, about 90%E H_2 when ϕ=0.5) for which the concentration of fuel bond N (free nitrogen) is too low to directly affect the rate of the reactions. Therefore for cases with very high hydrogen concentration in the fuel, a very low rate of NO production by the stated reactions has been observed. This overall trend applies for a wide range of equivalence ratios.

By using the data presented and discussed in the previous figure, one can differentiate the effect of thermal NO_x and calculate its contribution in the total NO_x emission. For this purpose, the constant flame temperature curve has been subtracted from the constant inlet temperature curve and plotted in Figure 3-11(b) after normalization with the total NO_x formation based on constant inlet temperature. The contribution of thermal NO_x is presenting a growing trend with increasing hydrogen content. As expected, the overall increase is mainly due to the increasing flame temperature with increasing hydrogen content of the mixture. Also, it manifests a high increase rate in the hydrogen enriched zone, where ammonia and fuel bond nitrogen is rare and therefore thermal NO_x is the dominant mechanism.

Effect of unburnt mixture temperature variation

Figure 3-12 shows the effect of the initial mixture temperature on the total NO_x mole fraction for different fuel mixture compositions. The total NO_x level increases as the unburnt mixture temperature rises. The slope of NO_x level increment for the pure hydrogen case is lower than that of the ammonia seeded mixtures. In addition, the amount of change in the flame temperature at the studied mixture temperature interval is almost equal for all the mixtures (about 140 K increase in flame T for unburnt gas T from 600 K to 765 K). Therefore the increasing trend of NO_x cannot be solely due to the increase in thermal NO_x. Also, it is observed that the increase in the fuel mixture hydrogen fraction up to 80% causes an increase in the NO_x level. However, by further

increasing the H_2 fraction the NO_x level plummeted. This is completely consistent with Figure 3-11.

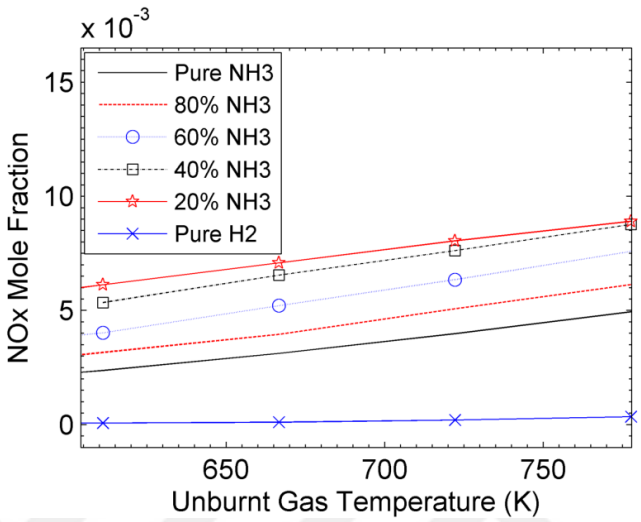

Figure 3-12 Total NO_x mole fraction as function of the unburnt gas temperature, P=17 bar, ϕ=0.5.

3.3.5 Effect of equivalence ratio variation

Effect of the equivalence ratio variation on the total NO_x formation is illustrated in Figure 3-13.

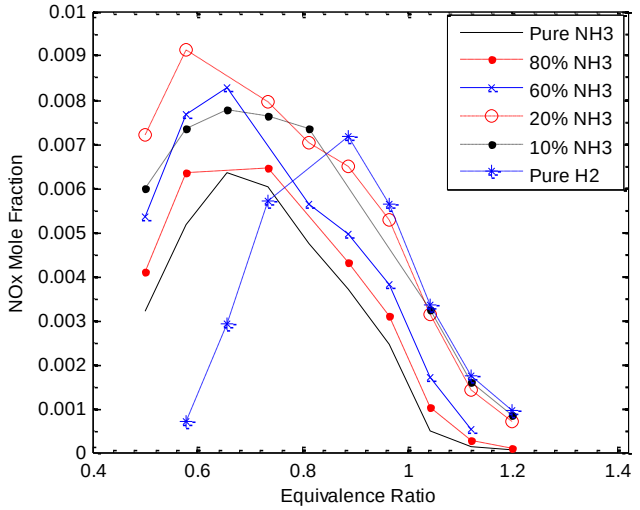

Figure 3-13 Total NO_x mole fraction as function of equivalence ratio, P=17 bar, T=673 K.

As shown in the figure, for all ammonia seeded flames the total NO_x formation in the fuel rich region is noticeably lower than it is in the lean region. For example, the NO_x mole fraction for ϕ = 1.1 is about an order of magnitude lower compared to that for ϕ = 0.5. This means a noticeable reduction in NO_x emission in engine applications by operating under local rich conditions. However, in engine applications, the compromise might be higher NH_3 slip level under the rich conditions which should be examined experimentally. As another important aspect, it is observed that when it comes to NO_x formation, H_2 is not always better than NH_3 under the studied conditions. It is just much better under lean conditions. In fact NH_3 seeded mixtures show better results for rich combustion.

To further understand the increasing/decreasing trend of NO_x with respect to the equivalence ratio, we analyze two different effects. As the first effect, increasing the equivalence ratio up to a certain level (~1-1.1 for studied cases) leads to an increase in the adiabatic flame temperature (Figure 3-14). As expected, the increased temperature causes higher thermal NO_x formation and therefore higher NO_x mole fraction. On the other hand, there is a second effect which is based on fuel NO formation behavior. The fuel NO in the ammonia seeded flames is mainly formed by the reaction of nitrogenous radicals with oxygenated species through Eq. (17).

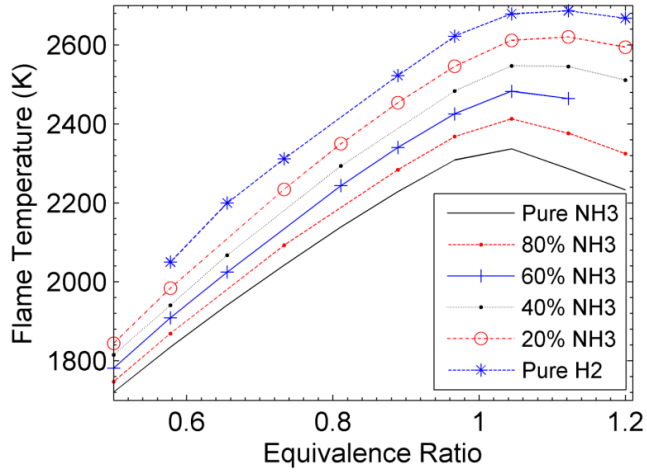

Figure 3-14 Flame temperature as function of equivalence ratio, P=17 bar.

$$NH_i + OX \rightarrow NO + H_iX \quad (17)$$

It implies that the NO formation can be reduced by reducing the oxygen available to participate in reaction Eq. (17). By increasing the equivalence ratio, the ratio of the oxygen to fuel decreases. Therefore, as a simple statement of the second effect, increasing the equivalence ratio leads to a decline in the fuel NO formation and thus reduction in the total NO_x formation. As a result, the increasing/decreasing trend of the total NO_x formation, which is shown in the Figure 3-13, is mainly controlled by the competition between the two stated effects. Also the figure shows that the influence of the both effects varies in different mixture compositions. For example, in the pure ammonia case the first effect is the dominant effect in the range $0.5 < \phi < 0.65$, while the second effect dominates for $\phi > 0.6$.

It is observed that the equivalence ratio is a critical parameter which strongly influences the NO_x formation. This implies that in engine applications flame stoichiometry should be well controlled to minimize the exhaust NO_x emission. Although the lean premixed combustion design is considered an effective way to reduce the combustion temperature, thereby the thermal NO_x formation, in gas turbines, it does not alleviate the fuel NO_x formation. Therefore in the case of ammonia doped flames the NO_x formation level is still noticeable. For practical applications there is need to reduce the NO_x level to meet the standards. As a numerical result obtained in the previous section, it seems that the total NO_x formation would noticeably decrease by having the combustion under fuel rich conditions. Also the challenging NO_x reduction task can be achieved by well-known methods such as treatment of exhaust gases or design modifications which are not in the scope of the present study.

3.3.6 Reduced mechanism

To model NH_3 combustion in an actual combustor by conducting CFD simulations, a reduced mechanism is required to predict the chemical kinetics properties with an acceptable accuracy and significantly reduced CPU requirement. For simulating

practical combustion cases, usually a reduction of species and reactions to less than 20 species and 100 reactions is needed.

Duynslaegher et al. [33] has developed a reduced chemical mechanism for ammonia combustion which has been established based on the Konnov mechanism. However, by comparing the results of NO_x formation and flame speed prediction with the results of full mechanism, noticeable discrepancies are observed which lead to inaccurate prediction for the NO_x formation and the flame speed. Therefore, there still exists the need for a reduced mechanism capable of producing more reliable results for ammonia chemistry in a wide range of conditions.

Validation of reduced mechanism

Flame speed and NO_x formation simulations

To check the validity of reduced mechanisms under different conditions, we compare the results with reference results obtained by the full mechanism and experiments. As the experimental reference data, we use the flame propagation speed measurements by Van Wonterghem et al. [24] and Duynslaegher et al. [23]. They measured the flame speed for various mixtures of $NH_3/O_2/N_2$ at atmospheric pressure condition with several N_2 dilution levels ranging from 0% N_2 to 35% N_2 for Van Wonterghem et al. measurements and from 35%N_2 up to 62% N_2 for the experiments by Duynslaegher et al.. The mixture compositions used in the experiments are presented in Table 3-4.

Results of flame speed variation with respect to the dilution level are shown in Figure 3-15. It includes the experimental data and the corresponding predictions by the reduced mechanisms.

Table 3-4 Mixture compositions of flame speed measurements, STP.

N_2 Dilution (%)	0	5	10	15	20	25	30
X_{NH3}	0.571	0.543	0.514	0.486	0.457	0.429	0.400
X_{O2}	0.429	0.407	0.386	0.364	0.343	0.321	0.300
X_{N2}	0.000	0.050	0.100	0.150	0.200	0.250	0.300
N_2 Dilution (%)	35	40	45	50	55	60	61.7
X_{NH3}	0.371	0.343	0.314	0.286	0.257	0.229	0.219
X_{O2}	0.279	0.257	0.236	0.214	0.193	0.171	0.164
X_{N2}	0.350	0.400	0.450	0.500	0.550	0.600	0.617

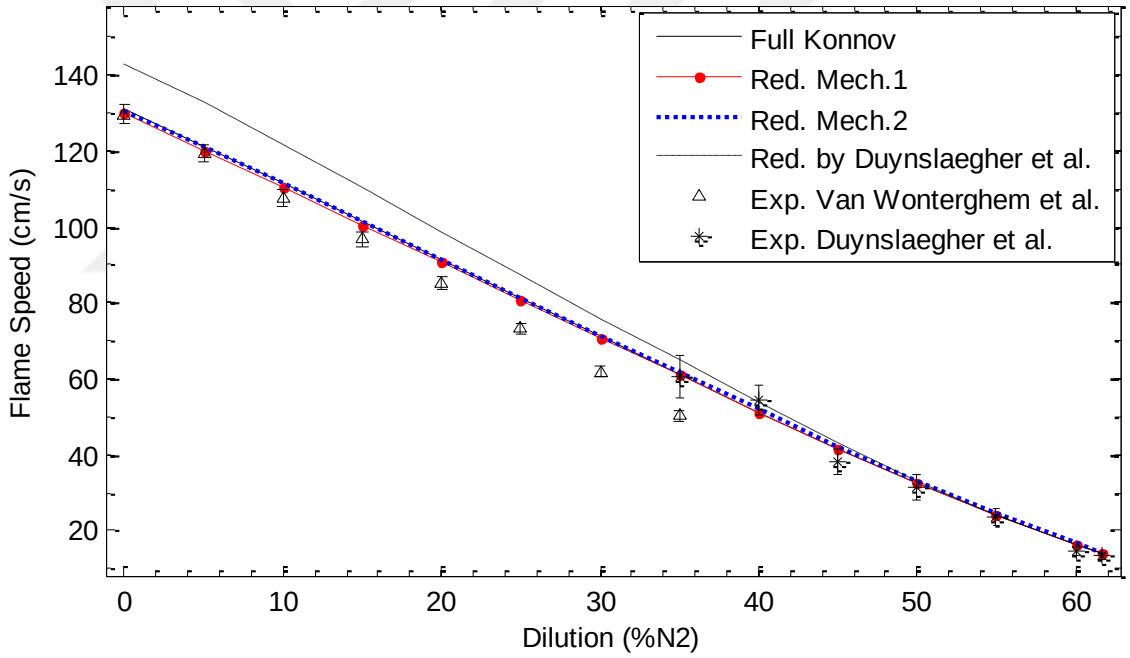

Figure 3-15 Flame speed variation with respect to dilution level; STP condition.

As expected, all the experimental data and numerical predictions show a decrease in flame speed with an increase in the dilution level. Despite the general agreement of the simulation trends with the experimental data, noticeable discrepancy is observed for the reduced mechanism of Duynslaegher et al. for lower dilution levels. To have a better insight into the accuracy of the reduced mechanisms, the deviation of predictions in the

Figure 3-15 is shown as percentage error with respect to the experimental data in Table 3-5.

Table 3-5 Deviation percentage of numerical predictions from the experimental data;STP condition.

	% N_2	**Konnov**	**Red. Mech.1**	**Red. Mech.2**	**Red. By**
Experiments of Van Wonterghem et al.	0	1.2	0.4	0.8	10.3
	5	1.5	0.6	1.3	11.2
	10	3.6	2.9	3.5	13.1
	15	4.7	3.8	4.8	13.8
	20	7.1	6.3	7.1	15.6
	25	11.3	10.0	10.7	19.2
	30	15.1	14.7	15.2	22.8
Experiments of Duynslaegher etal.	35	1.4	1.1	1.9	7.9
	40	5.9	6.0	4.5	1.4
	45	9.5	9.1	10.5	12.6
	50	3.8	3.6	5.8	4.7
	55	1.9	1.2	3.6	3.1
	60	12.1	14.0	15.5	12.8
	61.7	3.9	5.6	7.8	5.6

It is observed that both of the reduced mechanisms recommended in the present study provide better accuracy than the other reduced mechanism. This is more pronounced in lower dilution levels where the reduced mechanism of Duynslaegher et al. fails to predict the flame speed in an acceptable precision.

To further evaluate the performance of the reduced mechanisms, we aim to predict the laminar flame speed and NO_x formation level under high pressure conditions. For this aim we choose 17 bar and 10 bar pressures as target conditions and we compare the results obtained by the reduced mechanisms with the predictions of the full Konnov mechanism which are considered as the reference data.

The detailed comparison of predictions by reduced mechanisms at 17 bars is presented in the following figures. It is notable that only some of the cases are depicted in the following figures as the sample illustrations, while the detailed quantitative results will be presented later in Table 3-6. Figures 3-16 and 3-17 demonstrate the total NO_x prediction as function of equivalence ratio and ammonia content, respectively. Only the cases with equivalence ratios of 1 and 1.8 and ammonia contents of 80% and 60% are presented.

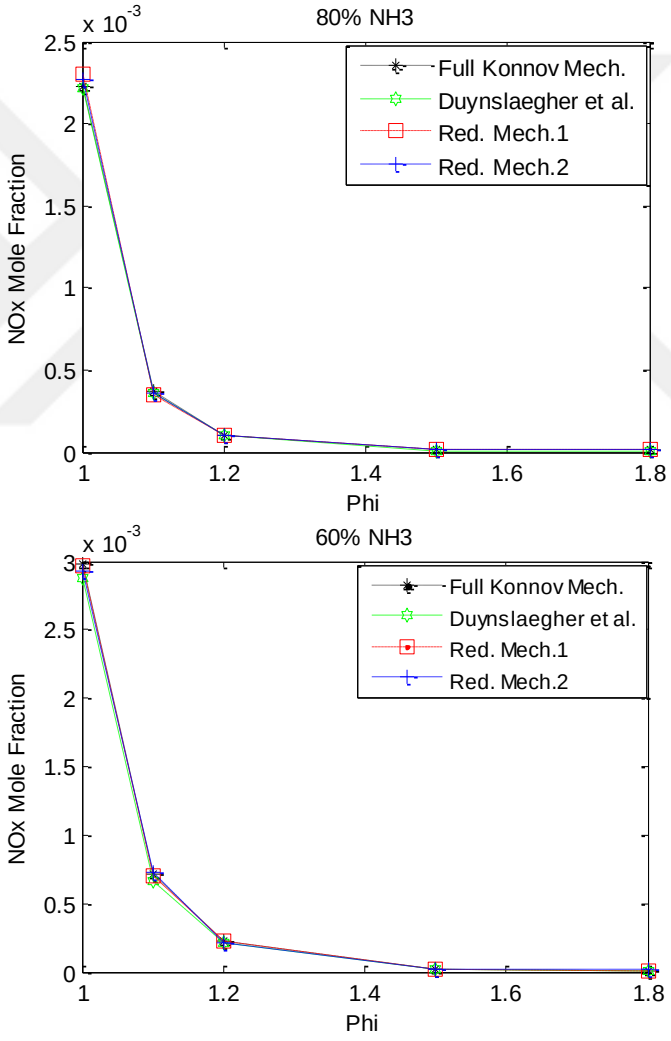

Figure 3-16 NO_x mole fraction as function of equivalence ratio, P=17 bar.

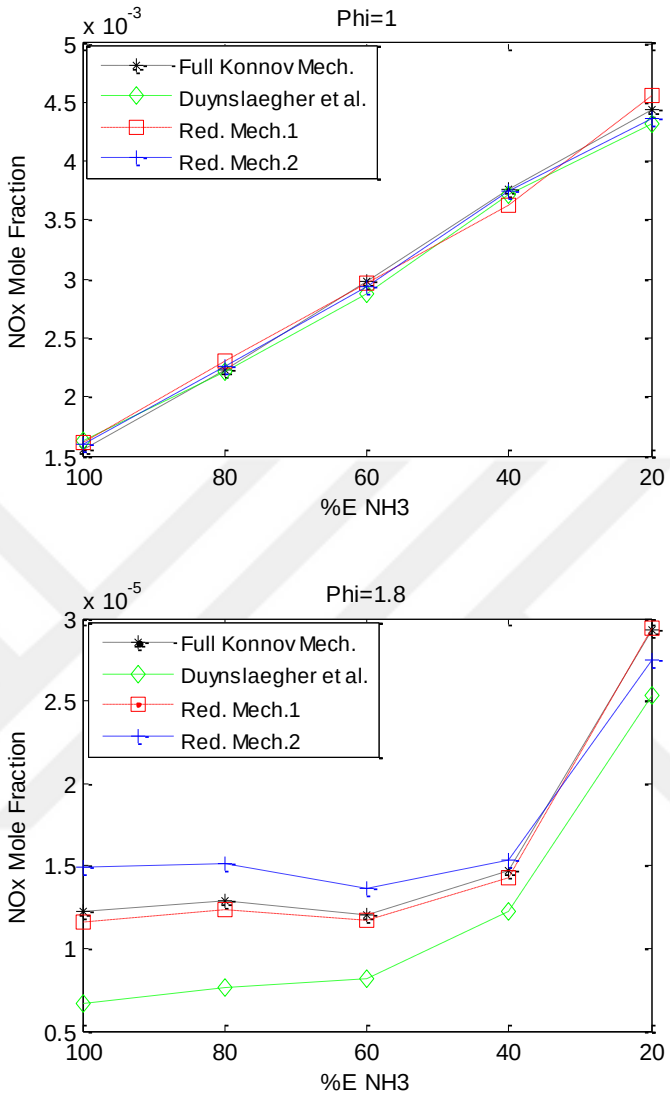

Figure 3-17 NO_x mole fraction as function of ammonia content, P=17 bar.

The NO_x prediction results show an overall agreement of reduced mechanisms with the full mechanism. However, as will be presented in Table 3-6, with equivalence ratio approaching the richest conditions, discrepancies are observed for the Duynslaegher et al. reduced mechanism. This is also the case to a lesser degree for the reduced mechanism # 2 for $\phi=1.8$. It is notable that the reduced mechanism # 1 shows to be consistent with the Konnov mechanism in the whole range of ammonia content. The flame speed values as function of equivalence ratio and ammonia content are presented in Figure 3-18 and 3-19, respectively.

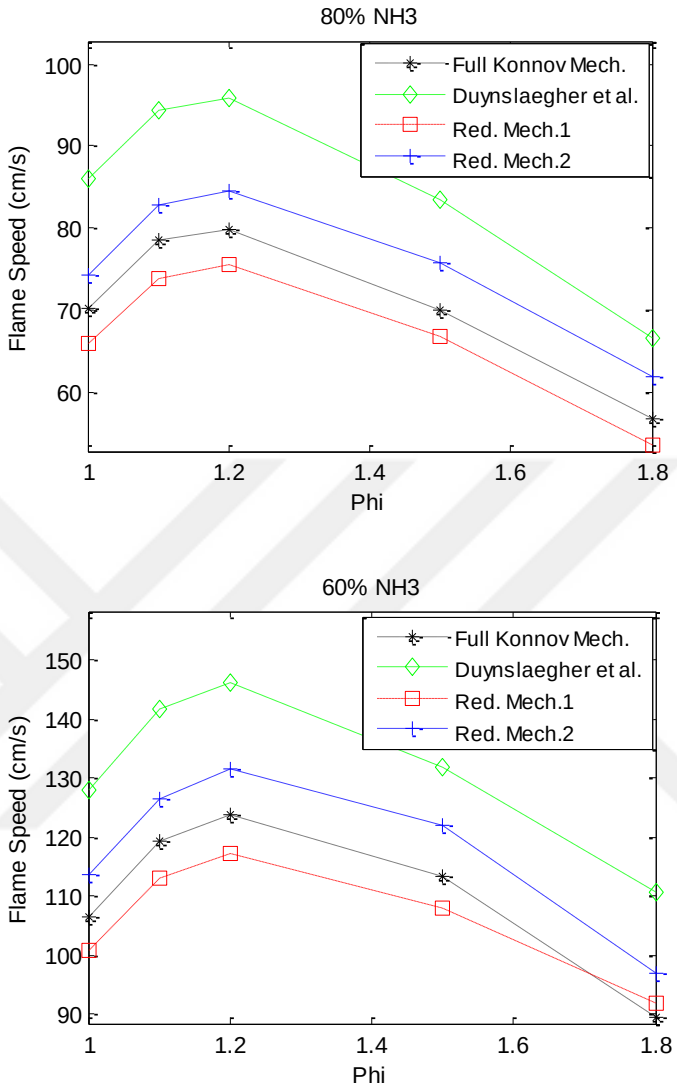

Figure 3-18 Flame speed as function of equivalence ratio, P=17 bar.

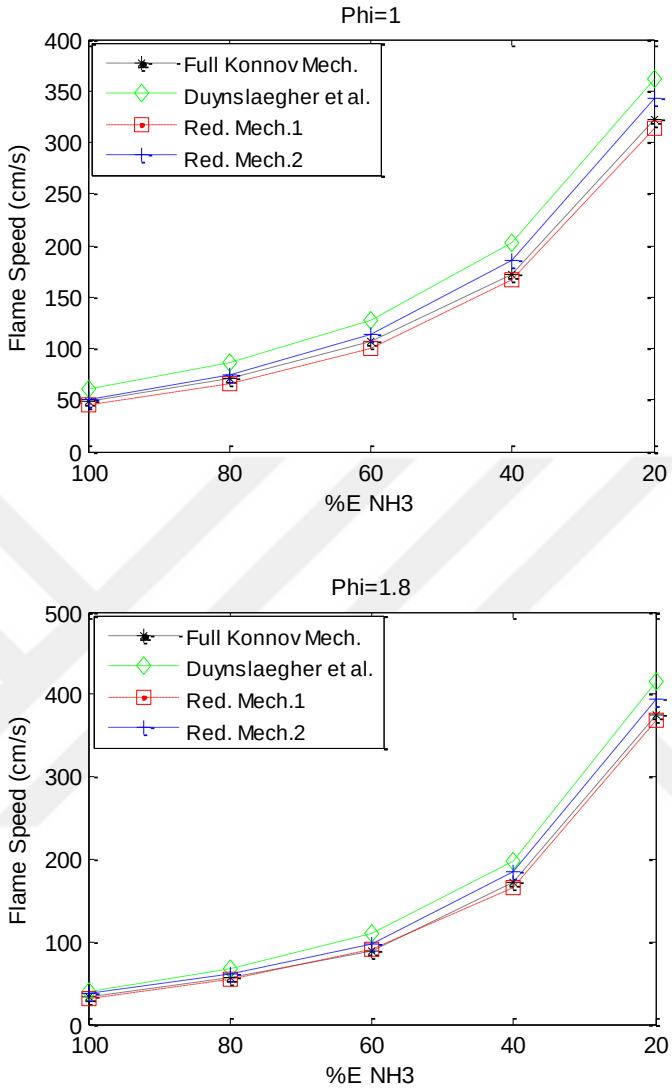

Figure 3-19 Flame speed as function of ammonia content, P=17 bar.

The better consistency of predictions by reduced mechanisms # 1 & 2 compared to that of Duynslaegher et al. is noticeable in the figures.

By averaging the difference of predictions of reduced mechanism with the Konnov mechanism for different fuel mixture compositions, average error for each equivalence ratios is obtained and presented in Table 3-6 for flame speed and NO_x formation cases.

Table 3-6 Average flame speed/NO_x formation prediction error (%), P=17 bar.

	FlameSpeed			**NO_xFormation**		
ϕ	Red. Mech.	Red. Mech.	Duynslaegher	Red. Mech. 1	Red. Mech. 2	Duynslaegher
0.5	8.4	5.6	30	7.5	5.6	10.6
1	4.8	6	19.6	2.8	1.8	2.5
1.1	4.9	5.9	18.3	5	2.8	5.5
1.2	4.6	6	19.4	3	2.7	2.8
1.5	4.4	6.7	18.3	3.2	4.5	10
1.8	4.2	7.7	16.8	3.2	12.8	29.7

The table shows the discrepancies of laminar flame speed and NO_x formation predictions with respect to the Konnov mechanism results. The results which are obtained for a wide range of equivalence ratios reveal the better agreement of reduced mechanism #1 and #2 compared to that of Duynslaegher et al. in most cases. Also, based on the NO_x formation results presented in the table, it is deduced that both reduced mechanisms almost always produce more reliable results. In terms of the NO_x formation prediction, the reduced mechanism of Duynslaegher et al. performs well under near stoichiometric conditions, however does not predict as well under very lean/very rich conditions. Also the reduced mechanism # 2 is not as accurate as mechanism #1 for very rich conditions.

Similar study is performed for the 10 bar pressure condition and the previous trends apply in this case as well. Figures 3-20 and 3-21 demonstrate the flame speed and total NO_x prediction with respect to the ammonia content and equivalence ratio, respectively.

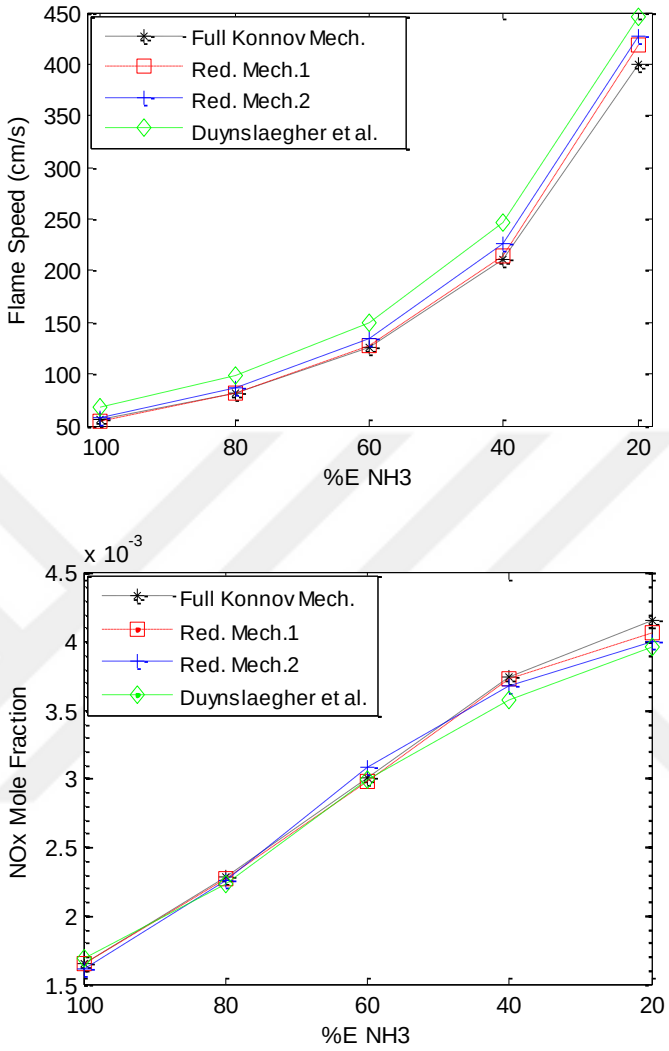

Figure 3-20 Flame speed and NO_x mole fraction as function of ammonia content at ϕ=1; P=10 bar.

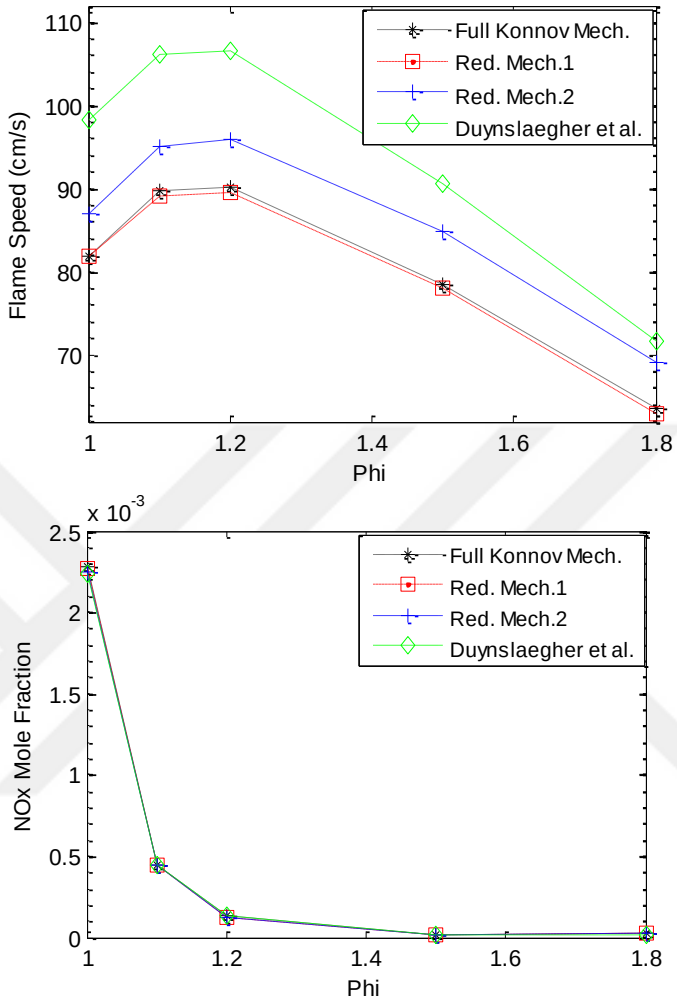

Figure 3-21 Flame speed and NO_x mole fraction as function of equivalence ratio at %E NH_3=80%; P=10 bar.

It is observed that the results follow the similar trend as discussed for the 17 bar case. Although the NO_x predictions are noticeably consistent with the full mechanism (not shown here), the flame speed results look more critical in the sense that there are noticeable deviations in some of the predictions generated by the reduced mechanisms. For instance, the flame speed profiles in the case of 80% NH_3 illustrate high accuracy of the reduced mechanism # 1 while discrepancies in predictions of the reduced mechanism # 2 and the reduced mechanism of Duynslaegher et al. are observed.

Based on the previously discussed evaluation results, it is deduced that the reduced mechanism # 1 is the most reliable reduced mechanism under wide range of conditions (stoichiometry and pressure) and it produces more consistent results with the full mechanism and the experiments.

Homogeneous Ignition Case

We have performed ignition delay simulations with the full Konnov mechanism and the reduced mechanisms. Despite the fact that the ignition delay times were not captured accurately by any reduced mechanism (our two mechanisms and the one by Duynslaegher et al.) compared to the full mechanism, our two mechanisms predicted the temporal profiles very well (once the time scale is translated to account for the differences in the delay times between the reduced mechanisms and the full Konnov mechanism). Also the final NO_x concentrations are very well predicted by the two reduced mechanisms. Figure 3-22 shows predictions of OH and NO concentration traces in time by reduced mechanisms in comparison to the counterpart predictions by the reference Konnov mechanism.

The error in the final NO concentration is very similar to the error calculated in the steady state case. Moreover, the final NO_x concentrations are very well predicted by the two reduced mechanisms as shown in the Table 3-7 for various initial temperatures and $\%NH_3$ levels. Note that the error in the final NO concentration is very similar to the errors calculated in the previous steady state case.

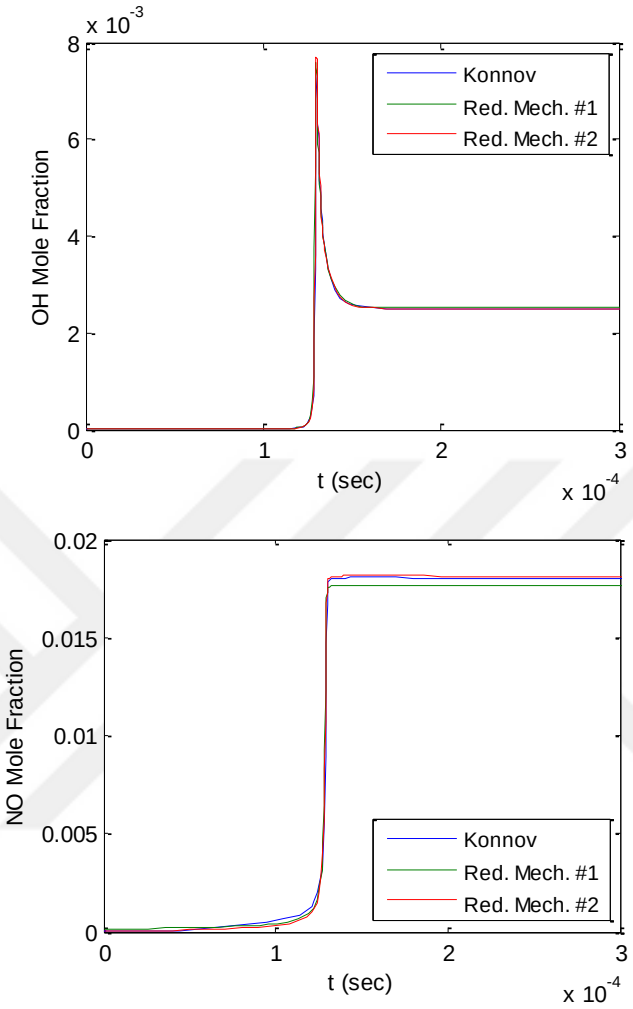

Figure 3-22 Temporal profiles of (a) OH and (b) NO predicted by the mechanism, ϕ=0.5, T=1300K.

Table 3-7 Final NO_x prediction error (ϕ=0.5)

Initial T	%NH3	Red Mech. 1 NOx %Error	Red Mech. 2 NOx %Error
1300	100	0,15	3,47
	80	0,22	1,03
	0	0,67	0,68
1400	100	0,98	1,58
	80	0,90	0,77
	0	0,51	0,52

It is noteworthy that there is no experimental data in the open literature for the combustion of NH_3/H_2 mixtures under the studied conditions that can be used to validate the results of the homogeneous ignition case for the full or reduced mechanisms.

Performance analysis

Reduced mechanisms which are established to be used in CFD simulations need to be efficient in terms of time expence and accuracy. Low CPU time usage and high accuracy are two most important efficiency criteria one expects for a reduced mechanism to fulfill. To have a rough estimation about the overall performance of the reduced mechanisms we find it beneficial to compare the CPU time usage and the accuracy with respect to the full mechanism and the experimental data, respectively. Therefore, based on the experimental data points presented in the Figure 3-15, we calculate the average deviation of results for each mechanism, including the Konnov mechanism, and consider it as the accuracy indicator. On the other hand, assuming the Konnov mechanism time of simulations as the reference value, the CPU time of reduced mechanisms for each case is normalized with the associated reference value and finally averaged for all the data points. As a result, an efficiency chart is established based on the two criteria which is demonstrated in Figure 3-23.

As expected the reduced mechanisms 1 and 2 noticeably decrease the simulation time which would be an important factor in practical CFD simulations. Furthermore, the prediction error for both the reduced mechanisms is considerably less than that of Duynslaegher et al.. There exist slight differences between the two mechanisms in terms of accuracy and simulation time. The reduced mechanism # 1 produces more accurate results than the reduced mechanism # 2 with the compromise in simulation time. Therefore, based on the purpose and type of intended simulation, either one of the mechanisms can be applied.

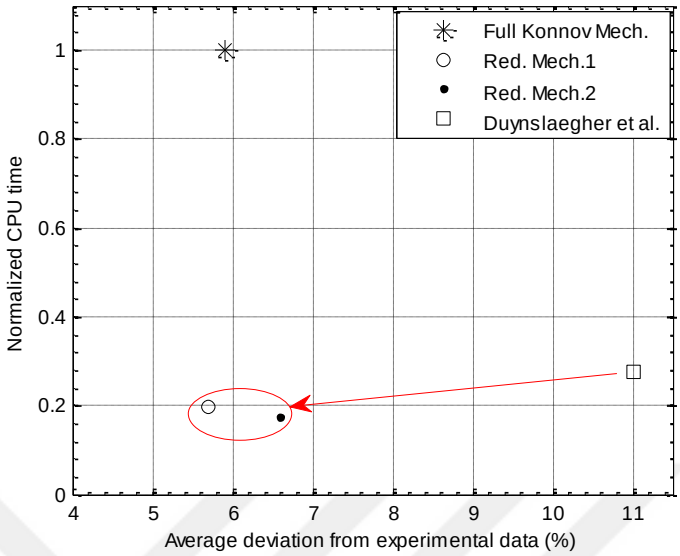

Figure 3-23 Efficiency chart for reduced mechanisms.

Generally it is observed that by applying the reduced mechanisms established in this study, we get almost the same accuracy as Konnov mechanism with about 5 times less CPU time expense.

3.4 Concluding Remarks

The combustion characteristics of NH_3/H_2/air mixtures at elevated pressures and under lean conditions are examined numerically. It is revealed that the radicals have strong influence on the combustion characteristics. Under high pressure and fuel lean conditions, OH is the most influential radical contributing to ammonia decomposition and flame speed, followed by other effective radicals such as H, O, and NH_2. By adding hydrogen to the fuel mixture, the combustion characteristics such as ignition delay time and laminar flame speed are noticeably improved. The improvement in combustion characteristics is of high importance in the real world applications in the sense that two of the major operational drawbacks (low flame speed and high ignition delay time of ammonia) are compensated.

The complex chemistry of NO_x formation is highly dependent on the fuel mixture composition which controls the contribution of fuel NO_x and thermal NO_x levels. This

could lead to a trade-off situation in choosing the optimal fuel composition for engine applications. It is deduced that the total NO_x formation of ammonia doped flames would noticeably decrease by operating under fuel rich conditions.

Two reduced reaction mechanisms are established based on the Konnov mechanism to predict the laminar flame speed and NO_x emission levels. The performance evaluation and efficiency analysis of the reduced mechanisms, regarding the full mechanism and the experimental data, reveal their acceptable accuracy in predicting the combustion characteristics in a wide range of equivalence ratios, mixture compositions, and pressures. It is inferred that the reduced mechanisms can effectively reduce the simulation time while maintaining the reliable accuracy of Konnov mechanism.

CHAPTER 4

Improving combustion characteristics of ammonia-hydrogen-air mixtures: experimental study

4.1 Introduction

Carbon free ammonia (NH_3) is a promising green energy carrier/storage medium due to its high hydrogen density and many practical advantages discussed in the literature[4,5]. As a clean fuel that can be used in various power generating systems, ammonia combustion has attracted many experimental and numerical studies especially in the last decade. Ammonia, which is one of the most produced chemicals in the world, has a relatively high volumetric and gravimetric energy density and power generation capacity[68]. Low flame speeds and fuel bond NO_x generation possibility are the two major drawbacks of ammonia as a potential fuel. There has been noticeable effort to figure out practical ways for addressing these challenges. Especially in the recent years, astonishingly growing interest is observed aiming at creating effective methods to address the challenges associated with ammonia combustion.

Despite the growing attention on ammonia combustion, the number of studies focusing on ammonia-hydrogen flames is quite limited. In an applied viewpoint regarding the fact that ammonia is a noticeable hydrogen carrier capable of being partially cracked to hydrogen prior to being combusted [69,70], ammonia-hydrogen is a practical mixture deserving further fundamental research. Better understanding of the flame characteristics, enhancement of the combustion quality, and effective application to combustors in power generation units still remain as challenges that need to be addressed. Following the previous comprehensive chemical kinetics study on the NH_3-H_2-air premixed flames [71], we present our experimental study on a porous media NH_3-H_2-air burner in this chapter. We apply SiC porous medium based burner for the

purpose of flame stabilization of NH_3-H_2-air flames over a wide range of mixture compositions and power output levels. As the main focus of the current experimental study, we examine the effects of equivalence ratio and mixture composition on the flame stability range. Combustion temperature is also measured and compared to the adiabatic flame temperature predicted by chemical kinetics models. A simplified CFD model based on volumetric heat release is also developed as a useful computational tool for examining the combustion efficiency of the burners by simulating the flow field and temperature distribution under the same conditions of the experiments. Subsequently, the effect of burner diameter on the stability range is discussed as a key design parameter which must be taken into account in power applications. Also a power density (output power per cross-sectional area of the burners) analysis is performed based on the maximum capacity of the burners for operating inside the flame stability boundaries. In the final section of this chapter, results of exhaust NO_x measurements are also presented.

It is important to note that in most studies reported in the open literature, flame holding of ammonia doped mixtures has been performed for lower mixture fractions of ammonia and lower flow rates (power outputs) [55,56,72]. For that reason, this study extends the knowledge base to conditions that more likely exist in practical power generating systems.

4.2 Materials and Methods

A fully premixed atmospheric combustion test rig [73] is modified in order to conduct the ammonia combustion experiments. Schematic drawing of the setup and a picture of the combustion chamber are illustrated in Figure 4-1. A premixed jet is formed at the exit of a stainless steel feed tube with an inner diameter of 22.3 mm. A passage length/diameter ratio of 50 is selected to ensure fully-developed pipe flow at the tube exit, entering the flame stabilizer which is placed on the tube rim. The mixture is spark-ignited downstream of the porous combustor. Upon ignition a premixed NH_3-H_2-air flame is formed and stabilized in the porous medium based burner.

Hydrogen and anhydrous ammonia fuels stored in high pressure cylinders are fed into the system at desired flow rates. The purities of hydrogen and ammonia gases stated by the gas company are 99.9% and 99.99%, respectively. As for the oxidizer, continuous dry air is provided by two tanks with capacities of 200 liters each, which are filled by an oil-less compressor. Flow rates of NH_3 and H_2 are controlled by separate mass flow controllers, Aalborg DFC 0-100 SLPM and 0-50 SLPM, respectively. These units have reported accuracies of ±1.0% of the full scale. The flow rate of air is adjusted by a rotameter with range of 2.5-25 m^3/hr and accuracy of 0.5 m^3/hr. The mass flow controllers are commanded by adjusting the voltage input from potentiometers. This simple method ensures easy, independent, and precise control of mixture composition and the tube exit velocity. A type R thermocouple with an accuracy of ±1.5 °C is used to measure the temperature 30 mm downstream of the burner exit. NO_x concentration is measured by a calibrated gas analyzer (MRU VARIOplus SE) at the exhaust port with an accuracy of 0.1-1.0 ppm.

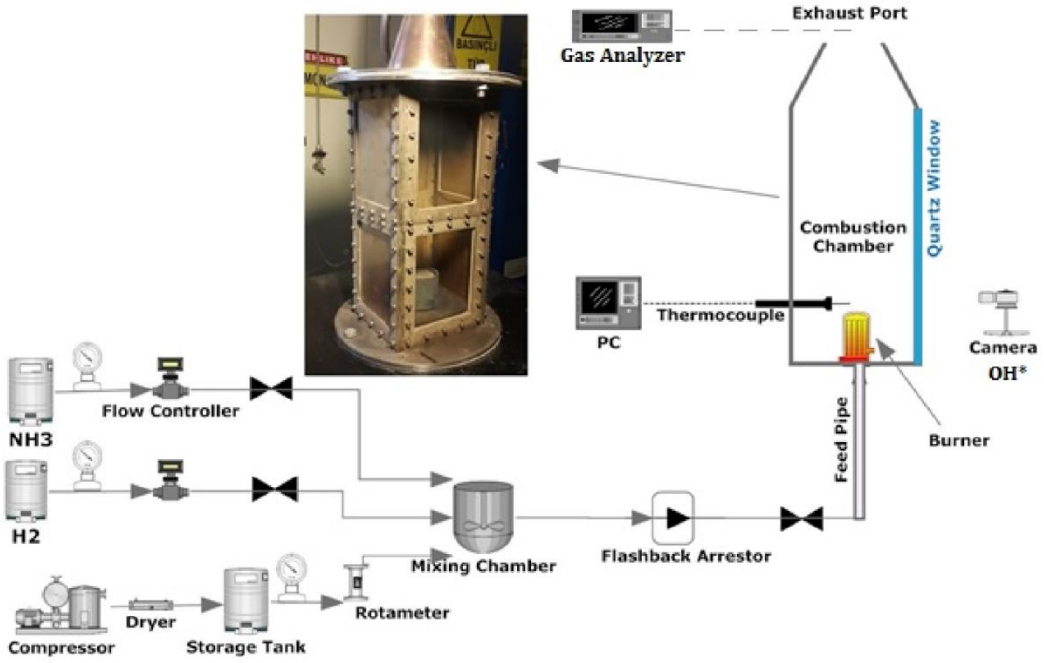

Figure 4-1 Schematic of experimental apparatus and combustion chamber.

Flame is enclosed in a stainless steel chamber (cross section and height of 194x200 mm and 640 mm, respectively) to resemble a practical combustion device by isolating the

flame from laboratory drafts. Quartz window installed on one side of the chamber enables optical access into the flame zone. The top of the chamber is a conic section with an opening port for exhaust gases to exit. To prevent any damage to the mixture supply system from flashback, flashback arresters are installed on the mixture line and the fuel feed lines.

Flame is stabilized by an inert SiC porous block burner with diameter of 7.62 cm, height of 7 cm, and a porosity level of 10 PPI. The measured pressure drop is negligible due to the high porosity level of the applied media. In fact, the pressure drop across the burner for all the tests conducted in this study is less than the accuracy of the manometer (0.2 bars) installed on the air supply line. The porous block is enclosed by a stainless steel shell with the thickness of 0.5 cm for improving rigidity of the burner as well as preventing air entrainment into the porous flame zone from the sides. Figure 4-2 depicts the burner, the ignitor plugs, and the thermocouple, which is placed 30 mm downstream of the burner surface.

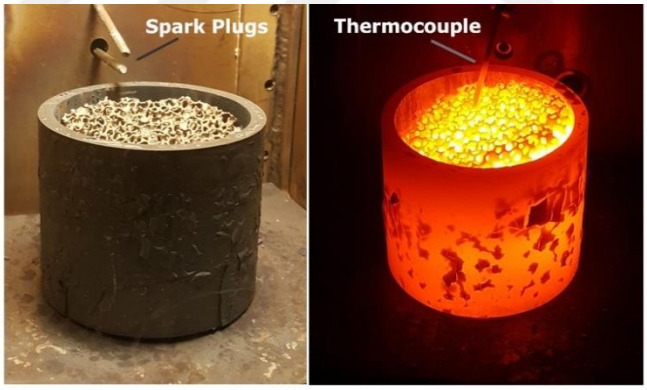

Figure 4-2 The SiC porous media based burner.

As a reliable tool for the assessment of the behavior of the attached flames, OH* chemiluminescence technique is applied. Distribution of the OH* radicals is a reliable indicator of the exact location of combustion (and flame shape). Time averaged two dimensional OH* chemiluminescence images are captured with an intensified HiSense MkII CCD camera equipped with an appropriate band pass filter. Resolution of the CCD camera is 1600 x 1200 pixels and the band pass filter captures light from OH* at

wavelength of 310 nm. For each image, the CCD array is gated for 10 μs and a total of 500 images are recorded for averaging and background noise removal.

At ambient temperatures of T =293 ± 3 K and atmospheric pressure (NTP), experiments were carried out for volume based %NH_3=60-90%, ϕ=0.9-1.5, and mixture inlet velocity range of V= 4-18 m/s (corresponding to a Reynolds number range of Re = 4500-25000; The Reynolds number is based on the inlet bulk velocity and inner diameter of the tube). It is worth mentioning that the burner is not capable of holding pure ammonia flames in a stable way. Based on the mixture ratio and flow rate capability of the system, the heating value input of the burner can be as high as 30 kW. In all of the tests flames were ignited at the conditions that corresponded to a stable regime, and then the flow rates were gradually adjusted to obtain the desired mixture composition, allowing some time for the porous block to heat up.

In the experiments conducted for this study, random measurement error is believed to be the largest source of uncertainty. The measurement uncertainty is minimized by repeating the temperature and NO_x measurements and stability tests several times (3 times on average). Error bars of the temperature and stability plots in the following sections present the standard error, $\sigma_{\bar{x}}$, calculated by dividing the standard deviation of the measured data by the number of repetitions as presented in Eq. 18.

$$\sigma_{\bar{x}} = \frac{(\frac{1}{N}\sum_{i=1}^{N}(x_i-\bar{x})^2)^{1/2}}{\sqrt{N}} \qquad (18)$$

Here x_i is the result of i^{th} measurement and N is the number of measurements.

In addition to the measurement errors in temperature and stability criteria, we would like to note that the equivalence ratio and the mixture ammonia fractions also have inaccuracies. Measurement errors are inevitable for hydrogen, ammonia, an air flows through the flow controllers and rotameter. For each gas, the measurement error, $\mathcal{E}_i$, is calculated by dividing the related flow controller inaccuracy stated by the manufacturer by the flow rate of the gas, q_i, as follows.

$$\boldsymbol{\varepsilon}_i = \frac{FC_{inaccuracy}}{q_i} \qquad (19)$$

Subsequently, the measurement errors of the equivalence ratio and the mixture fraction would include the measurement errors of all the gas flows involved in each case as calculated in Eq. 20.

$$\boldsymbol{\varepsilon}_{\emptyset} = \sqrt{\boldsymbol{\varepsilon}_{H_2}^2 + \boldsymbol{\varepsilon}_{NH_3}^2 + \boldsymbol{\varepsilon}_{air}^2} \qquad (20)$$

$$\boldsymbol{\varepsilon}_{\%NH_3} = \sqrt{\boldsymbol{\varepsilon}_{H_2}^2 + \boldsymbol{\varepsilon}_{NH_3}^2}$$

In this study, the maximum measurement errors calculated for the equivalence ratio and the ammonia mixture fraction are 8% and 5%, respectively.

Also to gain a better insight into the effect of heat loss on measured temperatures and to evaluate the combustion efficiency of the burner, a basic volumetric heat release CFD model is developed to simulate the experimental conditions (Figure 4-3).

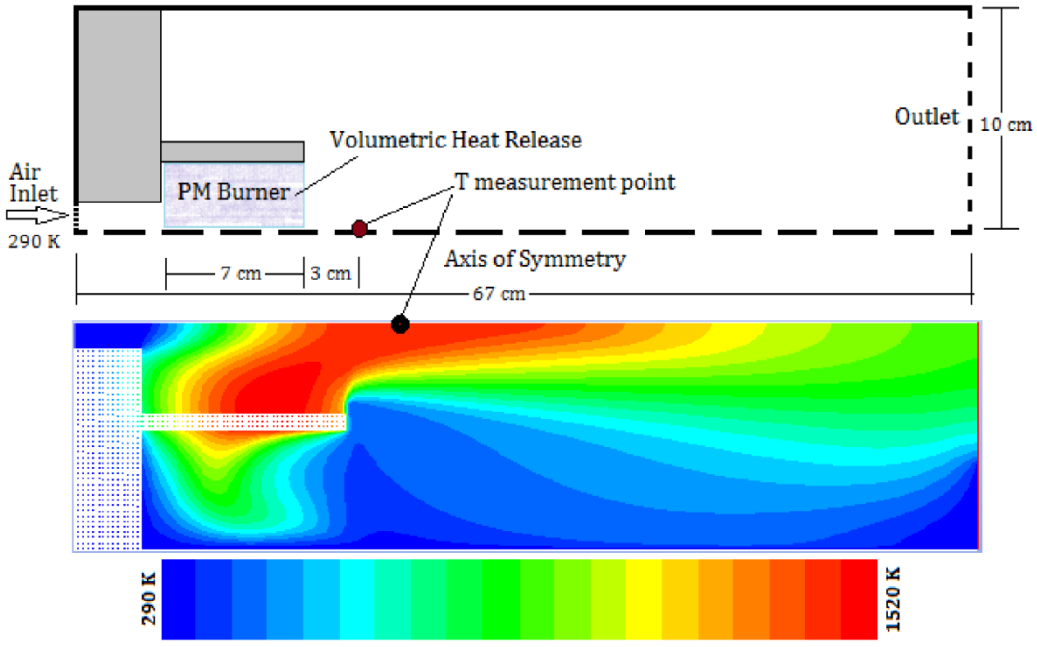

Figure 4-3 Volumetric heat release model schematic and sample temperature field for 80% NH_3, ϕ=1.1.

The porous core of the burner is defined as a uniform heat release source with a total power loading which is calculated regarding the combustion based power of the mixture composition entering the burner. A practical assumption in this simplified model is that

the combustion takes place homogeneously inside the porous volume of the burner. Velocity inlet and pressure outlet boundary conditions are used for the inlet and outlet boundaries, respectively. A realizable k-ε turbulence model with standard wall functions is used. Air entering the burner is heated up passing through the porous core loosing heat to the burner wall and the base panel. As the main purpose of the model, the temperature downstream of the burner (at the exact location of the thermocouple in the experiments) is obtained.

All the chemical kinetics predictions in this chapter are obtained by using a reduced reaction mechanism with 21 species and 91 reactions which was developed in a previous numerical study [71] and elaborated in chapter 3.

Taking into consideration the practical applications, our focus is on the mixture compositions with high fractions of ammonia (60-90% volume based), since it resembles the conditions at which a reasonable percentage of ammonia can be partially cracked to generate hydrogen before entering the burner. Based on the well-established fact that rich combustion of ammonia generates lower concentrations of NO_x [51,71], in this study we primarily focus on rich flames.

4.3 Results and Discussion

In the flame stability evaluation experiments, equivalence ratio and ammonia mixture fraction are set to fixed values and then the mixture exit velocity is varied to find the combustion stability limits. For each ϕ and $\%NH_3$, two combustion stability limits are observed in general: one at low velocities due to heat losses to the tube wall and ambient air (flashback or extinction) and another at high velocities due to insufficient burning velocity of the injecting mixture jet (blow-off). For the case of lower stability limits, exit velocities are obtained by establishing a stable flame at a relatively higher velocity and then gradually decreasing it to a value at which flashback or extinction is observed. Following the similar reverse procedure for the upper stability limit, flame is started at lower exit velocities and the velocity is slowly increased until the blow-off is observed. Depending on the mixture composition, flow rate, and equivalence ratio,

stable flames are formed either completely inside the burner or attached to the surface of the burner. Figure 4-4 depicts samples of stable flames with different mixture fractions and configurations for the porous medium based burner studies in this chapter.

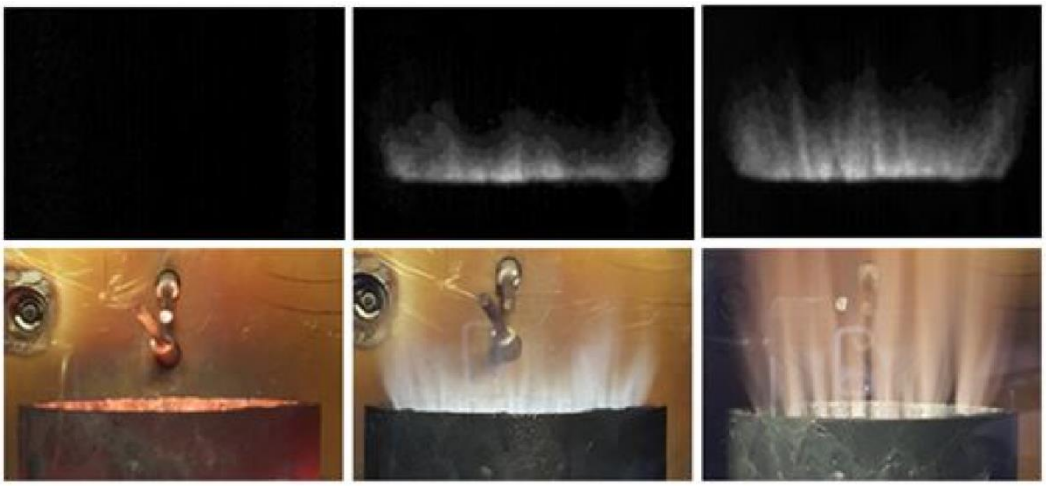

Figure 4-4 OH* chemiluminescence and visual images for ϕ=1.1 70% NH_3 7 m/s (left), ϕ=1.1 80% NH_3 13.5 m/s (center), and ϕ=1.1 90% NH_3 12 m/s (right).

When the combustion takes place inside the burner, as for the case of 70% NH_3 mixture, no trace of OH radicals is detected downstream of the burner. For the other two cases, i.e. 80% and 90% NH_3, the flames are extended beyond the surface of the burner. As expected, a longer flame is formed with 90% NH_3 compared to the case with 80% NH_3, because of the lower flame speed in the former case. It is important to state that each experiment is repeated several times for all the temperature, NO_x, and stability limits measurements.

4.3.1 Flame temperature and combustion efficiency

In a previous chemical kinetics study on premixed NH_3-H_2-air flames[71], effects of equivalence ratio and ammonia mixture fraction on adiabatic flame temperature were thoroughly investigated. As expected, for a specific mixture composition maximum flame temperature takes place close to the stoichiometric condition. Flame temperature decreases with increasing ammonia fraction in the mixture. In the current study to examine the sensitivity of temperature to the relevant parameters, we measure the gas

temperature downstream of the burner surface. It is important to note that the temperature measurements inside the porous media are difficult because of the physical limitations caused for both optical and mechanical probes by the presence of a solid matrix and the combustion chamber walls. Figures 4-5a and 4-5b demonstrate the effects of equivalence ratio and mixture fraction on adiabatic flame temperature and measured temperature, respectively. Also Figures 4-6a and 4-6b present the same data including the modeling results as well for the cases of 70% and 80% NH_3, respectively.

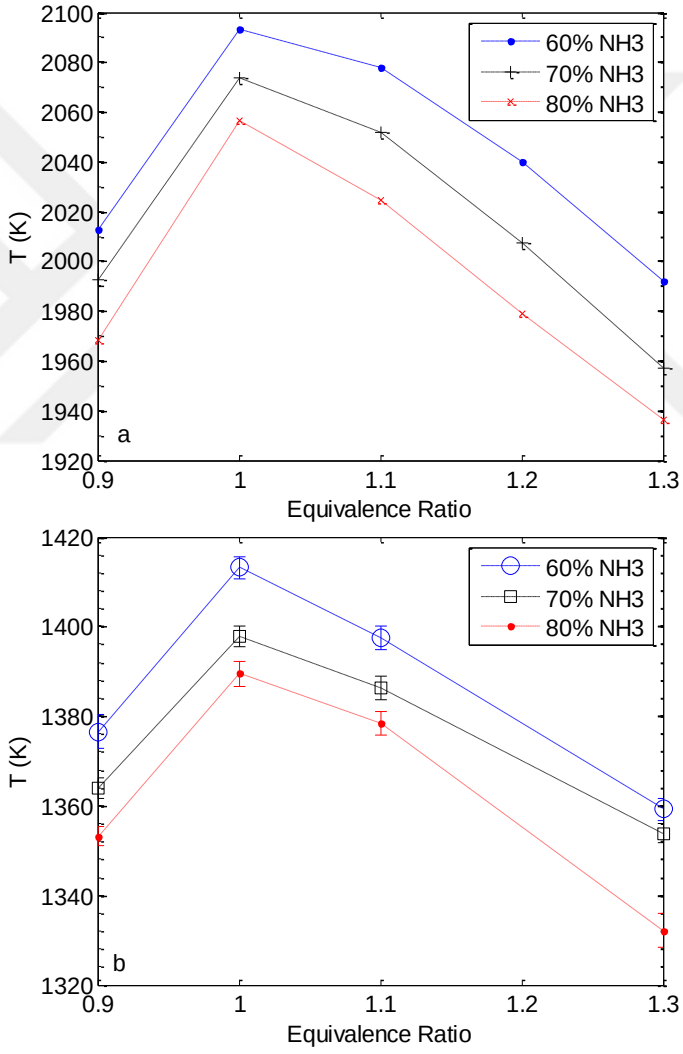

Figure 4-5 Effect of equivalence ratio and mixture fraction on adiabatic flame temperature (a) and measured temperature (b).

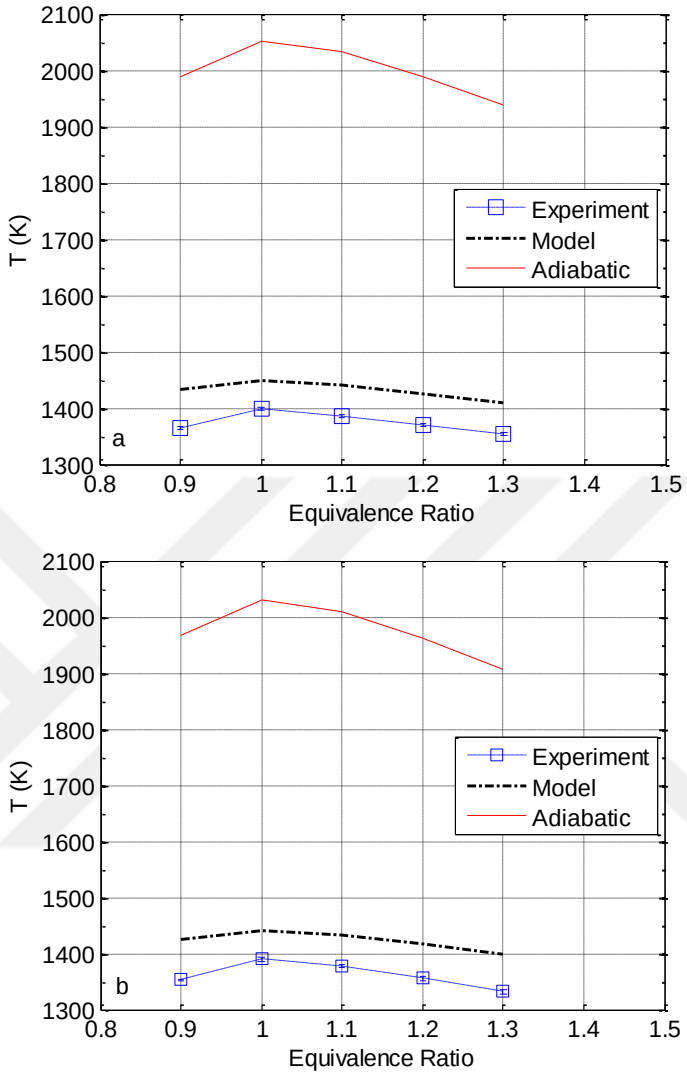

Figure 4-6 Adiabatic, experimental, and modeling temperature values with respect to equivalence ratio for 70% NH_3 (a) and 80% NH_3 (b).

Following the similar trend, all the temperature profiles show a peak near the stoichiometric ratio. Also consistent with the adiabatic flame temperature predictions, we observe a decrease in flame temperature with increasing ammonia content of the mixture in experimental and simulation data. Although the overall trend is well captured, we are dealing with a noticeable decrease in the experimental temperatures compared to the corresponding adiabatic flame temperatures. In the following subsection we discuss the possible reasons for the observed gap.

Measured and Calculated Temperature difference

To have a better insight into the nature of the difference between the measured temperatures and the adiabatic flame temperatures estimated using chemical kinetics, we consider a basic temperature index (T_{indx}) which is defined as the ratio of the measured temperature to the adiabatic flame temperature, as shown in Eq. 21.

$$(T_{indx})_i = (\frac{T_{measured}}{T_{ad}})_i \quad (21)$$

We intend to track the variation of the temperature index with respect to the equivalence ratio and ammonia percentage in order to determine whether the source of deficiency is incomplete combustion or heat loss. Figure 4-7 demonstrates the relation between the measured temperature and the temperature index. The points on the graph include all data points from Figure 4-5b.

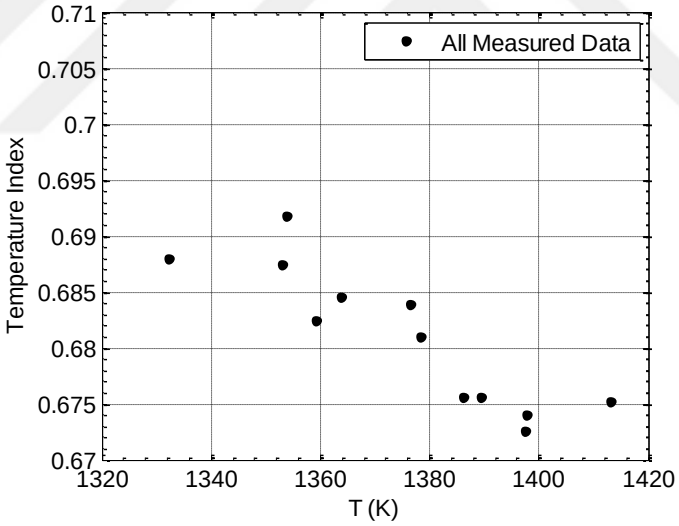

Figure 4-7 Distribution of the temperature index with respect to the measured temperature.

The figure shows a slight decrease in temperature index with an increase in the temperature. Note that the amount of decrease throughout the complete temperature range is less than 2%. In an overall outlook, despite a major change in the chemistry, i.e. in the equivalence ratio and the mixture fraction, we obtain almost the same level of temperature index. Based on this observation we deduce that the combustion inefficiency is almost completely resulted from the heat loss while combustion

incompleteness is not a major influential factor. We explain the slight decrease in temperature index as a result of relatively higher heat transfer level to the environment at higher temperatures. Once more, this confirms the heat loss as the dominant factor controlling the measured temperature drop with respect to the theoretical temperature.

Temperature variation with equivalence ratio

Regarding the non-adiabatic nature of the experiments due to the inevitable heat losses, to compare the temperature behavior with the adiabatic flame temperature trend, we define a scaled temperature. It is a non-dimensional quantity defined for adiabatic flame temperatures as well as the measured data points, resulted by dividing the temperature by the maximum value, i.e. stoichiometric temperature value, obtained in the related chemical kinetics or experimental data set, respectively. The scaled adiabatic flame temperature and measured temperature behaviors with respect to the equivalence ratio for 60% and 70% NH_3 are shown in Figure 4-8.

A general assessment of the results suggests that the measured temperatures for both mixture compositions have a satisfactory consistency with the predicted adiabatic flame temperatures. The trend is well captured with a maximum nonconformity of about 2%. The increasing-decreasing behavior is observed with respect to the equivalence ratio in measurements as well.

Also as previously depicted in Figure 4-6, experimentally measured temperatures and the temperatures from the numerical simulations are in good agreement. It has been observed that the difference between the numerical and experimental results is well within 5%. Since the thermocouple is close to the burner surface, the effect of mixing with the external air is small. We believe that the slightly lower experimental temperatures compared to the numerical predictions are related to the incomplete nature of the combustion in the burner.

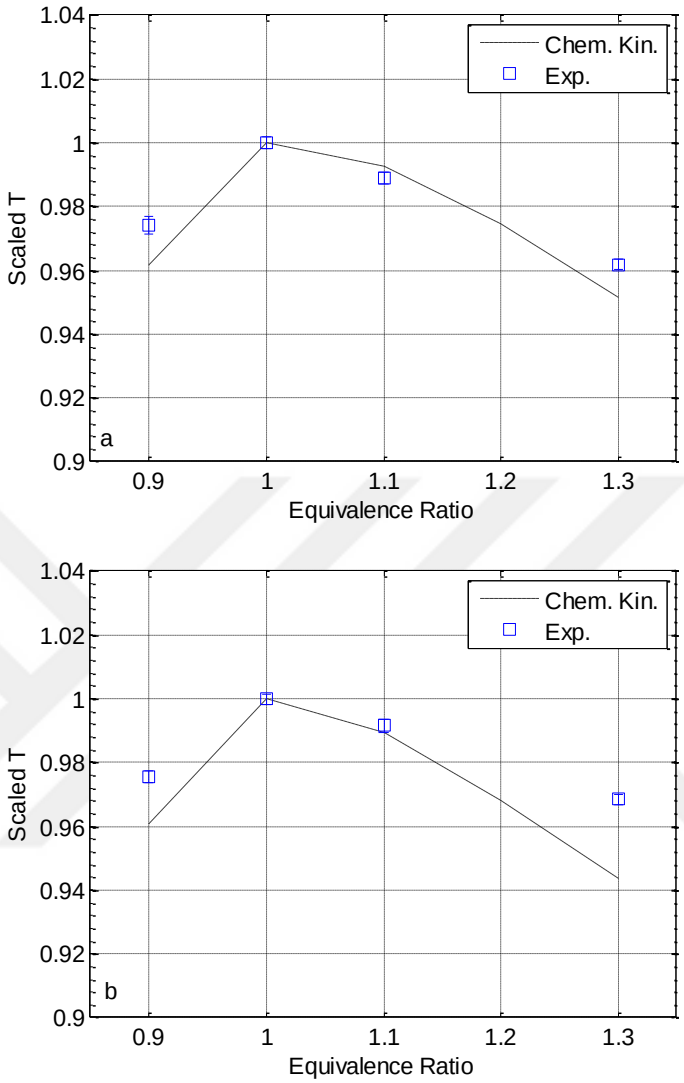

Figure 4-8 Scaled temperature behavior with respect to equivalence ratio for 60% NH_3 (a) and 70% NH_3 (b).

We consider the ratio of the experimental temperature to the corresponding modeling value as an indicator of the completeness of combustion in the burner or the estimated combustion efficiency of an actual combustor for which the heat losses are expected to be minimal. The variation of the estimated combustion efficiencies with respect to the equivalence ratio is shown for different mixture compositions in Figure 4-9.

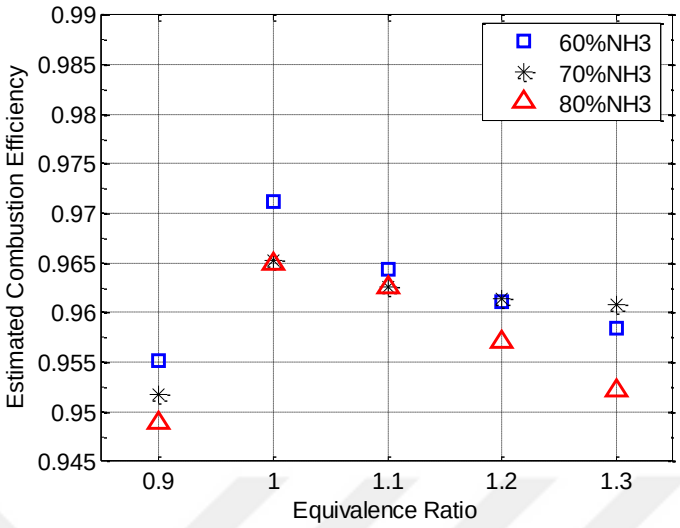

Figure 4-9 Combustion efficiency chart for the mixtures with 60%, 70%, and 80% NH_3.

The figure reveals that the combustion completeness level is higher than 95% for all the mixtures, which shows the excellent potential of the porous medium based burners for practical power generation applications. The chart also indicates a slight decrease in the combustion efficiency with increasing ammonia fraction in the mixture, which is a direct outcome of slower laminar flame speeds at lower hydrogen fractions.

4.3.2 Burner stability maps

By determining the upper and lower stability limits for each mixture composition, we obtain a stability map for the burner. The map demonstrates the region between the two criteria for which a stable flame is formed in the burner. The stability maps are helpful tools in adapting the burners to practical systems with an accurate prediction of operating range under similar test conditions. The stability maps for several equivalence ratios are shown in Figure 4-10.

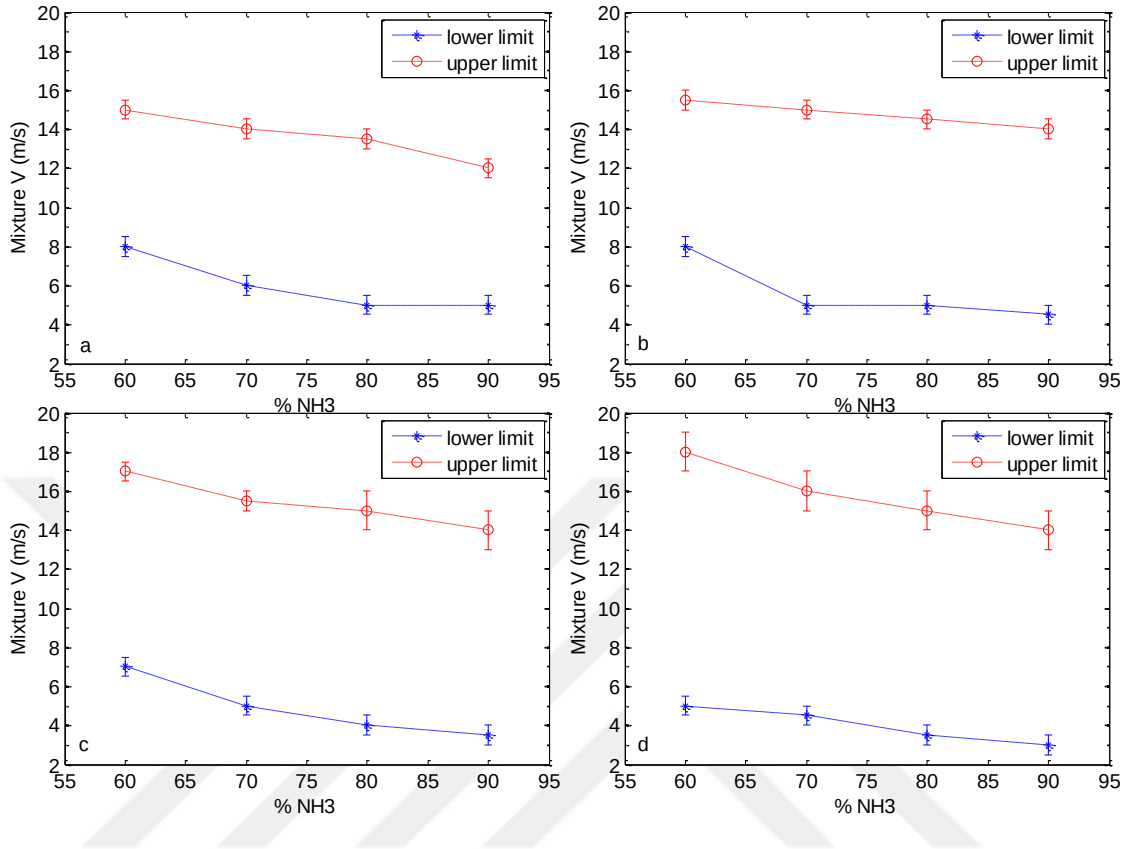

Figure 4-10 Flame stability maps for ϕ=0.9 (a), ϕ=1.1 (b), ϕ=1.3 (c), and ϕ=1.5 (d).

The results show decrease of the upper and lower limits with increase in the ammonia content. We also observe a broader stability region as we move from lean to rich conditions. This behavior is better demonstrated in Figure 4-11, which essentially presents the map in the mixture velocity/mixture composition space.

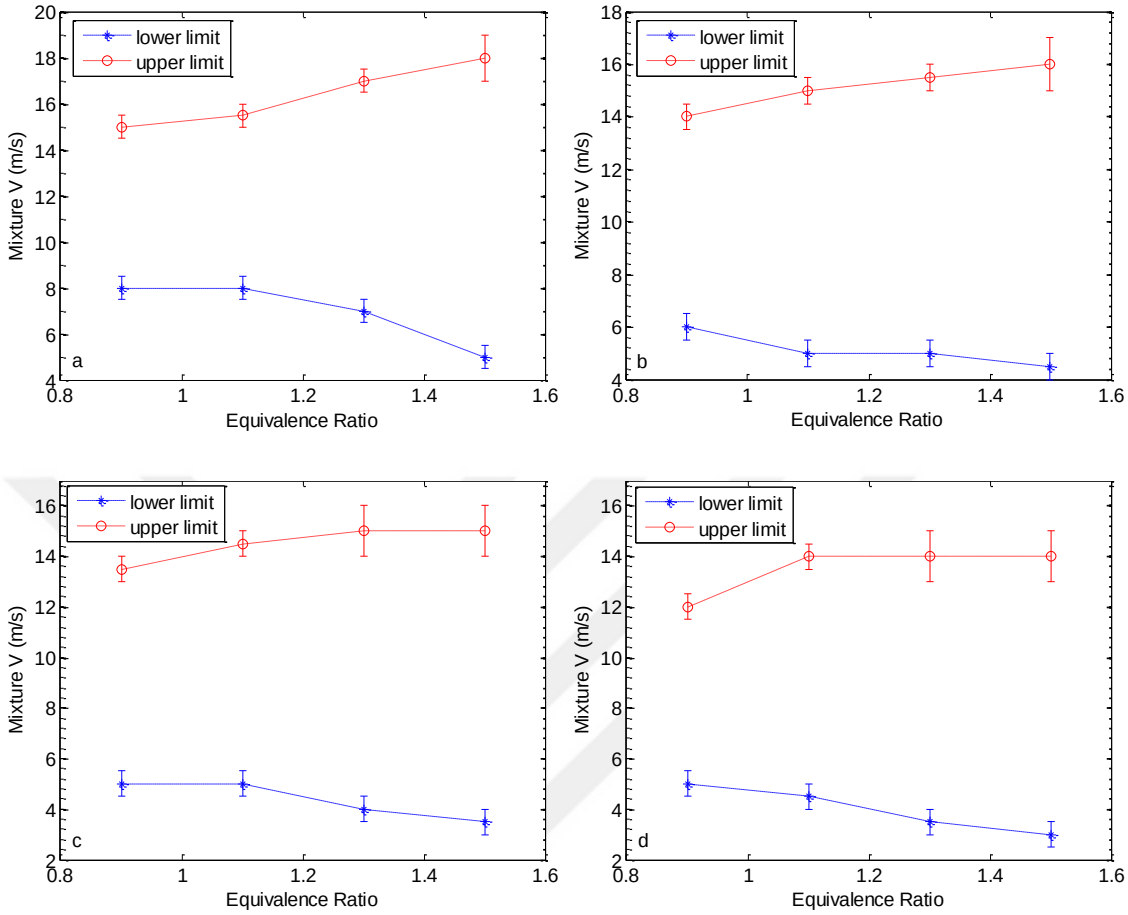

Figure 4-11 Flame stability maps for 60% NH_3 (a), 70% NH_3 (b), 80% NH_3 (c), and 90% NH_3 (d).

It can be deduced that with increasing equivalence ratio, the stability range extends in both the lower and upper stability limits. This behavior is the result of excess fuel remaining unreacted in the burner which reacts with the ambient air downstream of the burner postponing the flame extinction and blow-off. The elongated flame under the rich conditions is an indication of this phenomenon. In order to have a better insight into the underlying mechanisms controlling the upper and lower stability criteria, we discuss each case separately.

Lower stability limit

Lower stability limit is obtained for each condition, i.e. certain equivalence ratio and mixture composition, by gradually decreasing mixture exit velocity and finally

approaching to a value at which flashback or extinction is observed. The low stability limits for various conditions are depicted in Figure 4-12.

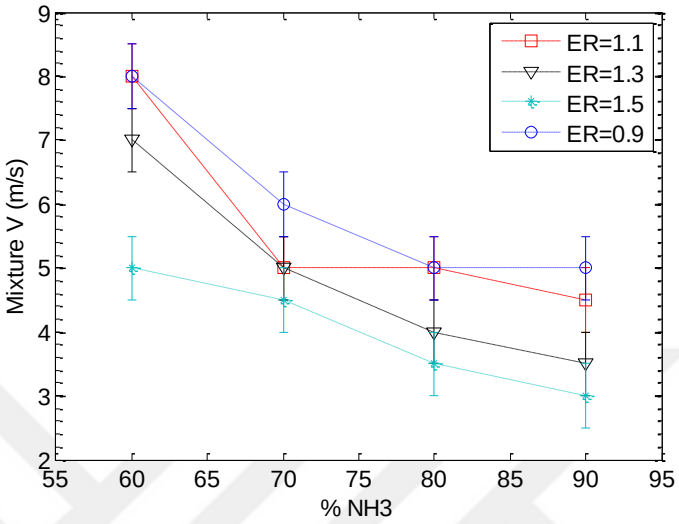

Figure 4-12 Low stability limits for various equivalence ratios.

Based on the noticeable increase in flame holding capability by the porous medium burner, two conditions can occur in the vicinity of the lower stability limit. When the burning speed exceeds the mixture jet velocity flashback happens. In this case flame propagates toward upstream of the burner into the feed tube. This is usually observed in the near-stoichiometric and lean conditions for which relatively vigorous flames are formed and propagated. In the case of flashback occurrence we observe acoustic instability upstream of the burner in the feed tube. Other behavior detected at the lower stability limit is extinction. Due to the noticeable heat losses to the tube walls and the ambient gases, flame extinguishes in the flame holder, lifts off, and extinction occurs. This process takes place in a short period of time just after ignition. The latter behavior is observed mostly in the case of the rich flames through which some fuel remains unburned due to the extreme heat losses near the tube rim and the burner. In a more detailed point of view we can associate the flame extinction to two parallel mechanisms. The reduced heat release at the low mixture energy input is unable to compete with the substantial heat loss to the burner wall and environment. On the other hand, as the flame gets closer to the upstream edge of the burner as the mixture inlet velocity approaches to the lower limit, the preheating length for the incoming unburnt mixture becomes

shorter. Therefore, the limited heat transfer from the solid walls to the unburnt gases cannot compensate the large heat losses anymore. Accordingly while no flame is formed in the burner due to the stated loss, the excess fuel reacts with the ambient air downstream of the porous block forming a weak lifted flame which extinguishes immediately. For all equivalence ratios, we observe a decrease in low stability limit with increase in ammonia content in the mixture. It is directly related to the lower flame speeds of the mixtures with high ammonia percentages.

Quenching distance

Quenching distance for ammonia-hydrogen-air flames is estimated using Eq. 22 based on the flame speed (S_l) and thermal diffusivity (α) of the mixtures [74].

$$d = \frac{2\alpha}{S_l} \qquad (22)$$

Laminar flame speeds were calculated in the previous chemical kinetics study for a wide range of conditions using a new reduced mechanism [71]. Figure 4-13 illustrates the variation of the laminar flame speed and the quenching distance with the equivalence ratio for various mixture compositions.

The figures indicate that the extremums happen around $\phi=1.1$ for the flame speed and accordingly for the quenching distance. Based on the calculation results the quenching distance is two orders of magnitude smaller than the feed tube diameter. Therefore, at least theoretically, a flame can be absorbed into the feed pipe.

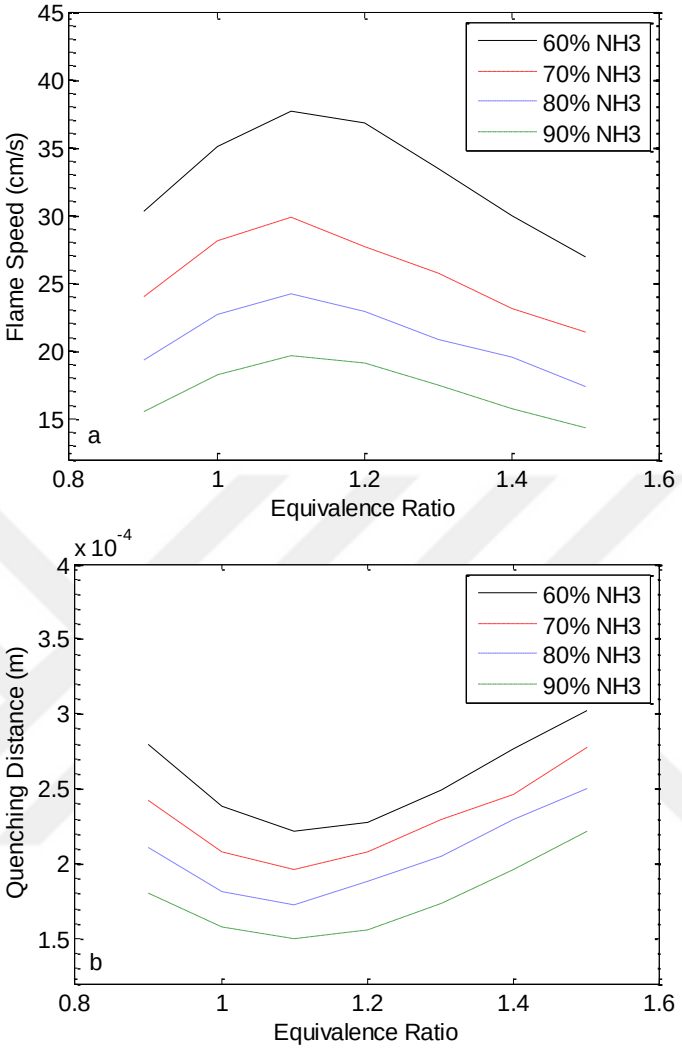

Figure 4-13 Effect of equivalence ratio on flame speed (a) and quenching distance (b) for various mixtures.

Upper stability limit

It is well established that the upper stability limit is directly related to the insufficient residence time for the incoming mixture in the burner. In general upper limit is a function of chemistry, i.e. equivalence ratio and mixture composition, as well as the burner properties. The upper stability limits for various conditions based on the equivalence ratio and ammonia mixture fraction are measured and shown in Figure 4-14.

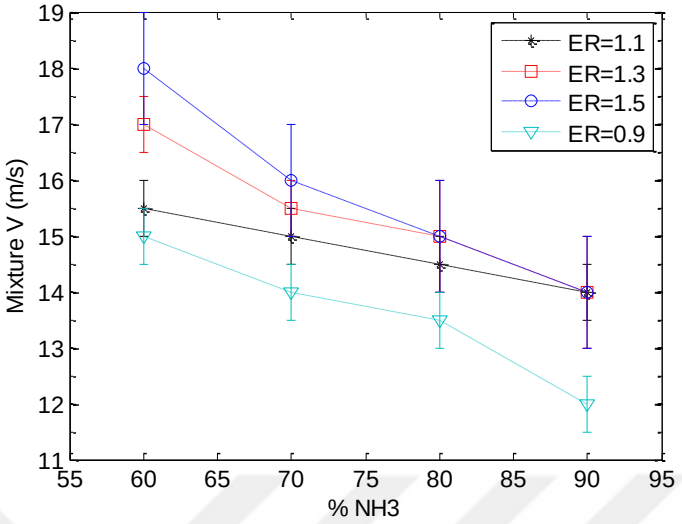

Figure 4-14 Upper stability limits for various equivalence ratios.

In the inert porous media, heat conduction from the post-flame zone to the pre-flame region is remarkably enhanced due to its excellent thermal conduction properties. The radiation and conduction feedback from the reaction zone to the unburnt gases leads to a significant enhancement of the flame speed. Thus the burner is able to operate at higher burning speeds extending the flame blow-off limit compared to many conventional flame holding methods [55,72].

In the present study, the upper stability limit is specified as the point at which unstable behavior in the form of erratic oscillations in the flame structure starts. In other words, when the mixture inlet velocity exceeds the upper limit by a small margin, a flame still exists on the burner. However, this is an unstable flame with its shape and length changing in an erratic manner. After a slight increase in the inlet velocity, the flame oscillations become augmented and finally the flame blows off. It is important to note that in the case of 90% ammonia, the blow-off limit exceeds the maximum limit of the ammonia flow controller for the equivalence ratios between 1.1 and 1.5. Thus, under these conditions the upper flammability limit could not be established.

Flame holding improvement

In order to quantify the effectiveness of the burner in its ability to hold the flame at higher flow velocities, we consider a scaled velocity parameter obtained by dividing the mixture velocity in the burner by the theoretical laminar flame speed of the mixture. The variation of the scaled velocity with the flame equivalence ratio is illustrated for various mixture compositions in Figure 4-15.

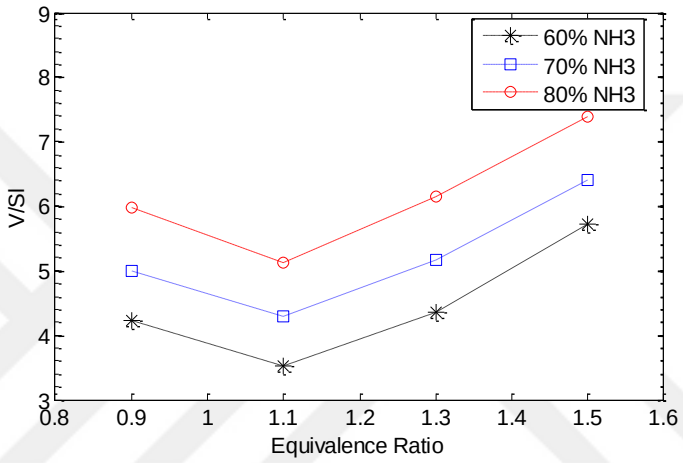

Figure 4-15 Burning speed elevation as a function of equivalence ratio.

Since flame speed takes its maximum value near the equivalence ratio of 1.1, we can see a local minimum in the normalized velocity in that vicinity. As stated previously, increase in the ammonia content of the mixture in a certain equivalence ratio results in a lower blow off velocity and also a reduced flame speed. Since the level of decrease in the flame speed exceeds the reduction in the mixture velocity, we observe an overall increase in the value of the normalized velocity.

For comparison purposes, a 7.62 cm diameter dump combustor (same diameter as the porous medium based burner) with a height of 18 cm is also tested under the same test conditions. Figure 4-16 depicts the flame holding performance of the burners for the mixtures with 60% and 70% ammonia content. Since a comparison of the maximum flame holding capabilities is intended, only the blow off limit is examined for the combustors in the figure.

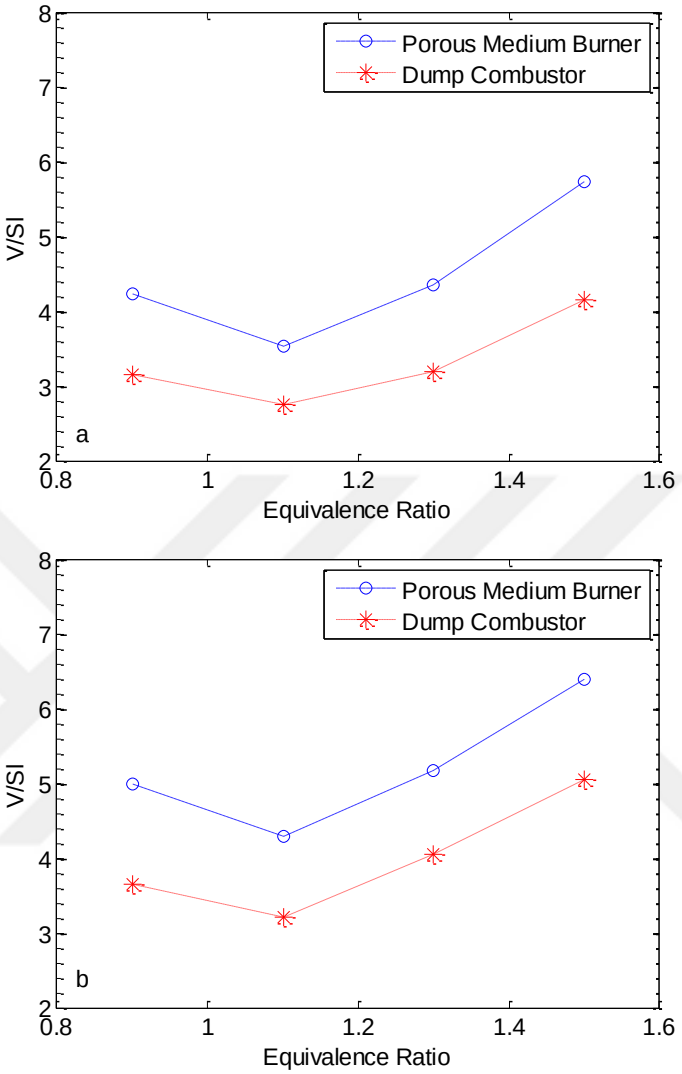

Figure 4-16 Normalized mixture velocity at the upper limit for the cases with 60% NH_3 (a) and 70% NH_3 (b).

From a practical perspective, it is fair to state that the porous medium based burner is capable of generating a remarkable elevation in the burning velocity for ammonia-hydrogen flames. Another critical point is that the effectiveness of the burner is even greater for higher ammonia content flames, highlighting the practical value of this particular burner concept. Comparing the two different burner types indicate that the effectiveness of the porous medium based burner for increasing the mixture burning velocities is up to 40% higher than the dump combustor with the same diameter. This is certainly a significant performance improvement when applied to practical power

generation systems. Additionally, it is worth mentioning that while the porous medium burner can hold flames for a wide range of mixture conditions (over 90% NH_3), the dump combustor is not capable of stabilizing the flames with high ammonia content, i.e. 80% or higher.

4.3.3 Effect of burner diameter

Since the maximum burner diameter is an important design constraint for a power generation systems, the effect of diameter on the stability limits should be carefully studied. Figure 4-17 shows a comparison between the upper stability limits for a burner with 7.62 cm diameter and a 5.08 cm diameter counterpart. Both burners have the same length and contain porous media with the same properties. Mixture flow rate, equivalence ratio, and mixture composition were matched for fair comparison. It is important to note that we did not observe a noticeable change in the lower stability limit by using a smaller burner.

The results indicate a drop in the upper stability limit with the smaller burner. Smaller diameter results in higher mass flux or energy flux at a given flow rate, which leads to a shorter residence time for the mixture in the burner. We cannot establish a stable flame for the mixture with 90% ammonia in the smaller burner. The figure infers that using a burner that is 45% smaller in area can cause the stability range to narrow down up to 15%. Generally for the cases with high ammonia content in which flame forms in the burner and extend to downstream of the burner, a longer flame is observed with the smaller burner compared to the larger counterpart.

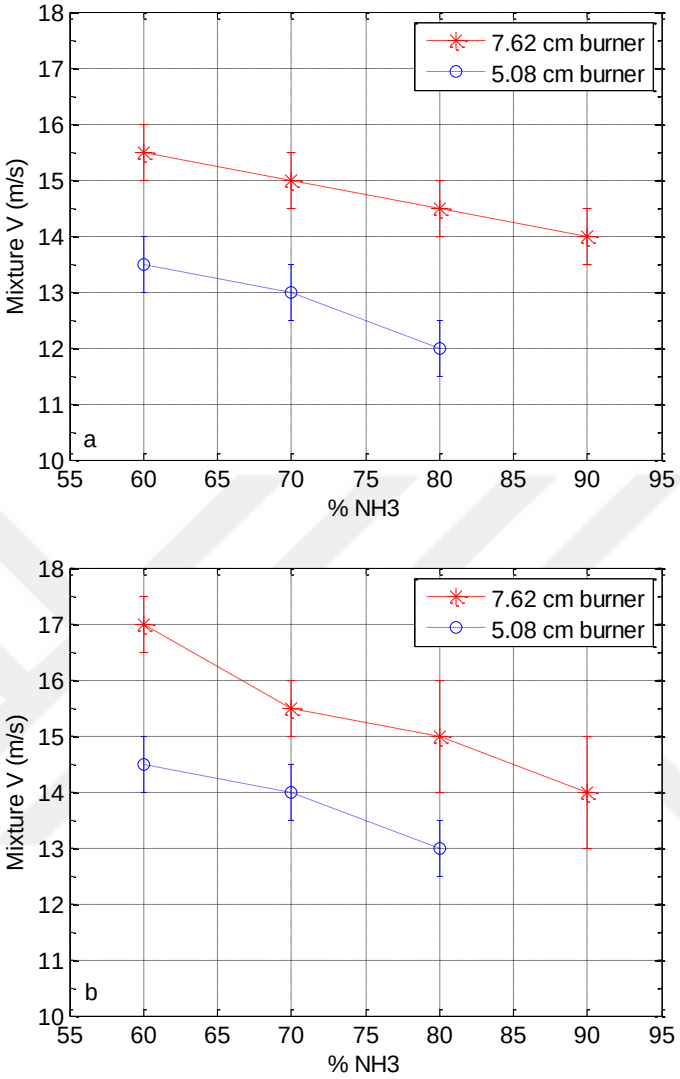

Figure 4-17 Upper stability limits for burners with different diameters for ϕ=1.1 (a) and ϕ=1.3 (b).

As a visual demonstration of the flame configurations, digital and OH* chemiluminescence images for both burners are shown in Figure 4-18 for an equivalence ratio of 1.1, ammonia fraction of 80%, and mixture inlet velocity of 11 m/s. With the aim of a more discernible comparison, we have purposely illustrated a condition for which the flame extends well beyond the surface of the burner.

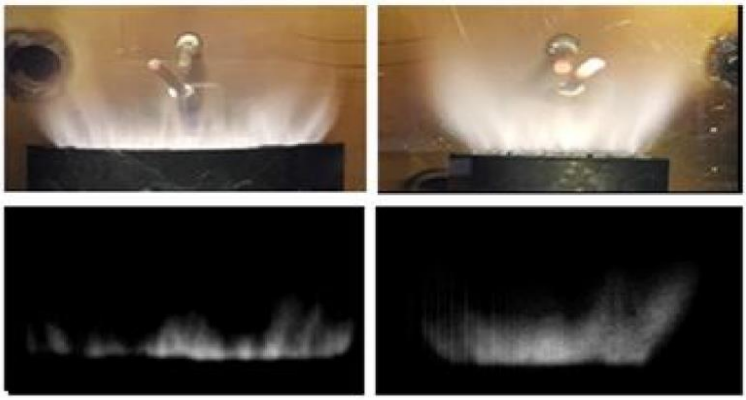

Figure 4-18 Flame formed on the burner with 7.62 cm (left) and 5.08 cm (right) diameter; ϕ=1.1, 80% NH_3, V=11 m/s.

It is worth mentioning that the stability region of the burners in practical combustion systems, such as gas turbines, is expected to be much wider because of the remarkable effect of elevated mixture temperatures on the burning speed of the studied mixtures. Although the flame speed has a reverse relation with chamber pressure, the pressure influence is expected to be insignificant compared to the strong effect of the elevated temperature [75].

4.3.4 Power density

The maximum power generation density of the porous medium based burners is evaluated based on the upper stability limits determined from combustion experiments at a given equivalence ratio and mixture composition. Power generation density is calculated based on the lower heating values of the fuel mixture and the combustor flow area. Figure 4-19 shows the power output density in terms of kilowatts per square centimeters for the equivalence ratios of 1.1 and 1.3.

Interestingly, a higher power output density is observed for the burner with smaller diameter. Although the upper stability limit based on mixture velocity is lower in the case of the smaller burner (Figure 4-17), its maximum power output density is higher than the larger burner. The two opposite effects offer a trade-off between wider stability range and higher power output density. For practical applications, in order to

compensate the narrower stability range for smaller diameters while maintaining the high power density merit, a longer burner can be used.

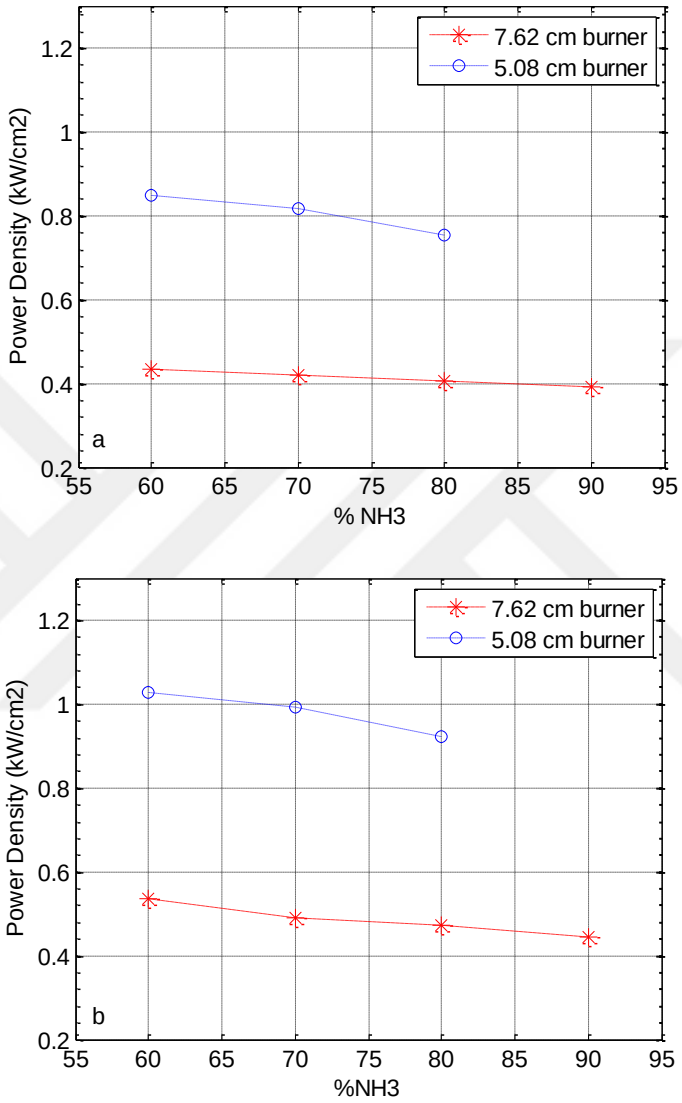

Figure 4-19 Maximum power output density criteria for burners with different diameters for ϕ=1.1 (a) and ϕ=1.3 (b).

It is useful to note that the maximum power density achieved by the methane-air premixed flame in the same experimental setup with a different flame stabilizing method was 0.45 kW/cm^2 [73]. Whereas the power generation density of the porous medium based burner system studied in this paper, even with a lower energy fuel, reaches up to 1.1 kW/cm^2.

4.3.5 NO_x emission

Direct NO_x measurements obtained at the combustor exhaust as well as the chemical kinetics predictions for the NO_x concentrations are presented in Figure 4-20 for mixtures with 70% and 80% NH_3.

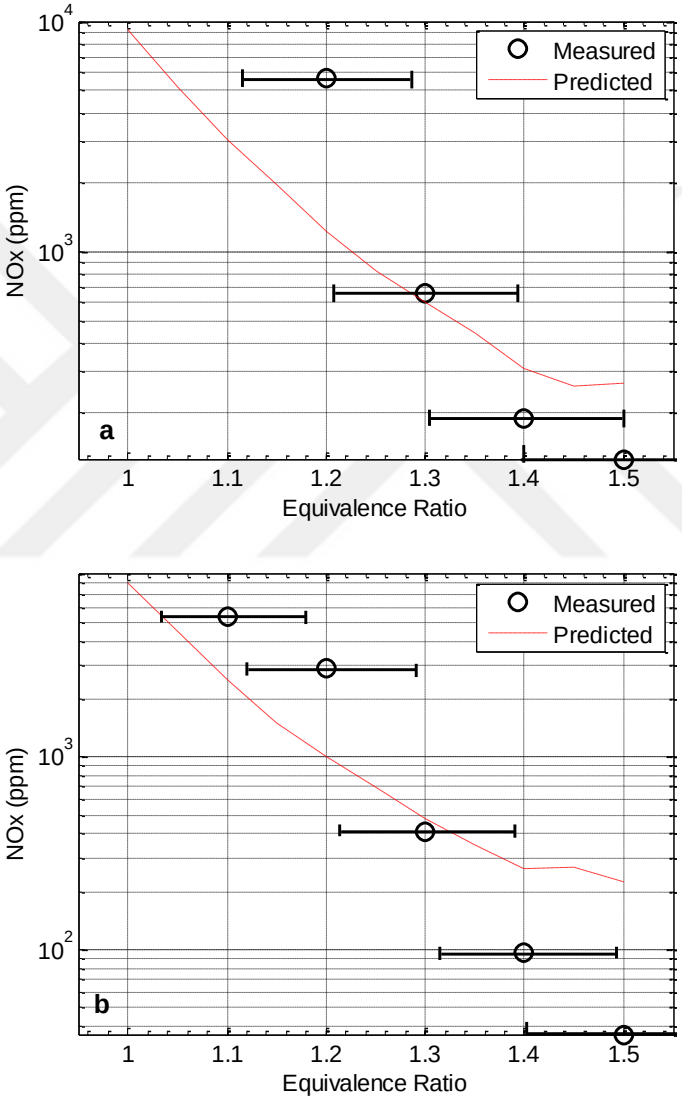

Figure 4-20 Exhaust NOx concentrations for (a) 70% NH_3 and (b) 80% NH_3.

The results indicate that the experimentally measured NO_x follows the trend of the chemical kinetics predictions. As presented in the figure, the high measurement errors associated with the air flow rotameter introduces a relatively wide uncertainty range in

the measured equivalence ratio. However, regardless of the uncertainty in the equivalence ratio values, we observe remarkably lower experimental NO_x concentrations at equivalence ratios higher than 1.3 approaching to a level of 35 ppm for the equivalence ratio of 1.5. We believe that this interesting behavior is a result of three possible mechanisms:

- With increasing equivalence ratio from stoichiometric to the richer end of the interval, flame temperature decreases dramatically (this effect was well discussed in chapter 3). This directly causes a drop in thermal NO_x formation.
- The well-known NO_x reduction mechanism caused by the small but finite concentration of ammonia molecules, that go through the burner under rich conditions, is potentially an influential factor [20].
- Higher equivalence ratio means lower concentration of oxygenated species in the flame zone. As discussed before, oxygenated spesies react with NH_i precursors to form fuel NO_x. Thus, with increasing the equivalence ratio less amount of fuel bond NO_x is expected.

It is notable that no significant mechanical or chemical change was observed in the inert porous blocks after being used for all the tests. However, it is critical to ensure structural resistance and durability of the blocks to be used in real combustors under long-term full-scale operational conditions. Furthermore, it should be stated that the porous media used in the experiments are easily available at minor cost.

4.4 Concluding remarks

Stability, combustion efficiency, and NO_x emissions of ammonia-hydrogen-air premixed flames have been investigated in this chapter. An inert porous medium based burner is introduced, which is capable of providing stable combustion at high burning speeds over a wide range of mixture compositions and equivalence ratios. Stability maps for the porous medium based burners, which can be applied to the design of practical combustors, have been established. The major conclusions can be summarized as the following.

- Measured temperature profile captures the adiabatic flame temperature trend with an acceptable level of accuracy.
- Heat loss is verified to be the main mechanism responsible for lower measured temperatures rather than incomplete combustion.
- Combustion efficiency, which is estimated by comparing the measured temperatures with the simulation results, is proved to be higher than 95% for all conditions studied in this chapter.
- A decrease in lower and upper stability limits occurs with increasing ammonia mixture fraction which is mainly resulted by lower flame speed of mixture with higher ammonia fraction.
- Flame holding capability is improved up to 40% for the porous medium burner compared to a same diameter dump combustor counterpart.
- Higher equivalence ratios provide a wider stability region by increasing the upper limit and also decreasing the lower limit. This behavior is rooted in the excess fuel remaining unreacted in the burner which reacts with the ambient air just downstream of the burner postponing the extinction and blow-off.
- Reducing the burner diameter leads to a narrowing in the flame stability region due to the shorter resistance time of the mixture in the burner.

- Power output density of the smaller burner is determined to be higher than the larger burner. Burner size is therefore an important design parameter directly affects the power density and the stability range.
- Noticeably higher power generation density is achieved for the ammonia-hydrogen mixtures (even at high ammonia concentrations such as 90%) in the porous medium based burners compared to the similar premixed methane-air flame on the same setup with a different type of burner.
- NO_x emission measurements show low levels of NO_x concentration at rich equivalence ratios.

The porous medium based burners open a new vista for combusting ammonia without increasing operational complexities or costs of existing power generation systems. We believe that there is still ample room for further improvements in the power generation densities, efficiencies, and NO_x emissions for this type of combustors following a rigorous optimization process.

CHAPTER 5

CONCLUSION

Due to its high hydrogen density and extensive experience base, ammonia is believed to be an excellent alternative fuel that can be used in energy generation and transportation systems. A huge benefit associated with a hypothetical "ideal fuel" would be the ability to produce it from any and all primary energy sources. As discussed in the introduction of this thesis, it takes a relatively small amount of additional energy to produce NH_3 once hydrogen has been produced via electrolysis or other means.

Combustion of ammonia has certain challenges (associated with its low flame speed and fuel bond NO_x emissions) that need to be addressed before its widespread use in practical systems. The successful application of ammonia as an alternative transportation or power generation fuel should be based on a profound understanding of its combustion characteristics.

The primary goal of the current Ph.D research is to find a way to combust ammonia in an efficient and environmentally benign way. Accordingly this dissertation encompasses the chemical kinetics and experimental investigation of important combustion characteristics of ammonia. In the third chapter the combustion characteristics of NH_3/H_2/air mixtures at elevated pressures and under lean conditions are examined numerically. It is revealed that the radicals have strong influence on the combustion characteristics. Under high pressure and fuel lean conditions, OH is the most influential radical contributing to ammonia decomposition and flame speed, followed by other effective radicals such as H, O, and NH_2. By adding hydrogen to the fuel mixture, the combustion characteristics such as ignition delay time and laminar flame speed are noticeably improved. The improvement in combustion characteristics is of high importance in the real world applications in the sense that the ammonia operational drawbacks (low flame speed and high ignition delay time) are compensated.

Also, a comprehensive NO_x formation sensitivity analysis is conducted. The complex chemistry of NO_x formation is highly dependent on the fuel mixture composition which controls the contribution of fuel NO_x and thermal NO_x levels. This could lead to a trade-off situation in choosing the optimal fuel composition for engine applications. It is deduced that the total NO_x formation of ammonia doped flames would noticeably decrease by operating under fuel rich conditions.

As an important outcome of the chemical kinetics study, two reduced reaction mechanisms are established based on the detailed Konnov mechanism to predict the laminar flame speed and NO_x emission levels. The performance evaluation and efficiency analysis of the reduced mechanisms (regarding the full mechanism and the experimental data) reveal their high accuracy in predicting the combustion characteristics in a wide range of equivalence ratios, mixture compositions, and pressures. It is inferred that the reduced mechanisms can effectively reduce the simulation time while maintaining the reliable accuracy of Konnov mechanism.

Following the chemical kinetics invesigatrion, an experimental study is conducted on a lab-scale combustion chamber through which the main challenges of ammonia doped flames are addressed. Stability, combustion efficiency, and NO_x emissions of ammonia-hydrogen-air premixed flames have been investigated in chapter 4. An inert porous medium based burner is introduced, which is capable of providing stable combustion at high burning speeds over a wide range of mixture compositions and equivalence ratios. Stability maps for the porous medium based burners, which can be applied to the design of practical combustors, have been established.

It is observed that the measured temperature profile captures the adiabatic flame temperature trend with an acceptable level of accuracy. Accordingly, the difference between the measured temperatures and the predicted counterparts is further studied. Heat loss is verified to be the main mechanism responsible for lower measured temperatures rather than incomplete combustion. Combustion efficiency, which is estimated by comparing the measured temperatures with the simulation results, is proved to be higher than 95% for all conditions studied in this project.

As another critical parameter in ammonia combustion, flame stability of ammonia-hydrogen-air mixtures is thoroughly investigated. By determining the upper and lower stability limits for each mixture composition, stability maps for the burner are obtained. The stability maps are helpful tools in adapting the burners to practical systems with an accurate prediction of operating range under similar test conditions. A decrease in lower and upper stability limits occurs with increasing ammonia mixture fraction which is mainly resulted by lower flame speed of mixture with higher ammonia fraction. Higher equivalence ratios provide a wider stability region by increasing the upper limit and also decreasing the lower limit. This behavior is rooted in the excess fuel remaining unreacted in the burner which reacts with the ambient air just downstream of the burner postponing the extinction and blow-off.

To verify the high effectiveness of the porous medium based burners in stabilizing the mixtures, a comparison is performed with a dump combustor burner regarding the flame stabilizing capability. It is observed that the flame holding capability is improved up to 40% for the porous medium burner compared to a same diameter dump combustor counterpart. Effect of burner diameter is also examined. It is concluded that reducing the burner diameter leads to a narrowing in the flame stability region due to the shorter resistance time of the mixture in the burner. As an important attribute of a combustor in applied-based perspective, power output density is evaluated for the porous medium based burners. Noticeably higher power generation density is achieved for the ammonia-hydrogen mixtures (even at high ammonia concentrations such as 90%) in the porous medium based burners compared to the similar premixed methane-air flame on the same setup with a different type of burner. Also power output density of the smaller burner is determined to be higher than the larger burner. Burner size is therefore an important design parameter directly affecting the power density and the stability range.

Finally, NO_x formation behavior is studied as a function of equivalence ratio. Emission measurements show noticeably low levels of NO_x concentration at rich equivalence ratios.

Putting together all the studied operational parameters of the porous medium based burners, it is concluded that the burners open a new vista for combusting ammonia without increasing operational complexities or costs of existing power generation systems. We believe that there is still ample room for further improvements in the power generation densities, efficiencies, and NO_x emissions for this type of combustors following a rigorous optimization process.

This thesis has brought some learnings and ideas on the potential use of ammonia as a fuel in power generation systems. The major challenges of ammonia combustion are addressed and methods to compensate the drawbacks are introduced. There is still a lot of room for improvement in developing methods for further improvement of the combustion quality of ammonia. Porous medium based burner is introduced as an effective method to elevate the stability and combustion efficiency, and to lower the NO_x emission. Further research is required to determine effects of the burner geometry on combustion characteristics. Followingly, configuration optimization can be established for various applications based on the operational requirements. Further elevation of power output density by integrating the porous burner with some other flame stabilizers can be investigated and optimized. Finally, numerical simulations should be performed to reproduce ammonia combustion under the engine conditions. The reduced ammonia combustion mechanism elaborated in this thesis should be integrated in a CFD code in order to perform these simulations.

Appendix 1

Flow charts

The mole fractions and corresponding volume flow rates of the fuel and air streams are presented in Tables A-1. The table established based on the burner inlet mixture velocity of 7 m/s. For all the studied mixture compositions the flames formed with this inlet velocity are stable.

Table A - 1 Mole fractions and inlet volume flow rates of fuel and air streams.

ϕ	%Vol. NH_3	X_{NH3}	X_{H2}	X_{air}	Q_{NH3}(lit/min)	Q_{H2}(lit/min)	Q_{air} (lit/min)
1,5	90	0,2727	0,0303	0,697	46,35	5,15	118,47
	85	0,2607	0,046	0,6933	44,31	7,82	117,84
	80	0,2483	0,0621	0,6896	42,20	10,56	117,21
	75	0,2357	0,0786	0,6857	40,06	13,36	116,55
	70	0,2228	0,0955	0,6817	37,87	16,23	115,87
	60	0,1959	0,1306	0,6735	33,30	22,20	114,48

ϕ	%Vol. NH_3	X_{NH3}	X_{H2}	X_{air}	Q_{NH3}(lit/min)	Q_{H2}(lit/min)	Q_{air} (lit/min)
1,4	90	0,2597	0,0289	0,7114	44,14	4,91	120,92
	85	0,2484	0,0438	0,7078	42,22	7,44	120,31
	80	0,2367	0,0592	0,7041	40,23	10,06	119,68
	75	0,2247	0,0749	0,7004	38,19	12,73	119,05
	70	0,2124	0,091	0,6965	36,10	15,47	118,40
	60	0,1869	0,1246	0,6885	31,77	21,18	117,03

ϕ	%Vol. NH_3	X_{NH3}	X_{H2}	X_{air}	Q_{NH3}(lit/min)	Q_{H2}(lit/min)	Q_{air} (lit/min)
1,3	90	0,2463	0,0274	0,7264	41,86	4,66	123,45
	85	0,2355	0,0416	0,7229	40,03	7,07	122,87
	80	0,2245	0,0561	0,7193	38,16	9,54	122,28
	75	0,2132	0,0711	0,7157	36,24	12,09	121,65
	70	0,2016	0,0864	0,7119	34,27	14,69	121,02
	60	0,1897	0,1022	0,7081	32,24	17,37	120,36

ϕ	%Vol. NH_3	X_{NH3}	X_{H2}	X_{air}	Q_{NH3}(lit/min)	Q_{H2}(lit/min)	Q_{air} (lit/min)
1,2	90	0,2322	0,0258	0,742	39,47	4,39	126,12
	85	0,2221	0,0392	0,7386	37,75	6,66	125,56
	80	0,2118	0,053	0,7352	36,00	9,01	124,96
	75	0,2012	0,0671	0,7317	34,20	11,41	124,37
	70	0,1903	0,0816	0,7281	32,35	13,87	123,76
	60	0,1677	0,1118	0,7205	28,50	19,00	122,47

ϕ	%Vol. NH_3	X_{NH3}	X_{H2}	X_{air}	Q_{NH3}(lit/min)	Q_{H2}(lit/min)	Q_{air} (lit/min)
1,1	90	0,2175	0,0242	0,7583	36,97	4,11	128,89
	85	0,2082	0,0367	0,7551	35,39	6,24	128,35
	80	0,1986	0,0496	0,7518	33,76	8,43	127,79
	75	0,1887	0,0629	0,7484	32,07	10,69	127,21
	70	0,1785	0,0765	0,745	30,34	13,00	126,63
	60	0,1574	0,1049	0,7377	26,75	17,83	125,39

ϕ	%Vol. NH_3	X_{NH3}	X_{H2}	X_{air}	Q_{NH3}(lit/min)	Q_{H2}(lit/min)	Q_{air} (lit/min)
1	90	0,2022	0,0225	0,7753	34,37	3,82	131,78
	85	0,1936	0,0342	0,7723	32,91	5,81	131,25
	80	0,1847	0,0462	0,7692	31,39	7,85	130,73
	75	0,1755	0,0585	0,7659	29,83	9,94	130,20
	70	0,1662	0,0712	0,7626	28,25	12,10	129,62
	60	0,1466	0,0977	0,7557	24,92	16,61	128,45

ϕ	%Vol. NH_3	X_{NH3}	X_{H2}	X_{air}	Q_{NH3}(lit/min)	Q_{H2}(lit/min)	Q_{air} (lit/min)
0,9	90	0,1862	0,0207	0,7932	31,65	3,52	134,81
	85	0,1783	0,0315	0,7903	30,31	5,35	134,31
	80	0,1701	0,0425	0,7873	28,91	7,22	133,84
	75	0,1618	0,0539	0,7843	27,50	9,16	133,31
	70	0,1532	0,0656	0,7812	26,04	11,15	132,78
	60	0,1352	0,0901	0,7747	22,98	15,31	131,68

Appendix 2

Ammonia safety

Safety factor associated with the use of ammonia is an important issue to be considered. Ammonia is a poisonous gas with an OSHA[1] exposure limit of 50 ppm [76]. Its health effects are summarized in Table A-2 [2] Nevertheless, ammonia is a commonly used industrial and agricultural chemical for which the safety handling protocols are well established and it is handled by skilled and professional people.

Table A - 2 Ammonia health effects.

Effect	Ammonia volumetric concentration in air (ppm)
Least perceptible odor	5
Readily detectable odor	20-50
No discomfort or impairment of health for prolonged exposure	50-100
General discomfort and eye tearing; no lasting effect on short exposure	150-200
Severe irritation of eyes, ears, nose and throat, no lasting effect on short exposure	400-700
Coughing, bronchial spasms	1700
Dangerous, less than ½ hour exposure may be fatal	2000-3000
Serious edema, strangulation, asphyxia, rapidly fatal	5000-10000

Although the low detectability level may be cited as a positive safety factor in detecting leaks, a pervasive odor in the vicinity of high use areas may be against the perception of

[1] Occupational safety and Health Adminstration

a “clean” fuel. However, ammonia used as a fertilizer and refrigerant has an excellent, decades-long safety record. Making ammonia acceptably safe from a statistical standpoint is an easily solved engineering design issue. There are risks associated with the use of ammonia as a fuel however all fuels have inherent dangers associated with their use.

Appendix 3

Reaction Mechanisms

Arrhenius rate expression

In most chemical reactions, the reaction rates are based on collisions of two reactants that may have the required conditions to react and form the products. If we consider an elementary reaction in the form of $A + B \rightarrow C + D$ the reaction rate expression can be presented as the following [74].

$$-RR = \frac{d[A]}{dt} = \frac{d[B]}{dt} = -\frac{d[D]}{dt} = -\frac{d[C]}{dt} = -k[A][B] \qquad (23)$$

The specific presentation of reaction does not mean the every collision of the reactants (A and B) would lead to reaction and formation of the products (C and D). Based on a theory by Arrhenius, temperature plays an important role in determining the reaction capability of the reactants. According to his theory, only the molecules which have greater energy than the activation energy (E) can react. In chemical kinetics studies a uniform expression is used for rate constant:

$$k = AT^{b}\exp(-E/(RT)) \qquad (24)$$

The term $(-E/(RT))$ is referred as Boltzmann factor. Basically the Boltzmann factor presents the fraction of collisions which have a transitional kinetic energy along the internuclear axis greater that the activation energy. Therefore the energy term in the factor can be considered as the barrier along a potential energy surface for the reactants towards the products.

A is referred as the kinetic pre-exponential factor. It takes into account the steric orientation factor and collision frequency. It is important to note that inclusion of the temperature term along with the pre-exponential factor provide a more general for to the Arrhenius expression and the resulting form is referred as modified Arrhenius

expression. Most elementary reactions show Arrhenius behavior, thus the temperature exponent is zero. However, because of the wide range of temperatures in combustion reactions, inclusion of the temperature term is essential for the reactions and temperature ranges exhibiting non-Arrhenius behavior. To better understand the effect of T-E combination on the reaction rate, the rate constant is plotted against the temperature reciprocal based on Arrhenius expression in Figure A-1.

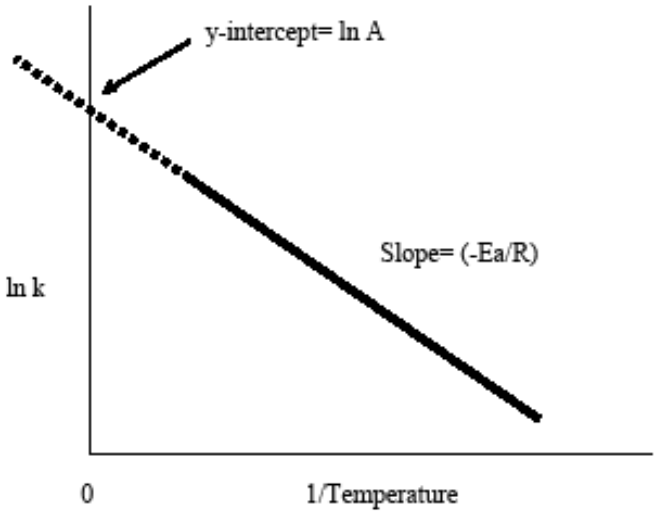

Figure A - 1 Effect of temperature on rate constant in Arrhenius expression.

Due to the graph it is inferred that at low temperatures, the processes with lower activation energies proceed faster and are less sensitive to temperature. However, at high temperatures, the reactions with high activation energy dominate due to the temperature sensitivity.

Appendix 3 Reaction Mechanisms

Reduced reaction mechanisms

The reduced mechanisms are presented in the following table.

Table A - 3 Reduced reaction mechanisms.

Red. Mech. # 2 Reactions	Red. Mech. # 1 Reactions	A (cm^3 mol^{-1} s^{-1})	b	E (cal/mole)
✓	H+H+M=H2+M	7.000E+17	-1.0	0.0
	Enhanced third-body efficiencies: H2=0.0, N2=0.0, H=0.0, H2O=14.3			
✓	H+H+N2=H2+N2	5.400E+18	-1.3	0.0
✓	O+O+M=O2+M	1.000E+17	-1.0	0.0
✓	O+H2=OH+H	5.060E+04	2.67	6290.0
✓	H+O2=OH+O	9.75E+13	0.0	14850.0
✓	H+O2(+M)=HO2(+M)	1.48E+12	0.6	0.0
	Low pressure limit	0.35000E+17	-0.41000E+00	-0.11160E+04
	TROE centering:	0.50000E+00	0.10000E+06	0.10000E+02
	Enhanced third-body efficiencies:H2O=10.6, H2=1.5			
✓	H+OH+M=H2O+M	2.200E+22	-2.0	0.0
	Enhanced third-body efficiencies: H2O=6.4			
✓	H2+OH=H2O+H	1.00E+08	1.6	3300.0
✓	OH+OH=H2O+O	1.50E+09	1.1	100.0
✓	HO2+OH=H2O+O2	2.89E+13	0.0	-500.0
✓	HO2+O=OH+O2	1.630E+13	0.0	-445.0
✓	H+HO2=H2+O2	4.280E+13	0.0	1411.0
✓	H+HO2=OH+OH	1.700E+14	0.0	875.0
✓	H+HO2=H2O+O	3.000E+13	0.0	1720.0
✓	N2+O=NO+N	1.800E+14	0.0	76100.0
✓	NH3+M=NH2+H+M	2.200E+16	0.0	93470.0
✓	NH3+H=NH2+H2	5.420E+05	2.4	9920.0
✓	NH3+O=NH2+OH	1.100E+06	2.1	5210.0
✓	NH3+OH=NH2+H2O	5.000E+07	1.6	950.0

✓	NH3+NH=NH2+NH2	3.160E+14	0.0	26770.0
✓	NH2+M=NH+H+M	3.160E+23	-2.0	91400.0
✓	NH2+N=N2+H+H	6.900E+13	0.0	0.0
✓	NH2+NH=N2H2+H	1.500E+15	-0.5	0.0
✓	NH2+NH=NH3+N	1.000E+13	0.0	2000.0
✓	NH2+NH2=N2H2+H2	1.000E+13	0.0	1500.0
✓	NH2+O=H2+NO	5.000E+12	0.0	0.0
✓	NH2+O=HNO+H	4.500E+13	0.0	0.0
✓	NH2+O=NH+OH	7.000E+12	0.0	0.0
✓	NH2+OH=NH+H2O	9.000E+07	1.5	-460.0
✓	NH2+HO2=HNO+H2O	5.680E+15	-1.12	707.0
✓	NH2+O2=HNO+OH	1.000E+13	0.0	26290.0
✓	NH2+NO=NNH+OH	2.290E+10	0.425	-814.0
✓	NH2+NO=N2+H2O	2.770E+20	-2.65	1258.0
✓	NH2+NO=H2+N2O	1.000E+13	0.0	33700.0
✓	NH2+NO2=N2O+H2O	1.620E+16	-1.44	270.0
✓	NH+H=N+H2	3.200E+13	0.0	325.0
✓	NH+N=N2+H	9.000E+11	0.5	0.0
✓	NH+NH=NNH+H	5.100E+13	0.0	0.0
✓	NH+O=NO+H	7.000E+13	0.0	0.0
✓	NH+O=N+OH	7.000E+12	0.0	0.0
✓	NH+OH=HNO+H	2.000E+13	0.0	0.0
✓	NH+OH=N+H2O	2.000E+09	1.2	0.0
✓	NH+OH=NO+H2	2.000E+13	0.0	0.0
✓	NH+O2=HNO+O	4.000E+13	0.0	17880.0
✓	NH+O2=NO+OH	4.500E+08	0.79	1190.0
✓	NH+H2O=HNO+H2	2.000E+13	0.0	13850.0
✓	NH+N2O=N2+HNO	2.000E+12	0.0	6000.0
✓	NH+NO=N2+OH	6.100E+13	-0.50	120.0

✓	N+OH=NO+H	2.800E+13	0.0	0.0
✓	N+O2=NO+O	9.000E+09	1.0	6500.0
✓	NO+O(+M)=NO2(+M)	1.30E+15	-0.8	0.0
	Low pressure limit:	0.47200E+25	-0.28700E+01	0.15510E+04
	TROE centering:	0.96200E+00	0.10000E+02	0.79620E+04
	Enhanced third-body efficiencies:NO2=6.2, NO =1.8, O2=0.8, N2O=4.4, H2O=10			
✓	H+NO(+M)=HNO(+M)	1.52E+15	-0.4	0.0
	Low pressure limit:	0.40000E+21	-0.17500E+01	0.0
	Enhanced third-body efficiencies:H2O=10, O2=1.5, H2=2			
✓	N2O(+M)=N2+O(+M)	1.260E+12	0.0	62620.0
	Low pressure limit:	4.000E+14	0.0	56640.0
	Enhanced third-body efficiencies: O2=1.4, N2=1.7, H2O=12.0, NO=3.0, N2O=3.5			
✓	N2O+O=N2+O2	1.000E+14	0.0	28200.0
✓	N2O+O=NO+NO	6.920E+13	0.0	26630.0
✓	N2O+NO=N2+NO2	2.750E+14	0.0	50000.0
✓	N2O+H=N2+OH	2.200E+14	0.0	16750.0
✓	N2O+OH=N2+HO2	1.000E+14	0.0	30000.0
✓	NO2+O=NO+O2	3.910E+12	0.0	-238.0
✓	NO2+H=NO+OH	1.320E+14	0.0	362.0
✓	NO2+OH=HO2+NO	1.810E+13	0.0	6676.0
✓	HNO+H=NO+H2	4.460E+11	0.72	655.0
✓	HNO+OH=NO+H2O	1.300E+07	1.88	-956.0
✓	HNO+O=OH+NO	5.000E+11	0.5	2000.0
✓	HNO+NH2=NH3+NO	2.000E+13	0.0	1000.0
✓	NNH=N2+H	3.000E+08	0.0	0.0
✓	NNH+M=N2+H+M	1.000E+13	0.5	3060.0
✓	NNH+O=NH+NO	2.000E+14	0.0	4000.0
✓	NNH+O2=N2O+OH	2.900E+11	-0.34	150.0
✓	NNH+NO=N2+HNO	5.000E+13	0.0	0.0

✓	N2H2+M=NNH+H+M	5.000E+16	0.0	50000.0
	Enhanced third-body efficiencies: H2O=15.0, O2=2.0, N2=2.0, H2=2.0			
✓	N2H2+H=NNH+H2	8.500E+04	2.63	-230.0
✓	N2H2+NH2=NH3+NNH	8.800E-02	4.05	-1610.0
✓	N2H2+O=NH2+NO	1.000E+13	0.0	0.0
✓	N2H2+O=NNH+OH	2.000E+13	0.0	1000.0
✓	N2H2+OH=NNH+H2O	5.920E+01	3.4	-1360.0
✓	N2H2+NO=N2O+NH2	3.000E+10	0.0	0.0
X	NH+H2=NH2+H	1.000E+14	0.0	20070.0
X	N2O+H=NH+NO	6.700E+22	-2.16	37155.0
X	H2NO+NO=HNO+HNO	2.000E+07	2.0	13000.0
X	NH2+HO2=H2NO+OH	2.91E+17	-1.3	1248.0
X	NH2+O2=H2NO+O	6.000E+13	0.0	29880.0
X	H2NO+O=HNO+OH	3.000E+07	2.0	2000.0
X	H2NO+H=HNO+H2	3.000E+07	2.0	2000.0
X	HNO+NH=NH2+NO	5.000E+11	0.5	0.0
X	H2NO+H=NH2+OH	5.000E+13	0.0	0.0
X	N2H4(+M)=NH2+NH2(+M)	5.000E+14	0.0	60000.0
	Low pressure limit:	1.50E+15	0.0	39000.0
	Enhanced third-body efficiencies: N2=2.4, NH3=3.0, N2H4=4.0			
X	N2H4+O=N2H2+H2O	8.500E+13	0.0	1200.0
X	NH3+NH2=N2H3+H2	1.000E+11	0.5	21600.0
X	N2H4+NH=NH2+N2H3	1.000E+09	1.5	2000.0
X	N2H3+M=N2H2+H+M	1.000E+16	0.0	37000.0

Appendix 3 Reaction Mechanisms

Konnov Mechanism

ELEMENTS H O N

SPECIES

H H2 O O2 OH HO2 H2O H2O2 N NH NO N2O NH2 N2O3 HNO NO2 NNH NH3 N2H2 HONO NO3 HNO3 N2H3 N2H4 N2O4 NH2OH HNOH H2NO HNNO

REACTION STEPS

			A (cm3 mol-1 s-1)	b	E (cal mole-1)
1. H+H+M=H2+M			7.00E+17	-1.0	0.0
H2	Enhanced by	0.000E+00			
N2	Enhanced by	0.000E+00			
H	Enhanced by	0.000E+00			
H2O	Enhanced by	1.430E+01			
2. H+H+H2=H2+H2			1.00E+17	-0.6	0.0
3. H+H+N2=H2+N2			5.40E+18	-1.3	0.0
4. H+H+H=H2+H			3.20E+15	0.0	0.0
5. O+O+M=O2+M			1.00E+17	-1.0	0.0
O	Enhanced by	7.100E+01			
O2	Enhanced by	2.000E+01			
NO	Enhanced by	5.000E+00			
N2	Enhanced by	5.000E+00			
N	Enhanced by	5.000E+00			
H2O	Enhanced by	5.000E+00			
6. O+H+M=OH+M			6.20E+16	-0.6	0.0
H2O	Enhanced by	5.000E+00			
7. H2+O2=OH+OH			2.50E+12	0.0	39000.0
8. O+H2=OH+H			5.06E+04	2.7	6290.0
9. H+O2=OH+O			9.75E+13	0.0	14850.0
10. H+O2(+M)=HO2(+M)			1.48E+12	0.6	0.0

Low pressure limit: 0.35000E+17 -0.41000E+00 -0.11160E+04				
TROE centering: 0.50000E+00 0.10000E+06 0.10000E+02				
H2O	Enhanced by 1.060E+01			
H2	Enhanced by 1.500E+00			
11. H+OH+M=H2O+M		2.20E+22	-2.0	0.0
H2O	Enhanced by 6.400E+00			
12. H2+OH=H2O+H		1.00E+08	1.6	3300.0
13. OH+OH=H2O+O		1.50E+09	1.1	100.0
14. HO2+OH=H2O+O2		2.89E+13	0.0	-500.0
15. HO2+O=OH+O2		1.63E+13	0.0	-445.0
16. H+HO2=H2+O2		4.28E+13	0.0	1411.0
17. H+HO2=OH+OH		1.70E+14	0.0	875.0
18. H+HO2=H2O+O		3.00E+13	0.0	1720.0
19. HO2+HO2=H2O2+O2		4.20E+14	0.0	12000.0
20. HO2+HO2=H2O2+O2		1.30E+11	0.0	-1640.0
21. OH+OH(+M)=H2O2(+M)		7.20E+13	-0.4	0.0
Low pressure limit: 0.22000E+20 -0.76000E+00 0.00000E+00				
TROE centering: 0.50000E+00 0.10000E+06 0.10000E+02				
H2O	Enhanced by 0.000E+00			
22. OH+OH(+H2O)=H2O2(+H2O)		7.20E+13	-0.4	0.0
Low pressure limit: 0.14500E+19 0.00000E+00 0.00000E+00				
23. H2O2+OH=HO2+H2O		1.00E+12	0.0	0.0
24. H2O2+OH=HO2+H2O		5.80E+14	0.0	9560.0
25. H2O2+H=HO2+H2		1.70E+12	0.0	3755.0
26. H2O2+H=H2O+OH		1.00E+13	0.0	3575.0
27. H2O2+O=HO2+OH		2.80E+13	0.0	6400.0
28. N2+O=NO+N		1.80E+14	0.0	76100.0
29. N+O2=NO+O		9.00E+09	1.0	6500.0
30. NO+M=N+O+M		9.64E+14	0.0	148300.0

N2	Enhanced by	1.500E+00		
NO	Enhanced by	3.000E+00		
31. NO+NO=N2+O2			3.00E+11	0.0	65000.0
32. N2O(+M)=N2+O(+M)			1.26E+12	0.0	62620.0
Low pressure limit:	0.40000E+15	0.00000E+00	0.56640E+05		
O2	Enhanced by	1.400E+00		
N2	Enhanced by	1.700E+00		
H2O	Enhanced by	1.200E+01		
NO	Enhanced by	3.000E+00		
N2O	Enhanced by	3.500E+00		
33. N2O+O=N2+O2			1.00E+14	0.0	28200.0
34. N2O+O=NO+NO			6.92E+13	0.0	26630.0
35. N2O+N=N2+NO			1.00E+13	0.0	20000.0
36. N2O+NO=N2+NO2			2.75E+14	0.0	50000.0
37. NO+O(+M)=NO2(+M)			1.30E+15	-0.8	0.0
Low pressure limit:	0.47200E+25	-0.28700E+01	0.15510E+04		
TROE centering:	0.96200E+00	0.10000E+02	0.79620E+04		
NO2	Enhanced by	6.200E+00		
NO	Enhanced by	1.800E+00		
O2	Enhanced by	8.000E-01		
N2O	Enhanced by	4.400E+00		
H2O	Enhanced by	1.000E+01		
38. NO2+O=NO+O2			3.91E+12	0.0	-238.0
39. NO2+N=N2O+O			8.40E+11	0.0	0.0
40. NO2+N=NO+NO			1.00E+12	0.0	0.0
41. NO2+NO=N2O+O2			1.00E+12	0.0	60000.0
42. NO2+NO2=NO+NO+O2			3.95E+12	0.0	27590.0
43. NO2+NO2=NO3+NO			1.13E+04	2.6	22720.0
44. NO2+O(+M)=NO3(+M)			1.33E+13	0.0	0.0

Low pressure limit: 0.14900E+29 -0.40800E+01 0.24670E+04				
TROE centering: 0.86000E+00 0.10000E+02 0.28000E+04				
H2O	Enhanced by 1.000E+01			
O2	Enhanced by 8.000E-01			
H2	Enhanced by 2.000E+00			
45. NO3=NO+O2		2.50E+06	0.0	12120.0
46. NO3+NO2=NO+NO2+O2		1.20E+11	0.0	3200.0
47. NO3+O=NO2+O2		1.02E+13	0.0	0.0
48. NO3+NO3=NO2+NO2+O2		5.12E+11	0.0	4870.0
49. N2O4(+M)=NO2+NO2(+M)		4.05E+18	-1.1	12840.0
Low pressure limit: 0.19600E+29 -0.38000E+01 0.12840E+05				
N2O4	Enhanced by 2.000E+00			
NO2	Enhanced by 2.000E+00			
50. N2O4+O=N2O3+O2		1.21E+12	0.0	0.0
51. NO2+NO(+M)=N2O3(+M)		1.60E+09	1.4	0.0
Low pressure limit: 0.10000E+34 -0.77000E+01 0.00000E+00				
N2	Enhanced by 1.360E+00			
52. N2O3+O=NO2+NO2		2.71E+11	0.0	0.0
53. N2+M=N+N+M		1.00E+28	-3.3	225000.0
N	Enhanced by 5.000E+00			
O	Enhanced by 2.200E+00			
54. NH+M=N+H+M		2.65E+14	0.0	75500.0
55. NH+H=N+H2		3.20E+13	0.0	325.0
56. NH+N=N2+H		9.00E+11	0.5	0.0
57. NH+NH=NNH+H		5.10E+13	0.0	0.0
58. NH+NH=NH2+N		5.95E+02	2.9	-2030.0
59. NH+NH=N2+H2		1.00E+08	1.0	0.0
60. NH2+M=NH+H+M		3.16E+23	-2.0	91400.0
61. NH+H2=NH2+H		1.00E+14	0.0	20070.0

62. NH2+N=N2+H+H			6.90E+13	0.0	0.0
63. NH2+NH=N2H2+H			1.50E+15	-0.5	0.0
64. NH2+NH=NH3+N			1.00E+13	0.0	2000.0
65. NH3+NH=NH2+NH2			3.16E+14	0.0	26770.0
66. NH2+NH2=N2H2+H2			1.00E+13	0.0	1500.0
67. N2H3+H=NH2+NH2			5.00E+13	0.0	2000.0
68. NH3+M=NH2+H+M			2.20E+16	0.0	93470.0
69. NH3+M=NH+H2+M			6.30E+14	0.0	93390.0
70. NH3+H=NH2+H2			5.42E+05	2.4	9920.0
71. NH3+NH2=N2H3+H2			1.00E+11	0.5	21600.0
72. NNH=N2+H			3.00E+08	0.0	0.0
73. NNH+M=N2+H+M			1.00E+13	0.5	3060.0
74. NNH+H=N2+H2			1.00E+14	0.0	0.0
75. NNH+N=NH+N2			3.00E+13	0.0	2000.0
76. NNH+NH=N2+NH2			2.00E+11	0.5	2000.0
77. NNH+NH2=N2+NH3			1.00E+13	0.0	0.0
78. NNH+NNH=N2H2+N2			1.00E+13	0.0	4000.0
79. N2H2+M=NNH+H+M			5.00E+16	0.0	50000.0
H2O	Enhanced by	1.500E+01			
O2	Enhanced by	2.000E+00			
N2	Enhanced by	2.000E+00			
H2	Enhanced by	2.000E+00			
80. N2H2+M=NH+NH+M			3.16E+16	0.0	99400.0
H2O	Enhanced by	1.500E+01			
O2	Enhanced by	2.000E+00			
N2	Enhanced by	2.000E+00			
H2	Enhanced by	2.000E+00			
81. N2H2+H=NNH+H2			8.50E+04	2.6	-230.0
82. N2H2+N=NNH+NH			1.00E+06	2.0	0.0

83. N2H2+NH=NNH+NH2	1.00E+13	0.0	6000.0
84. N2H2+NH2=NH3+NNH	8.80E-02	4.0	-1610.0
85. N2H3+NH=N2H2+NH2	2.00E+13	0.0	0.0
86. N2H3+NNH=N2H2+N2H2	1.00E+13	0.0	4000.0
87. N2H3+M=NH2+NH+M	5.00E+16	0.0	60000.0
88. N2H3+M=N2H2+H+M	1.00E+16	0.0	37000.0
89. N2H3+H=N2H2+H2	1.00E+13	0.0	0.0
90. N2H3+H=NH+NH3	1.00E+11	0.0	0.0
91. N2H3+N=N2H2+NH	1.00E+06	2.0	0.0
92. N2H3+NH2=NH3+N2H2	1.00E+11	0.5	0.0
93. N2H3+N2H2=N2H4+NNH	1.00E+13	0.0	6000.0
94. N2H3+N2H3=NH3+NH3+N2	3.00E+12	0.0	0.0
95. N2H3+N2H3=N2H4+N2H2	1.20E+13	0.0	0.0
96. N2H4(+M)=NH2+NH2(+M)	5.00E+14	0.0	60000.0
Low pressure limit: 0.15000E+16 0.00000E+00 0.39000E+05			
N2 Enhanced by 2.400E+00			
NH3 Enhanced by 3.000E+00			
N2H4 Enhanced by 4.000E+00			
97. N2H4+M=N2H3+H+M	1.00E+15	0.0	63600.0
N2 Enhanced by 2.400E+00			
NH3 Enhanced by 3.000E+00			
N2H4 Enhanced by 4.000E+00			
98. N2H4+H=N2H3+H2	7.00E+12	0.0	2500.0
99. N2H4+H=NH2+NH3	2.40E+09	0.0	3100.0
100. N2H4+N=N2H3+NH	1.00E+10	1.0	2000.0
101. N2H4+NH=NH2+N2H3	1.00E+09	1.5	2000.0
102. N2H4+NH2=N2H3+NH3	1.80E+06	1.7	-1380.0
103. N+OH=NO+H	2.80E+13	0.0	0.0
104. N2O+H=N2+OH	2.20E+14	0.0	16750.0

105. N2O+H=NH+NO	6.70E+22	-2.2	37155.0
106. N2O+H=NNH+O	5.50E+18	-1.1	47290.0
107. N2O+H=HNNO	8.00E+24	-4.4	10530.0
108. N2O+OH=N2+HO2	1.00E+14	0.0	30000.0
109. HNO+NO=N2O+OH	8.50E+12	0.0	29580.0
110. HNO+NO+NO=HNNO+NO2	1.60E+11	0.0	2090.0
111. NH+NO+M=HNNO+M	1.63E+23	-2.6	1820.0
112. HNNO+H=N2O+H2	2.00E+13	0.0	0.0
113. HNNO+H=NH2+NO	1.00E+12	0.0	0.0
114. HNNO+O=N2O+OH	2.00E+13	0.0	0.0
115. HNNO+OH=H2O+N2O	2.00E+13	0.0	0.0
116. HNNO+OH=HNOH+NO	1.00E+12	0.0	0.0
117. HNNO+NO=N2+HONO	2.60E+11	0.0	1610.0
118. HNNO+NO=NNH+NO2	3.20E+12	0.0	540.0
119. HNNO+NO=N2O+HNO	1.00E+12	0.0	0.0
120. HNNO+NO2=N2O+HONO	1.00E+12	0.0	0.0
121. HNNO+NO2=NNH+NO3	1.00E+13	0.0	17000.0
122. NO2+H=NO+OH	1.32E+14	0.0	362.0
123. NO2+OH=HO2+NO	1.81E+13	0.0	6676.0
124. NO2+HO2=HONO+O2	4.64E+11	0.0	-479.0
125. NO2+H2=HONO+H	7.33E+11	0.0	28800.0
126. NO2+NH=N2O+OH	8.65E+10	0.0	-2270.0
127. NO2+NH=NO+HNO	1.24E+11	0.0	-2270.0
128. NO3+H=NO2+OH	6.62E+13	0.0	0.0
129. NO3+OH=NO2+HO2	1.21E+13	0.0	0.0
130. NO3+HO2=HNO3+O2	5.55E+11	0.0	0.0
131. NO3+HO2=NO2+OH+O2	1.51E+12	0.0	0.0
132. N2O4+H2O=HONO+HNO3	2.52E+14	0.0	11590.0
133. N2O3+H2O=HONO+HONO	3.79E+13	0.0	8880.0

134. H+NO(+M)=HNO(+M)	1.52E+15	-0.4	0.0
Low pressure limit: 0.40000E+21 -0.17500E+01 0.00000E+00			
H2O Enhanced by 1.000E+01			
O2 Enhanced by 1.500E+00			
H2 Enhanced by 2.000E+00			
135. HNO+H=NO+H2	4.46E+11	0.7	655.0
136. HNO+OH=NO+H2O	1.30E+07	1.9	-956.0
137. HNO+O=OH+NO	5.00E+11	0.5	2000.0
138. HNO+O=NO2+H	5.00E+10	0.0	2000.0
139. HNO+O2=NO+HO2	2.20E+10	0.0	9140.0
140. HNO+N=NO+NH	1.00E+11	0.5	2000.0
141. HNO+N=H+N2O	5.00E+10	0.5	3000.0
142. HNO+NH=NH2+NO	5.00E+11	0.5	0.0
143. HNO+NH2=NH3+NO	2.00E+13	0.0	1000.0
144. HNO+HNO=N2O+H2O	3.63E-03	4.0	1190.0
145. HNO+HNO=HNOH+NO	2.00E+08	0.0	4170.0
146. HNO+NO2=HONO+NO	6.02E+11	0.0	2000.0
147. NO+OH(+M)=HONO(+M)	2.00E+12	-0.1	-721.0
Low pressure limit: 0.50800E+24 -0.25100E+01 -0.67600E+02			
TROE centering: 0.62000E+00 0.10000E+02 0.10000E+06			
H2O Enhanced by 1.000E+01			
O2 Enhanced by 2.000E+00			
H2 Enhanced by 2.000E+00			
148. NO2+H+M=HONO+M	1.40E+18	-1.5	900.0
149. HONO+H=HNO+OH	5.64E+10	0.9	4970.0
150. HONO+H=NO+H2O	8.12E+06	1.9	3840.0
151. HONO+O=OH+NO2	1.20E+13	0.0	5960.0
152. HONO+OH=H2O+NO2	1.69E+12	0.0	-517.0
153. HONO+NH=NH2+NO2	1.00E+13	0.0	0.0

154. HONO+HONO=H2O+NO2+NO	1.00E+13	0.0	8540.0
155. HONO+NH2=NO2+NH3	5.00E+12	0.0	0.0
156. NO2+OH(+M)=HNO3(+M)	2.41E+13	0.0	0.0
Low pressure limit: 0.64200E+33 -0.54900E+01 0.23500E+04			
TROE centering: 0.10000E+01 0.10000E+02 0.11680E+04			
H2O Enhanced by 1.000E+01			
O2 Enhanced by 2.000E+00			
H2 Enhanced by 2.000E+00			
157. NO+HO2+M=HNO3+M	1.50E+24	-3.5	2200.0
158. HNO3+H=H2+NO3	5.56E+08	1.5	16400.0
159. HNO3+H=H2O+NO2	6.08E+01	3.3	6290.0
160. HNO3+H=OH+HONO	3.82E+05	2.3	6980.0
161. HNO3+OH=NO3+H2O	1.03E+10	0.0	-1240.0
162. NH3+O=NH2+OH	1.10E+06	2.1	5210.0
163. NH3+OH=NH2+H2O	5.00E+07	1.6	950.0
164. NH3+HO2=NH2+H2O2	3.00E+11	0.0	22000.0
165. NH2+HO2=NH3+O2	1.65E+04	1.6	2027.0
166. NH2+O=H2+NO	5.00E+12	0.0	0.0
167. NH2+O=HNO+H	4.50E+13	0.0	0.0
168. NH2+O=NH+OH	7.00E+12	0.0	0.0
169. NH2+OH=NH+H2O	9.00E+07	1.5	-460.0
170. NH2+OH=NH2OH	1.79E+13	0.2	0.0
171. NH2+HO2=HNO+H2O	5.68E+15	-1.1	707.0
172. NH2+HO2=H2NO+OH	2.91E+17	-1.3	1248.0
173. NH2+O2=HNO+OH	1.00E+13	0.0	26290.0
174. NH2+O2=H2NO+O	6.00E+13	0.0	29880.0
175. NH2+NO=NNH+OH	2.29E+10	0.4	-814.0
176. NH2+NO=N2+H2O	2.77E+20	-2.6	1258.0
177. NH2+NO=H2+N2O	1.00E+13	0.0	33700.0

178. NH2+NO2=N2O+H2O	1.62E+16	-1.4	270.0
179. NH2+NO2=H2NO+NO	6.48E+16	-1.4	270.0
180. NH+O=NO+H	7.00E+13	0.0	0.0
181. NH+O=N+OH	7.00E+12	0.0	0.0
182. NH+OH=HNO+H	2.00E+13	0.0	0.0
183. NH+OH=N+H2O	2.00E+09	1.2	0.0
184. NH+OH=NO+H2	2.00E+13	0.0	0.0
185. NH+HO2=HNO+OH	1.00E+13	0.0	2000.0
186. NH+O2=HNO+O	4.00E+13	0.0	17880.0
187. NH+O2=NO+OH	4.50E+08	0.8	1190.0
188. NH+H2O=HNO+H2	2.00E+13	0.0	13850.0
189. NH+N2O=N2+HNO	2.00E+12	0.0	6000.0
190. NNH+O=NH+NO	2.00E+14	0.0	4000.0
191. NH+NO=N2+OH	6.10E+13	-0.5	120.0
192. N2H4+O=N2H2+H2O	8.50E+13	0.0	1200.0
193. N2H4+O=N2H3+OH	2.50E+12	0.0	1200.0
194. N2H4+OH=N2H3+H2O	3.00E+10	0.7	1290.0
195. N2H4+OH=NH3+H2NO	3.67E+13	0.0	0.0
196. N2H4+HO2=N2H3+H2O2	4.00E+13	0.0	2000.0
197. N2H3+O=N2H2+OH	2.00E+13	0.0	1000.0
198. N2H3+O=NNH+H2O	3.16E+11	0.5	0.0
199. N2H3+O=NH2+HNO	1.00E+13	0.0	0.0
200. N2H3+OH=N2H2+H2O	3.00E+10	0.7	1290.0
201. N2H3+OH=NH3+HNO	1.00E+12	0.0	15000.0
202. N2H3+O2=N2H2+HO2	3.00E+12	0.0	0.0
203. N2H3+HO2=N2H2+H2O2	1.00E+13	0.0	2000.0
204. N2H3+HO2=N2H4+O2	8.00E+12	0.0	0.0
205. N2H3+NO=HNO+N2H2	1.00E+12	0.0	0.0
206. N2H2+O=NH2+NO	1.00E+13	0.0	0.0

207. N2H2+O=NNH+OH	2.00E+13	0.0	1000.0
208. N2H2+OH=NNH+H2O	5.92E+01	3.4	-1360.0
209. N2H2+HO2=NNH+H2O2	1.00E+13	0.0	2000.0
210. N2H2+NO=N2O+NH2	3.00E+10	0.0	0.0
211. NNH+O=N2+OH	1.70E+16	-1.2	500.0
212. NNH+OH=N2+H2O	2.40E+22	-2.9	2444.0
213. NNH+O2=N2+HO2	1.20E+12	-0.3	150.0
214. NNH+O2=N2O+OH	2.90E+11	-0.3	150.0
215. NNH+HO2=N2+H2O2	1.00E+13	0.0	2000.0
216. NNH+NO=N2+HNO	5.00E+13	0.0	0.0
217. NH2OH+OH=HNOH+H2O	2.50E+13	0.0	4250.0
218. H2NO+M=H2+NO+M	7.83E+27	-4.3	60300.0
H2O Enhanced by 1.000E+01			
219. H2NO+M=HNO+H+M	2.80E+24	-2.8	64915.0
H2O Enhanced by 1.000E+01			
220. H2NO+M=HNOH+M	1.10E+29	-4.0	43980.0
H2O Enhanced by 1.000E+01			
221. H2NO+H=HNO+H2	3.00E+07	2.0	2000.0
222. H2NO+H=NH2+OH	5.00E+13	0.0	0.0
223. H2NO+O=HNO+OH	3.00E+07	2.0	2000.0
224. H2NO+OH=HNO+H2O	2.00E+07	2.0	1000.0
225. H2NO+HO2=HNO+H2O2	2.90E+04	2.7	-1600.0
226. H2NO+NH2=HNO+NH3	3.00E+12	0.0	1000.0
227. H2NO+O2=HNO+HO2	3.00E+12	0.0	25000.0
228. H2NO+NO=HNO+HNO	2.00E+07	2.0	13000.0
229. H2NO+NO2=HONO+HNO	6.00E+11	0.0	2000.0
230. HNOH+M=HNO+H+M	2.00E+24	-2.8	58935.0
H2O Enhanced by 1.000E+01			
231. HNOH+H=HNO+H2	4.80E+08	1.5	380.0

232. HNOH+H=NH2+OH	4.00E+13	0.0	0.0
233. HNOH+O=HNO+OH	7.00E+13	0.0	0.0
234. HNOH+O=HNO+OH	3.30E+08	1.5	-360.0
235. HNOH+OH=HNO+H2O	2.40E+06	2.0	-1190.0
236. HNOH+HO2=HNO+H2O2	2.90E+04	2.7	-1600.0
237. HNOH+NH2=HNO+NH3	1.80E+06	1.9	-1150.0
238. HNOH+NO2=HONO+HNO	6.00E+11	0.0	2000.0
239. HNOH+O2=HNO+HO2	3.00E+12	0.0	25000.0
240. HNOH+HNO=NH2OH+NO	1.00E+12	0.0	3000.0

BIBLIOGRAPHY

[1] Schlapbach L, Züttel A. Hydrogen-storage materials for mobile applications. Nature 2001;414:353–8. doi:10.1038/35104634.

[2] Thomas G, Parks G. Potential Roles of Ammonia in a Hydrogen Economy. 2006.

[3] Karabeyoglu A, Stevens J, Geyzel D, Cantwell B. High Performance Hybrid Upper Stage Motor. 47th AIAA/ASME/SAE/ASEE Jt. Propuls. Conf. Exhib., San Diego, California: 2011. doi:http://dx.doi.org/10.2514/6.2011-6025.

[4] Zamfirescu C, Dincer I. Ammonia as a green fuel and hydrogen source for vehicular applications. Fuel Process Technol 2009;90:729–37. doi:10.1016/j.fuproc.2009.02.004.

[5] Zamfirescu C, Dincer I. Using ammonia as a sustainable fuel. J Power Sources 2008;185:459–65. doi:10.1016/j.jpowsour.2008.02.097.

[6] Agency IE. HYDROGEN PRODUCTION AND STORAGE. 2006.

[7] Zeldovic Y. The oxidation of nitrogen in combustion and explosions. Acta Phys Chim USSR 1946;21:577{628.

[8] Karabeyoglu A, Evans B. Selection of NH3 for Gas Turbine Use. 8th NH3 Conf - Portl 2011.

[9] Kaskan WE, Hughes DE. Mechanism of decay of ammonia in flame gases from an NH3/O2 flame. Combust Flame 1973;20:381–8. doi:10.1016/0010-2180(73)90030-8.

[10] Miller JA, Smooke MD, Green RM, Kee RJ. Kinetic Modeling of the Oxidation of Ammonia in Flames. Combust Sci Technol 1983;34:149–76. doi:10.1080/00102208308923691.

[11] Dean AM, Chou M-S, Stern D. Kinetics of rich ammonia flames. Int J Chem Kinet 1984;16:633–53. doi:10.1002/kin.550160603.

[12] Salimian S, Hanson RK, Kruger CH. Ammonia oxidation in shock-heated NH3-N2O-Ar mixtures. Combust Flame 1984;56:83–95. doi:10.1016/0010-2180(84)90007-5.

[13] Miller JA, Bowman CT. Mechanism and modeling of nitrogen chemistry in combustion. Prog Energy Combust Sci 1989;15:287–338. doi:10.1016/0360-1285(89)90017-8.

[14] Davidson DF, Kohse-Höinghaus K, Chang AY, Hanson RK. A pyrolysis mechanism for ammonia. Int J Chem Kinet 1990;22:513–35. doi:10.1002/kin.550220508.

[15] Mertens JD, Chang AY, Hanson RK, Bowman CT. Reaction kinetics of NH in the shock tube pyrolysis of HNCO. Int J Chem Kinet 1989;21:1049–67. doi:10.1002/kin.550211107.

[16] Davidson DF, Hanson RK. High temperature reaction rate coefficients derived from N-atom ARAS measurements and excimer photolysis of NO. Int J Chem Kinet 1990;22:843–61. doi:10.1002/kin.550220805.

[17] Bian J, Vandooren J, Van Tiggelen PJ. Experimental study of the formation of nitrous and nitric oxides in H2−O2−Ar flames seeded with NO and/or NH3. Symp Combust 1991;23:379–86. doi:10.1016/S0082-0784(06)80282-1.

[18] Vandooren J, Bian J, Van Tiggelen PJ. Comparison of experimental and calculated structures of an ammonia-nitric oxide flame. Importance of the NH2 + NO reaction. Combust Flame 1994;98:402–10. doi:10.1016/0010-2180(94)90178-3.

[19] LINDSTEDT RP, LOCKWOOD FC, SELIM MA. Detailed Kinetic Modelling of Chemistry and Temperature Effects on Ammonia Oxidation. Combust Sci Technol 1994;99:253–76. doi:10.1080/00102209408935436.

[20] Lindstedt RP, Lockwood FC, Selim M a. A Detailed Kinetic Study of Ammonia Oxidation. Combust Sci Technol 1995;108:231–54. doi:10.1080/00102209508960400.

[21] Smith GP, Golden DM, Frenklach M, Moriarty NW, Eiteneer B, Goldenberg M, et al. GRI-MECH 3.0 n.d. http://www.me.berkeley.edu/gri_mech/.

[22] The combustion division of the Center for Energy Research at the University of California "San Diego reaction mechanism" 2005. www.maeweb.ucsd.edu/combustion/cermech/index.html.

[23] BENDTSEN AB, GLARBORG P, DAM-JOHANSEN K. Low temperature oxidation of methane: the influence of nitrogen oxides. Combust Sci Technol 1999;151:31–71. doi:10.1080/00102200008924214.

[24] Glarborg P, Per G. Kristensen A, Dam-Johansen K, Miller JA. Branching Fraction of the NH2 + NO Reaction between 1210 and 1370 K. J Phys Chem 1997. doi:10.1021/JP970264G.

[25] Skreiberg Ø, Kilpinen P, Glarborg P. Ammonia chemistry below 1400 K under fuel-rich conditions in a flow reactor. Combust Flame 2004;136:501–18. doi:10.1016/j.combustflame.2003.12.008.

[26] Konnov a. a., Ruyck J De. Kinetic Modeling of the Thermal Decomposition of Ammonia. Combust Sci Technol 2000;152:23–37. doi:10.1080/00102200008952125.

[27] Konnov AA. Implementation of the NCN pathway of prompt-NO formation in the detailed reaction mechanism. Combust Flame 2009;156:2093–105. doi:10.1016/j.combustflame.2009.03.016.

[28] Harrison JA, Whyte AR, Phillips LF. Kinetics of reactions of NH with NO and NO2. Chem Phys Lett 1986;129:346–52. doi:10.1016/0009-2614(86)80356-6.

[29] Lozovsky VA, Ioffe MA, Sarkisov OM. On the reaction of the NH2 radical with

oxygen. Chem Phys Lett 1984;110:651–4. doi:10.1016/0009-2614(84)85481-0.

[30] Cheskis SG, Nadtochenko VA, Sarkisov OM. Study of the HNO + HNO and HNO + NO reactions by intracavity laser spectroscopy. Int J Chem Kinet 1981;13:1041–50. doi:10.1002/kin.550131005.

[31] Zabielski MF, Seery DJ. High temperature measurements of the rate of the reaction of OH with NH3. Int J Chem Kinet 1985;17:1191–9. doi:10.1002/kin.550171105.

[32] Duynslaegher C. Thèse (Dissertation) " Experimental and numerical study of ammonia combustion " Référence bibliographique n.d.

[33] Duynslaegher C, Contino F, Vandooren J, Jeanmart H. Modeling of ammonia combustion at low pressure. Combust Flame 2012;159:2799–805. doi:10.1016/j.combustflame.2012.06.003.

[34] Kumar P, Meyer TR. Experimental and modeling study of chemical-kinetics mechanisms for H2–NH3–air mixtures in laminar premixed jet flames. Fuel 2013;108:166–76. doi:10.1016/j.fuel.2012.06.103.

[35] Xiao H, Howard M, Valera-Medina A, Dooley S, Bowen PJ. Study on Reduced Chemical Mechanisms of Ammonia/Methane Combustion under Gas Turbine Conditions. Energy & Fuels 2016:acs.energyfuels.6b01556. doi:10.1021/acs.energyfuels.6b01556.

[36] Xiao H, Valera-Medina A, Marsh R, Bowen PJ. Numerical study assessing various ammonia/methane reaction models for use under gas turbine conditions. Fuel 2017;196:344–51. doi:10.1016/j.fuel.2017.01.095.

[37] Macq A. Emploi de l'ammoniaque comme combustible de remplacement. Compte-rendu des Journées d'Etudes sur les Combust. Carburants Nationaux, Louvain , 286, 1941.

[38] Starkman ES, Newhall HK, Sutton R, Maguire T, Farbar L. Ammonia as a Spark Ignition Engine Fuel: Theory and Application, 1966. doi:10.4271/660155.

[39] Grannell SM, Assanis DN, Bohac S V., Gillespie DE. The Operating Features of a Stoichiometric, Ammonia and Gasoline Dual Fueled Spark Ignition Engine. Energy Convers. Resour., vol. 2006, ASME; 2006, p. 15–27. doi:10.1115/IMECE2006-13048.

[40] Grannell SM, Assanis DN, Bohac S V., Gillespie DE. The Fuel Mix Limits and Efficiency of a Stoichiometric, Ammonia, and Gasoline Dual Fueled Spark Ignition Engine. J Eng Gas Turbines Power 2008;130:42802. doi:10.1115/1.2898837.

[41] Mathis J. Mr. clean hits the road ammonia-gas blend to fuel a drive to San Francisco. Ann Arbor News 2007.

[42] Grannell SM, Assanis DN, Gillespie DE, Bohac S V. Exhaust Emissions From a Stoichiometric, Ammonia and Gasoline Dual Fueled Spark Ignition Engine.

ASME 2009 Intern. Combust. Engine Div. Spring Tech. Conf., ASME; 2009, p. 135–41. doi:10.1115/ICES2009-76131.

[43] Mørch CS, Bjerre a., Gøttrup MP, Sorenson SC, Schramm J. Ammonia/hydrogen mixtures in an SI-engine: Engine performance and analysis of a proposed fuel system. Fuel 2011;90:854–64. doi:10.1016/j.fuel.2010.09.042.

[44] Gross CW, Kong S-C. Performance characteristics of a compression-ignition engine using direct-injection ammonia–DME mixtures. Fuel 2013;103:1069–79. doi:10.1016/j.fuel.2012.08.026.

[45] Reiter AJ, Kong S-C. Combustion and emissions characteristics of compression-ignition engine using dual ammonia-diesel fuel. Fuel 2011;90:87–97. doi:10.1016/j.fuel.2010.07.055.

[46] Boretti A. Novel dual fuel diesel-ammonia combustion system in advanced TDI engines. Int J Hydrogen Energy 2016:1–6. doi:10.1016/j.ijhydene.2016.11.208.

[47] Solar Devision of International Harvester Company. Development of an ammonia-burning gas turbine engine. 1968.

[48] Pratt DT. Performance of ammonia-fired gas-turbine combustors. 1967.

[49] Karabeyoglu A, Evans B, Stevens J, Cantwell B, Micheletti D. Development of Ammonia Based Fuels for Environmentally Friendly Power Generation. 10th Int. Energy Convers. Eng. Conf., Atlanta, Georgia: American Institute of Aeronautics and Astronautics; 2012. doi:10.2514/6.2012-4055.

[50] Valera-Medina A, Marsh R, Runyon J, Pugh D, Beasley P, Hughes T, et al. Ammonia–methane combustion in tangential swirl burners for gas turbine power generation. Appl Energy 2016:1–10. doi:10.1016/j.apenergy.2016.02.073.

[51] Jun Li, Hongyu Huang, Noriyuki Kobayashi ZH and YN. Study on using hydrogen and ammonia as fuels: Combustion characteristics and NOx formation. Int J Energy Res 2014;38:1214–23. doi:10.1002/er.3141.

[52] Um DH, Joo JM, Lee S, Kwon OC. Combustion stability limits and NOx emissions of nonpremixed ammonia-substituted hydrogen-air flames. Int J Hydrogen Energy 2013;38:14854–65. doi:10.1016/j.ijhydene.2013.08.140.

[53] Frigo S, Gentili R. Analysis of the behaviour of a 4-stroke Si engine fuelled with ammonia and hydrogen. Int J Hydrogen Energy 2013;38:1607–15. doi:10.1016/j.ijhydene.2012.10.114.

[54] Ichikawa A, Hayakawa A, Kitagawa Y, Kunkuma Amila Somarathne KD, Kudo T, Kobayashi H. Laminar burning velocity and Markstein length of ammonia/hydrogen/air premixed flames at elevated pressures. Int J Hydrogen Energy 2015;40:9570–8. doi:10.1016/j.ijhydene.2015.04.024.

[55] Joo JM, Lee S, Kwon OC. Effects of ammonia substitution on combustion stability limits and NO x emissions of premixed hydrogen-air flames. Int J Hydrogen Energy 2012;37:6933–41. doi:10.1016/j.ijhydene.2012.01.059.

[56] Choi S, Lee S, Kwon OC. Extinction limits and structure of counterflow nonpremixed hydrogen-doped ammonia/air flames at elevated temperatures. Energy 2015;85:503–10. doi:10.1016/j.energy.2015.03.061.

[57] Mujeebu MA, Abdullah MZ, Bakar MZA, Mohamad AA, Muhad RMN, Abdullah MK. Combustion in porous media and its applications - A comprehensive survey. J Environ Manage 2009;90:2287–312. doi:10.1016/j.jenvman.2008.10.009.

[58] Su S, Hwang S, Lai W. On a porous medium combustor for hydrogen flame stabilization and operation. Int J Hydrogen Energy 2014;39:21307–16. doi:10.1016/j.ijhydene.2014.10.059.

[59] Howell JR, Hall MJ, Ellzey JL. Combustion of hydrocarbon fuels within porous intert media. Prog Energy Combust Sci 1996;22:121–45.

[60] Gauthier S, Nicolle A, Baillis D. Investigation of the flame structure and nitrogen oxides formation in lean porous premixed combustion of natural gas / hydrogen blends. Int J Hydrogen Energy 2008;33:4893–905. doi:10.1016/j.ijhydene.2008.06.012.

[61] Ingham DB, Pop I. Transport Phenomena in Porous Media III. Elsevier; 2005.

[62] Alavandi SK, Agrawal AK. Experimental study of combustion of hydrogen-syngas/methane fuel mixtures in a porous burner. Int J Hydrogen Energy 2008;33:1407–15. doi:10.1016/j.ijhydene.2007.12.005.

[63] Su S, Lai W, Hwang S. ScienceDirect Experimental study of the heat recovery rate in a porous medium combustor under different hydrogen combustion modes. Int J Hydrogen Energy 2016;41:15043–55. doi:10.1016/j.ijhydene.2016.06.119.

[64] Ströhle J, Myhrvold T. Reduction of a detailed reaction mechanism for hydrogen combustion under gas turbine conditions. Combust Flame 2006;144:545–57. doi:10.1016/j.combustflame.2005.08.011.

[65] Rotexo. Cosilab, the combustion simulation laboratory 2007. www.rotexo.com.

[66] Konnov AA. Remaining uncertainties in the kinetic mechanism of hydrogen combustion. Combust Flame 2008;152:507–28. doi:10.1016/j.combustflame.2007.10.024.

[67] Duynslaegher C, Jeanmart H, Vandooren J. Ammonia combustion at elevated pressure and temperature conditions. Fuel 2010;89:3540–5. doi:10.1016/j.fuel.2010.06.008.

[68] Dinçer I, Zamfirescu C. Sustainable Energy Systems and Applications. Springer; 2011.

[69] Grannel S, Gillespie DE. Ammonia flame cracker system, method and apparatus. US 8,623,285 B2, 2014.

[70] Karabeyoglu A, Evans B. Fuel Conditioning System for Ammonia-Fired Power Plants. 9th Annu. NH3 Fuel Assoc. Conf., 2012.

[71] Nozari H, Karabeyoglu A. Numerical study of combustion characteristics of ammonia as a renewable fuel and establishment of reduced reaction mechanisms. Fuel 2015;159:223–33. doi:10.1016/j.fuel.2015.06.075.

[72] Brackmann C, Alekseev V a., Zhou B, Bengtsson PE, Li Z, et al. Structure of premixed ammonia + air flames at atmospheric pressure: Laser diagnostics and kinetic modeling. Combust Flame 2016;163:370–81. doi:10.1016/j.combustflame.2015.10.012.

[73] Tunçer O, Kaynaroğlu B, Karakaya MC, Kahraman S, Çetiner-Yıldırım O, Baytaş C. Preliminary investigation of a swirl stabilized premixed combustor. Fuel 2014;115:870–4. doi:10.1016/j.fuel.2012.11.085.

[74] Glassman I, Yetter RA. Combustion. 4th ed. Elsevier; 2008.

[75] Nozari H, Karabeyoglu A. Combustion characteristics of ammonia as a renewable energy source and development of reduced chemical mechanisms. 13th Int. Energy Convers. Eng. Conf. AIAA Propuls. Energy Forum, Orlando, FL: AIAA; 2015. doi:10.2514/6.2015-3917.

[76] Occupational Safety and Health Administration n.d. https://www.osha.gov/.